SCALE-UP BEHAVIOUR OF THE FROTH STABILITY MEASUREMENT

By

Armand Stefan Geldenhuys

BEng (Chemical), University of Stellenbosch

A thesis submitted to the faculty of Engineering and the Built Environment, University of Cape Town in fulfilment of the requirements for the degree of Master of Science in Engineering

Supervised by: Dr Belinda McFadzean

Centre for Minerals Research

Department of Chemical Engineering

University of Cape Town

December 2018

DECLARATION

I, Stefan Geldenhuys, hereby declare that I understand what plagiarism is and that it is unethical to do so. The Harvard referencing system has been used throughout this document. Each significant contribution to, and quotation in, this document from the work, or works, of other people has been attributed, and has been referenced appropriately. I declare that this is my own work and I have not allowed, or will not allow, anyone to copy this work with the intention of passing it off as his or her or their own work.

Stefan Geldenhuys

Signed by candidate

_____ 15/10/2018_____

_ Signature Date

ACKNOWLEDGEMENTS

I would like to acknowledge the following people who made it possible, and probably bearable, for me to complete this project:

- My supervisor, Dr. Belinda McFadzean, for all the advice, insights and guidance throughout this project. Your approach to problem solving, albeit very different than mine, is truly something inspiring. Much appreciation also for the open-door policy and the fact that I could bother at any time.
- My advisor, Mr. Martin Harris, for always challenging my opinions and leading me towards new levels of understanding. Your approach to managing someone like me, albeit a bit harsh sometimes, is much appreciated.
- The Centre for Minerals Research (CMR), UCT, for funding this project and allowing me to do my master's while employed.
- The current MPTech manager, Mr. Andre van der Westhuizen, for understanding and supporting me while doing this project.
- The previous MPTech manager, Mrs. Jenni Sweet, for giving me the opportunity to join the CMR family and supporting me while doing this project.
- Mr. Kenneth Maseko for all the technical support in the laboratory as well as all the help and support during the experimental work.
- Mr. Monde Bekaphi for all the help and support during the experimental work.
- The CMR staff in general for creating such a wonderful work atmosphere.
- Finally, to my family and friends, for all the support and love. Without you this would truly not be possible.

ABSTRACT

Froth flotation is a widely used physio-chemical separation method in the minerals processing industry. Two distinct phases are present, namely: the pulp and froth phase. Flotation research has heavily focussed on the pulp performance; however only recently it was found that the froth performance contributes significantly to the overall flotation performance. Numerous parameters have been investigated to accurately quantify froth performance with the most notably being froth recovery. That being said, experimentally gathering data to obtain froth recovery is challenging and prone to large experimental errors. For this reason, the stability of the froth phase has been highlighted as a possible characterisation tool. Froth stability is defined as the time of persistence of the froth and is usually measured using either a dynamic and/or static methodology. Although measurement of froth stability has become common place in numerous flotation research articles, little to no attention has been given to the scale-up behaviour of the measurement. It is easily thought of that a froth constrained within a froth column will behave significantly different to one in an industrial flotation cell. Two common scale parameters, froth column diameter and initial pulp bubble size, was chosen to illustrate the dependence of the current methodology on scale. This does not mean that there are not vastly more parameters that would affect the measurement (column material of construction and/or column shape); however, these are two of the most easily changed parameters from experimental setup to setup.

Four different column diameters were used for this study. Column diameter experiments were done on an industrial scale by means on manual tracking of froth growth versus time. Pulp bubble size experiments was performed on a laboratory scale by using different pore size glass frits while maintaining a constant superficial gas velocity. Dynamic stability for the pulp bubble size experiments were done by means of video tracking of froth growth versus time.

The column diameter data sets highlighted similar behaviour – an increase in measured dynamic stability is seen with increasing column diameter up until a maximum is reached. This behaviour was attributed to the fact that wall films are thought to drain much faster than interstitial Plateau borders. As the column diameter decreases, the relative ratio of column surface area to bulk area increases and therefore results in an increased drainage rate a subsequently less stable froth. An empirical relationship was proposed to correct for the column diameter effect which is based on a ratio of bubble size to column diameter.

The pulp bubble size data sets highlighted similar behaviour – an exponential decrease in measured dynamic stability is seen with increasing pulp bubble size. This

behaviour was attributed to two fundamental mechanisms occurring within larger bubbled froths. Firstly, an increase in drainage rate as well as change in the drainage regime is seen as a function of bubble size; where in general froths of larger bubble sizes drain significantly faster. Secondly, on average froths consisting of large bubbles will have less water per volume of froth due to the decrease in bubble surface area. The effect of water content in a froth is well known and it can be said that wet froths experience less coalescence and bursting events. Therefore, the combination of the two mechanism is put forth as an explanation of the observed behaviour of the experimental systems.

TABLE OF CONTENTS

LIST OF FIGURES

LIST OF TABLES

LIST OF ABBREVIATIONS

Abbreviation	Description
APBS	Anglo American Platinum Bubble Sizer
BMS	Base Metal Sulphide
CCC	Critical Coalescence Concentration
CFH	Corrected Froth Height
CMC	Carboxymethyl Cellulose
CMR	Centre for Minerals Research
PCF	Pressure Correction Factor
PGM	Platinum Group Minerals
POR0	Glass frit ID with geometric mean pore size of 200 µm
POR1	Glass frit ID with geometric mean pore size of 126 µm
POR2	Glass frit ID with geometric mean pore size of 63 µm
POR3	Glass frit ID with geometric mean pore size of 25 µm
POR4	Glass frit ID with geometric mean pore size of 13 µm
SIBX	Sodium Isobutyl Xanthate
SLS	Sodium Lauryl Sulfate
SOF	Side-of-froth
SPW	Synthetic Plant Water
TOF	Top-of-froth
UCT	University of Cape Town
UG2	Upper Group 2 reef

LIST OF SYMBOLS

Symbol	Description	Units
ΔP	Net applied pressure	Pa
ΔP_{loss}	Pressure loss	Pa
$\sum$	Dynamic froth stability	s
$\sum_{\infty}$	Dynamic froth stability in an infinitely large system	s
$\sum_{measured}$	Apparent/measured dynamic froth stability	s
μ	Dynamic viscosity	kg/m·s
A	Area	m^2
A_b	Total surface area of bubbles in contact with column	mm^2
A_c	Surface area of column in contact with froth	mm^2
A_{column}	Area of column	cm^2
A_{frit}	Area of glass frit	cm^2
A_{PB}	Area of Plateau border	mm^2
D	Diameter	m
d_{32}	Sauter mean bubble diameter	mm
D_b / d_b	Bubble diameter	mm
D_C / d_c	Froth column diameter	mm
d_i	Diameter of bubble in class i	mm
g	Standard acceleration due to gravity	m/s^2
H(t)	Froth/foam height at time t	mm
$H_{foam,\ max}$	Equilibrium froth/foam height (static)	mm
H_{foam}	Froth/foam height at time t (static)	mm
H_i	Froth/foam height	mm
H_{max} / H_{∞}	Equilibrium froth/foam height (dynamic)	mm
H_p	Distance from pulp surface to end of APBS probe	m
H_w	Distance from end of measuring mark to end of APBS probe	m

Symbol	Description	Units
J_g	Superficial gas velocity	cm/s
L	Pipe length	m
N_b	Total number of spherical bubbles	-
P_{atm}	Atmospheric pressure	kPa
P_{film}	Applied film pressure	Pa
P_{PB}	Applied Plateau border pressure	Pa
Q	Volumetric flow rate	L/s
$r_{bubbles}$	Radius of bubbles	mm
r_{PB}	Radius of curvature of the Plateau border	mm
S_b	Bubble surface area flux	s^{-1}
t	Time	s
$t_{1/2}$	Froth/foam half-life (static stability indicator)	s
V_{bubble}	Volume of a spherical bubble	mm^3
V_{froth}	Volume of froth	mm^3
v_f	Front velocity/ propagation velocity	mm/s
V_S	Applied superficial liquid velocity	mm/s
v_s	Superficial fluid velocity	m/s
α	Fitting parameter (static)	-
ε_g	Gas hold-up fraction of pulp	-
ρ_p	Density of pulp/slurry	kg/m^3
ρ_w	Density of water	kg/m^3
τ	Average bubble lifetime (dynamic)	s
Φ	Gas hold-up fraction of froth/foam	-

CHAPTER ONE: INTRODUCTION

1.1. BACKGROUND

The flotation process is usually divided into two distinct sections, namely: the pulp and froth phase (Wills & Napier-Munn, 2006). Recent flotation research has focussed on the froth phase and it has been identified as a major contributor to the overall metallurgical performance of a flotation cell (Barbian, et al., 2005; Gorain, et al., 1998; Zanin, et al., 2009). Numerous parameters have been investigated to quantify froth performance, most notably froth recovery (Seaman, et al., 2004). Experimentally gathering data to determine froth recovery is challenging and for this reason other factors have been identified to characterise froth performance; one being the stability of the froth.

Several proxies can be used to estimate froth stability (Farrokhpay, 2011); however, two quantitative methods have found traction, namely: the dynamic and static froth stability tests. The dynamic froth stability test is based on the work done by Bikerman (1973) where it was proposed that the maximum froth volume achieved divided by the volumetric air flow rate is an indication of the stability. Barbian, et al., (2005) took this idea further and proposed an exponential equation that will describe the froth growth with time. That being said, Iglesias, et al., (1995) proposed that a static test would be a better approximation of froth stability. In static froth stability tests, a foam/froth is generated up until the maximum height is achieved then the air input is discontinued and the froth decay with time is measured.

Although measurement of froth stability has become common place in most froth studies within literature, little to no attention has been given to the scale-up behaviour. Please note that scale-up effects simply refer to going from an industrial scale to a laboratory scale and therefore things such as column material of construction, column shape, and bubble size, just to mention a few all fall under this broad descriptor. In fact, the only mention of scale effects in froth flotation literature is from a review paper by Farrokpay (2011); where it states that a froth constrained within a stability column might behave significantly differently to one in an industrial flotation cell. The development of a more predictive mechanistic froth model has numerous high-level benefits, such as: better plant simulation models for optimisation as well as increased design capacity and confidence. However, it is the operation of flotation plants where the model would possibly add the most value, allowing for a cell-by-cell mass pull control strategy by model predictive control. The dynamic and static froth stability methodologies provide a quantitative manner to establish froth stability numbers that could feed a mechanistic model; however, it is of critical importance that these experiments should be independent of scale to generate realistic predictions.

1.2. PROBLEM STATEMENT

As mentioned before scale effects have received little to no attention within froth literature. Following from this all results presented in this thesis will be to the authors` knowledge the first study in froth literature where scale parameter effects are studied. Figure 1 displays measured dynamic froth stability as a function of time for four different froth column diameters. Please note, the data displayed in Figure 1 was generated by the Centre for Minerals Research and is currently unpublished.

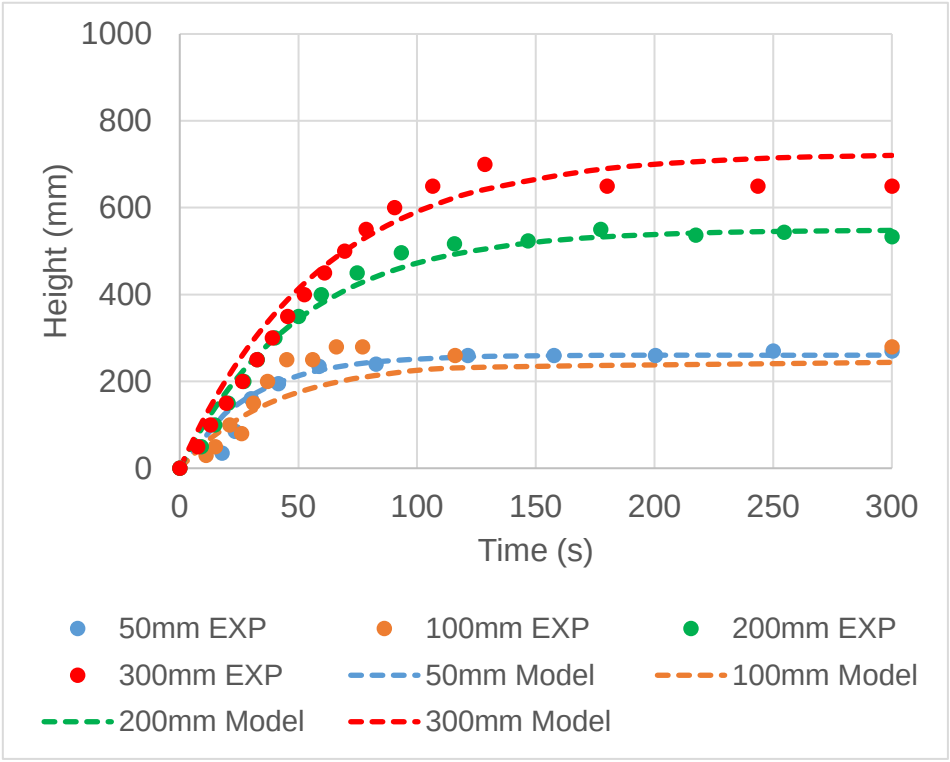

Figure 1: Dynamic froth height as a function of time for four different frothing column diameters performed on the third rougher cell of a PGM operation (McFadzean, 2013)

Even though no changes were made to the experimental conditions during the gathering of the data displayed in Figure 1, a large difference can be seen for the equilibrium froth height of the largest column diameter. Column diameter changes of laboratory column setup is quite common seeing as it directly impacts the amount of material needed to run a test. From the results displayed in Figure 1, if a froth stability test of an identical ore was done in a 100 mm and 200 mm column; the resulting dynamic froth stability would be vastly different.

This thesis aims to illustrate that scale parameters have a drastic effect on the outcomes of the experiment. For this study two of the most readily changed scale parameters will be investigated, namely: pulp bubble size and column diameter. The author, however, does not limit scale effects to only these two parameters as there might be vastly more parameters that would significantly affect the outcome, such as

column material of construction, column shape, bubble generation method, etc. just to mention a few.

1.3. RESEARCH OBJECTIVES

There are numerous outcomes from this research project which stems from the lack of scale dependent studies in flotation froth literature. In general, the following overall objectives will be addressed:

a. Gather data that illustrates the fact that froth column diameter influences the measured froth stability; as far as reasonably practicable find a common trend which will be published in flotation froth literature.
b. Gather data that illustrates the effect of pulp bubble size on the measured froth stability; as far as reasonably practicable find a common trend which will be published in flotation froth literature.
c. From the learnings of the project, propose a standard manner in which froth stability measurements should be performed. This could go as far as the fact that if initial bubble size is a significant factor; measurement of this parameter should be included in new froth stability equipment.

1.4. SCOPE OF RESEARCH

Firstly, scale parameters as referred to within this thesis will translate to physical changes to the measurement equipment and not changes to the material feeding it. Hence, parameters such as particle size, hydrophobicity, reagent dosage and type are not considered to fall under scale parameters. Furthermore, only two scale parameters will be studied during this research, namely: column diameter and pulp bubble size. These parameters were chosen since its changed quite often between experimental setups. For instance, column diameter is always decreasing in laboratory setups because smaller columns lead to less material needed to run experiments. Pulp bubble size is not measured in many of the experimental setups because it is thought to be less critical than parameters such as air rate.

Secondly, it should be noted that this is a first pass at a very complex problem and therefore it is the sole purpose of this research to highlight the effects. Little attention will be given to modelling the effects seen and therefore simple and robust experimental methodologies will be used. Numerous more accurate, high cost measurements may be amenable to this study; however, without a clear question to answer these methodologies will only complicate the analysis.

Lastly, most of the data will be collected from mineral slurries common in South African concentrators. Although numerous fundamental 2-phase studies have shown promise within foam literature; it is thought that these fundamental systems significantly depart from realistic applications.

1.5. BRIEF OUTLINE OF THESIS

This thesis will have the following outline:

- Chapter 1 – This will introduce the area of research. A short background will be given and a problem statement. This is followed by the overall objectives of this study and the scope of the research.
- Chapter 2 – Relevant literature to the area of research will be discussed. Please note, scale effects on the measurement of dynamic froth stability has not been studied in froth literature and therefore various other areas will be introduced where this is known. The hypotheses and key questions will be defined at the end of this chapter.
- Chapter 3 – This gives all the relevant experimental details of the test program. In general, it will be divided into subsections dealing with material and equipment, experimental procedures, and data analysis. The interesting aspect of this section is that both industrial scale and laboratory scale experiments were used throughout.
- Chapter 4 – In this chapter all the results and discussion relevant to the effect of column diameter on measured dynamic stability will be highlighted. Please note, the results present in section 4.2 and 4.3 were generated by exclusively using the industrial scale experimental setup and procedures. Whereas, the results presented in Section 4.4 were generated using a 100 mm and 200 mm laboratory experimental setup and procedure.
- Chapter 5 – This will deal with all the results and discussion regarding the effect of pulp bubble size on measured dynamic froth stability. Seeing as the glass frits used to generate the different pulp bubble sizes are central to the research a whole section (Section 5.2) was dedicated to the characterisation of the bubble size produced at various conditions. All the results displayed in Sections 5.3 and 5.4 were generated using a laboratory 200 mm column experimental setup.
- Chapter 6 – This chapter gives a detailed breakdown of the conclusions and recommendations of this research.

CHAPTER TWO: LITERATURE REVIEW, HYPOTHESIS AND KEY QUESTIONS

2.1. LITERATURE REVIEW

2.1.1. FROTH FLOTATION

Froth flotation is a widely used physio-chemical separation method used in the mineral processing industry. The process relies on separating material based on its affinity to air (hydrophobicity). In most mined ores there are valuable minerals that are naturally floating together with unwanted gangue minerals. The degree to which the valuables and/or gangue is naturally floating will depend on the respective mineralogy of the region from where it is mined.

To increase the flotation response and separation efficiency of mined ores, reagents are used to adjust the pulp chemistry. Some of the commonly used reagents are:

- Collector to induce hydrophobicity in valuable minerals,
- Depressant to induce hydrophilic behaviour in naturally floating unwanted gangue minerals,
- Promoters/Activators to achieve increased collector interaction with certain minerals, and
- Frother to prevent bubble coalescence and provide favourable froth conditions.

The flotation cell is usually divided into two distinct phases, namely: pulp and froth phase. The pulp phase is where minerals selectively adhere to air bubbles and the froth phase takes the material provided from the pulp phase, further separation occurs, and then transfers it into the concentrate launder. A graphical representation of this process is given in Figure 2.

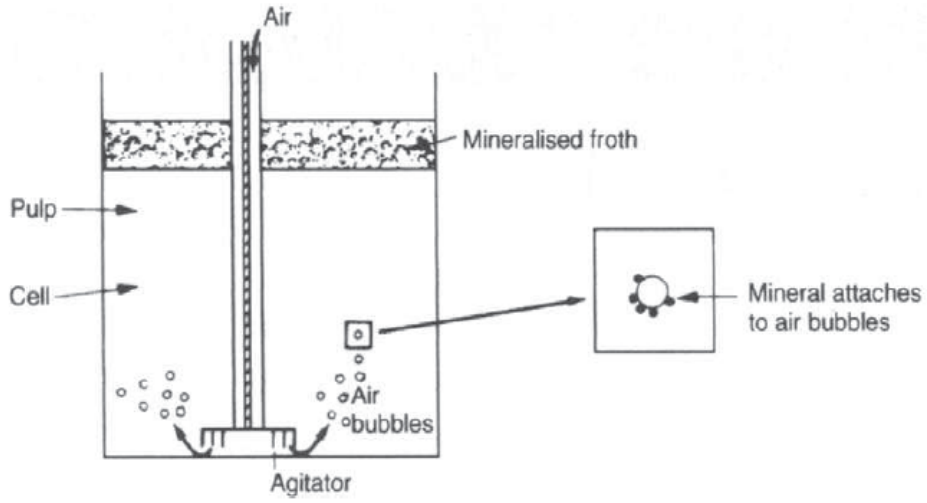

Figure 2: Graphical representation of flotation process (Wills & Napier-Munn, 2006)

2.1.2. FROTH STABILITY

Froth stability is defined as the time of persistence of the froth and is affected by numerous factors, such as drainage of the liquid in the lamellae, viscosity at the bubble surface and the thickness of the electrical double layer (Aktas, et al., 2008). Foam stability in an isolated system (isolated system is defined as a foam system not influenced by thermal and/or mechanical factors) is defined by Beneventi, et al., (2001) as the foam's resistance to gravitational drainage, drainage by capillary forces (caused by regions with different radii of curvature) and gas diffusion through liquid films (caused by pressure differences between bubbles). A more stable foam/froth is expected to be more resistant to coalescence and bursting events, to have on average a smaller bubble size and to carry more water (Farrokhpay, 2011).

This section will aim to give a brief background to the importance of froth stability, the measurements currently used, and the considerations and limitations of the measurements.

2.1.2.1. IMPORTANCE OF FROTH STABILITY

The froth phase has been identified as one of the most important components of the flotation process and defines both the final product quality as well as recovery (Ata, 2012).

Froth Stability and Valuable Mineral Recovery

Figure 3 displays experimental data for overall copper recovery as a function of froth recovery for two different flotation feed streams. The experiments were performed on a pilot scale 3 m^3 RCS^{TM} flotation cell and froth recovery values were calculated from the mass of copper measured over the cell lip compared to the mass of copper reporting from the pulp phase to the froth phase measured by using the device described by Seaman, et al., (2004).

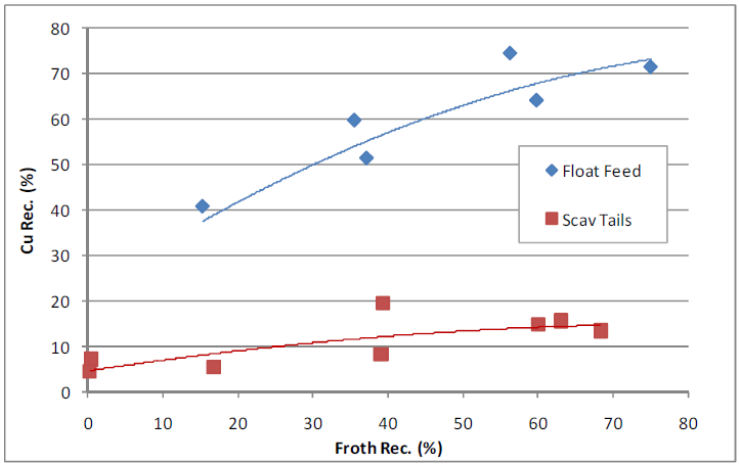

Figure 3: Overall copper recovery as a function of froth recovery for two different feed materials (Crosbie, et al., 2009)

The trend seen in the data of Figure 3 simply states that overall cell performance is closely linked to the froth performance. Froth performance is affected by numerous parameters; of which froth stability or persistence of the froth will definitely be paramount. Unfortunately, the experiments conducted by Crosbie, et al., (2009) did not measure froth stability explicitly and therefore experimental studies where this was done will reinforce the statement made above.

Figure 4 displays overall recovery for various valuable elements as a function of measured froth stability. A linear trend line is used to judge the dependence of recovery on froth stability and therefore it is not suggested that this function should be linear. A strong dependence between recovery and measured froth stability can be seen for all the elements displayed and therefore it can be concluded that froth stability does heavily affect the froth performance which in turn heavily affects the overall performance

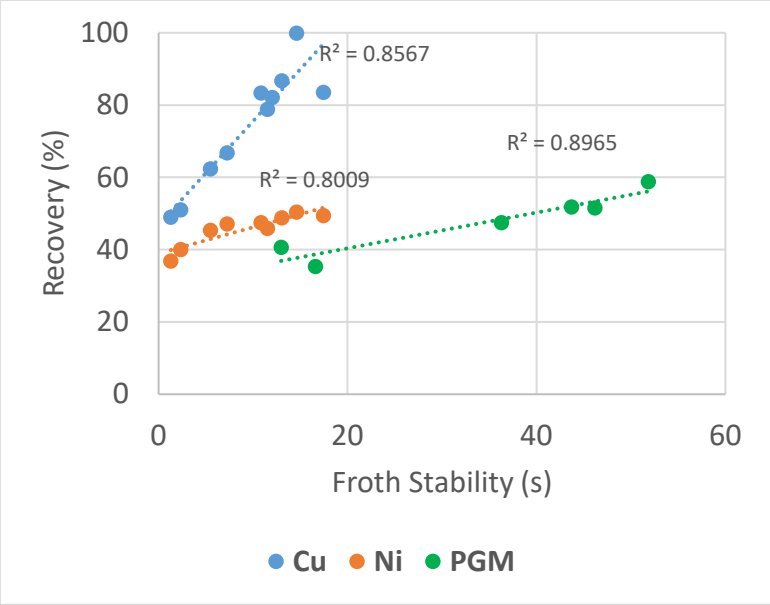

Figure 4: Measured valuable mineral recovery as a function of the measured froth stability for the specific experiments (Achaye, et al., 2015; Hu & Mokgosi, 2014)

Froth Stability and Final Product Grade

The water recovery during a laboratory batch flotation test has long been used as a proxy for froth stability in the absence of dynamic and/or static measurements (Wiese, et al., 2010; Wiese, et al., 2011; Wiese & Harris, 2012).

Figure 5 displays data that was drawn from two independent studies and shows that with increasing dynamic froth stability an increase in water recovery is seen.

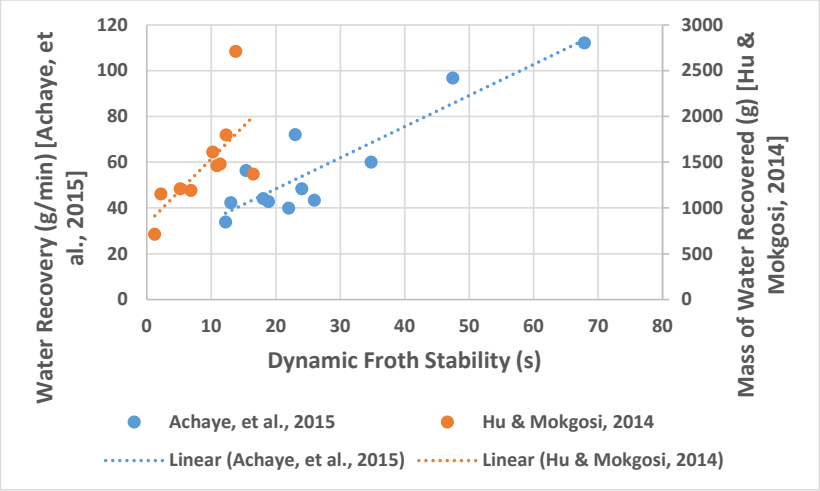

Figure 5: Water recovery as a function of measured dynamic froth stability (Achaye, et al., 2015; Hu & Mokgosi, 2014)

Figure 5 further emphasises the point of view that was initially expressed, i.e. water recovery is closely linked to froth stability and therefore can be used as a proxy measurement. A study by Banford, et al., (1998) performed on coal flotation also found that the coal recovery and grade are heavily dependent on the water recovery of the system. It was proposed that the relationship between water recovery and froth stability is due to the fact that water drainage relies on processes, such as bubble coalescence and bursting, which also defines the froth stability (Banford, et al., 1998).

The relationship between water recovery and entrainment of gangue material is well established in literature (Neethling & Cilliers, 2002; Wang, et al., 2015; Wiese, et al., 2010; Zheng, et al., 2006). Entrainment usually follows water recovery and therefore higher water recoveries will lead to higher recovery of gangue by entrainment.

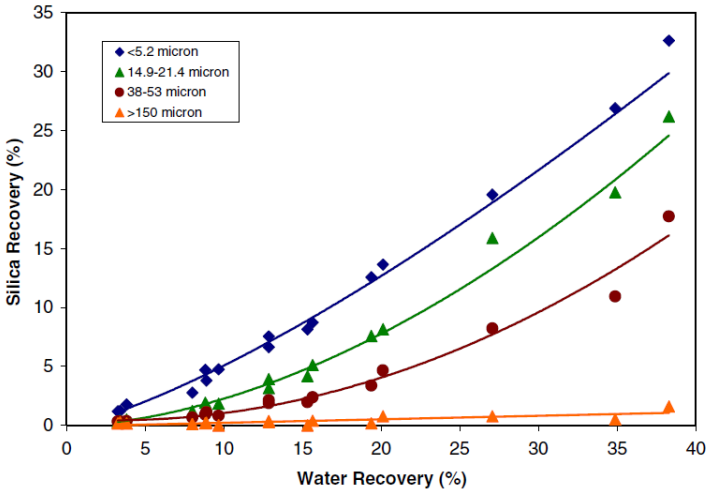

Figure 6: Overall silica recovery as a function of water recovery and particle size (Zheng, et al., 2006)

Figure 6 shows that the recovery of hydrophilic silica, which cannot be recovered by true flotation and thus is recovered due to entrainment, increases with an increase in the water recovery. Moreover, Figure 6 also shows that this effect is most pronounced at very small silica particle sizes and decreases with size since entrainment of large particles is less likely.

From this it can be said that more water recovery will lead to more unselective recovery of gangue by entrainment and thus decrease the grade of the concentrate produced (Wang, et al., 2015). A close relationship between froth stability and water recovery has also been highlighted. Hence, froth stability plays an important role in the grade achieved and a very stable froth, although beneficial for froth recovery, may not be desirable because of lower grades.

2.1.2.2. MEASURING FROTH STABILITY

Numerous methods have been used to quantify froth stability, these include but are not limited to (Farrokhpay, 2011):

- Static stability measurements (froth half-life and equilibrium height),
- Bubble growth across the froth phase,
- Air recovery and solid loading at the top of the froth,
- Froth velocity and rise velocity,
- Image processing focussing on bubble size and colour variations,
- Water recovery,
- Dynamic stability measurements (average bubble life-time, froth growth rate, and equilibrium height), and
- Froth retention/residence time.

A review paper on the subject of froths in flotation by Farrokhpay (2011) goes into detail on some of these methods and supplies the reader with a large number of references to the original papers. The majority of literature is however focussed on two methods which are commonly used, namely dynamic and static froth stability (Barbian, et al., 2003). This section will go into more detail regarding the aforementioned methods.

Dynamic Froth Stability

Bikerman (1973) proposed that the ratio of steady state foam volume to the air input is an indication of the foaminess of foams. In the Bikerman test, gas is passed (at varying flow rates, Q) through an open column containing a solution with known concentration of surfactant. As air is introduced foam generation will start and thus the foam height will increase with time up until a point where the rate of foam generation and decay is equal and equilibrium is achieved. The height of the foam at this point is denoted as the equilibrium foam height and is then used to calculate the dynamic foam stability as follows (Barbian, et al., 2003):

$$\Sigma = \frac{V_f}{Q} = \frac{H_{max} * A}{Q}$$ **Equation 1**

Where:

- ∑ is the dynamic foam stability (s),
- H_{max} is the equilibrium foam height (cm),
- A is the cross sectional area of the foam column (cm^2), and
- Q is the volumetric feed flow rate of air (cm^3/s).

In experiments done by Barbian, et al., (2005) the foam height was recorded as a function of time and an exponential model (Equation 2) was fitted to the resulting data.

$$H(t) = H_{max}\left(1 - e^{-\frac{t}{\tau}}\right)$$ **Equation 2**

Where:

- H(t) is the foam height at time t (cm),
- H_{max} is the equilibrium foam height (cm),
- t is time (s), and
- τ is the average bubble life time, a measure of froth stability (s).

Figure 7 displays the typical output from a Bikerman test as well as the exponential model displayed in Equation 2 fitted to the data.

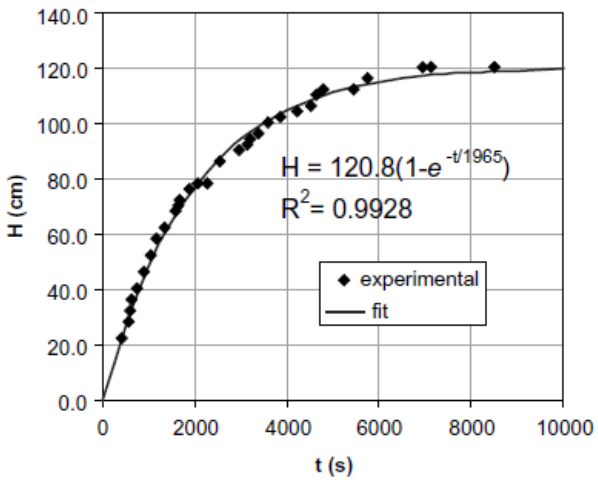

Figure 7: Typical dynamic froth stability test output (Barbian, et al., 2005)

It is well known that measuring dynamic foam stability in two-phase systems can be easily done; however, with the introduction of solids the structure and stability of the froth is significantly influenced (Barbian, et al., 2003). The exponential model allows froth stability measurements to be made without heavily relying on an accurate measure of H_{max} thus increasing the accuracy of Bikerman tests.

Figure 8 shows data collected by Barbian, et al., (2006) on an industrial flotation cell treating PGM ore.

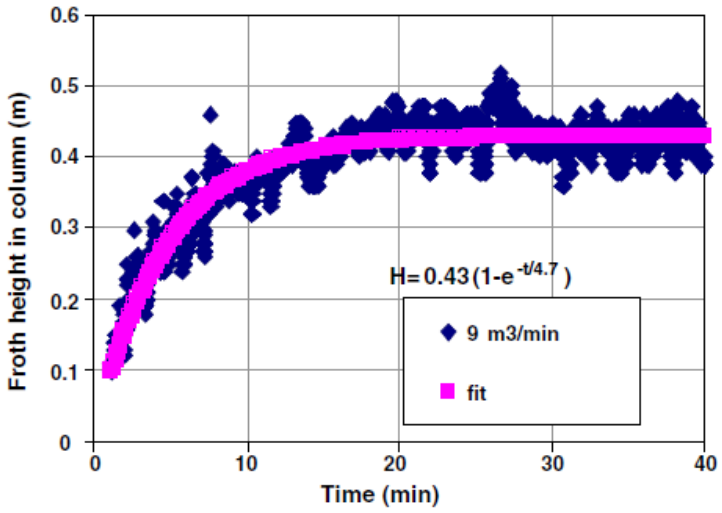

Figure 8: Froth height as a function of time from the second rougher cell in an industrial operation (Barbian, et al., 2006)

As was previously discussed the increased accuracy provided by the methodology is well suited to industrial measurements. Due to the fact that H_{max} is determined by a model fitting procedure it allows for accurate measurements even when there is significant variation in the experimental H_{max}.

Static Froth Stability

Iglesias, et al., (1995) first proposed a decay method for determining foam stability where the time taken for the foam to collapse to one-half of the initial height is determined. This method entails the same experimental setup as the aforementioned Bikerman method. An open column is used to generate foam until the characteristic equilibrium height is achieved, after which air supply is discontinued and the foam height with time is recorded as the foam colapses. It is thought that the static method would give a more accurate representation of the foam stability as opposed to the combined effect of stability and foamability which is determined in the dynamic test (Iglesias, et al., 1995). A mathematical representation of the method is given in Equation 3.

$$\frac{H_{foam}}{H_{foam,max}} = \frac{1}{2} - \alpha * ln\left(\frac{t}{t_{1/2}}\right) \qquad \textbf{Equation 3}$$

Where:

- H_{foam} is the foam height at time t (cm),
- $H_{foam,\,max}$ is the equilibrium foam height (cm),
- α is a dimensionless empirical constant (usually between 0.3 and 0.4),

- t is time (s), and
- $t_{1/2}$ is the foam half-life (s).

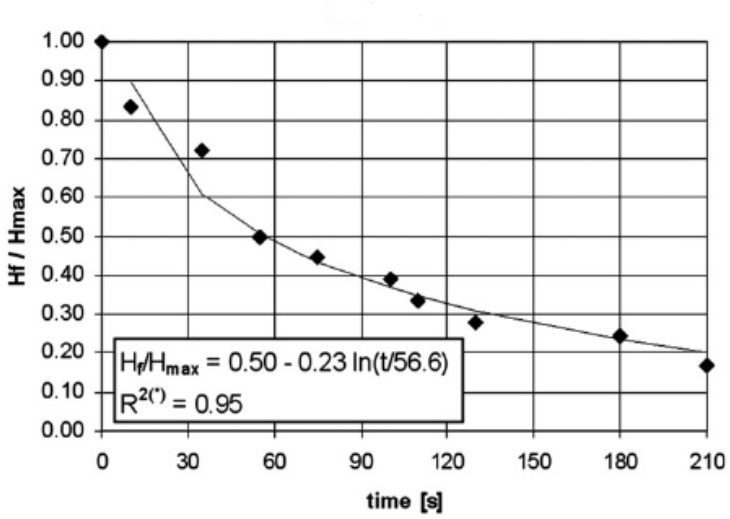

Figure 9: Froth decay as a function of time from an industrial flotation cell (Zanin, et al., 2009)

Figure 9 displays the froth decay data collected form an industrial flotation cell and a rather good fit of Equation 3 was achieved. This serves to prove that this method can also be used on a mineralised froth and several studies have applied this technique to characterise froth stability (Tsatouhas, et al., 2006; Zanin, et al., 2009).

Limitations and Considerations

When comparing the methods, dynamic and static, from a practical point of view the following can be said:

- The dynamic method gives a better fit which stems from the fast collapse of froths in the static regime which subsequently complicates data acquisition, and
- The application of the dynamic method is easier on an industrial scale as the static method involves discontinuing the air flow.

When interrogating the dynamic method the argument can be made that achieving equilibrium would be near impossible due to the non-overflow column that is employed. Following this train of thought, achieving an equilibrium height will be difficult as fluctuation in the height will occur due to the froth continuous loading with solids which then collapses from weight and then starts to load again. However, this effect is countered by the use of the exponential model for which an accurate experimental equilibrium height is not required, but rather model-fitted. Also, in the dynamic experiment two competing effects are present, i.e. froth collapse, a true measure of bubble stability and froth generation, which is related to foamability of the solution (Iglesias, et al., 1995). Iglesias, et al., 1995, argued that the combination of these two effects in the dynamic method make the static method a more accurate

measure of a froth's stability. A counter argument to this would be the fact that the dynamic method more closely simulates what is occurring in an actual flotation froth, i.e. air sparged continuously and froth starts to growth from the bottom upward while liquid drains downward (Farrokhpay, 2011).

Both methods have been widely used in laboratory and industrial studies (Aktas, et al., 2008; Barbian, et al., 2006; Barbian, et al., 2003; Tsatouhas, et al., 2006; Zanin, et al., 2009). Therefore, currently the choice between which method is used is mainly based on practical considerations. That being said, both these methods suffer from a similar fundamental problem. The underlying mechanisms are the same for both methods; however, the froth phase constrained in the stability column will differ significantly from the froth phase which is freely moving towards the overflow weir (Farrokhpay, 2011). Thus, it can be concluded that both methods will give different froth stabilities to the true condition (Farrokhpay, 2011).

2.1.3. FOAM/FROTH STRUCTURE AND MECHANICS

2.1.3.1. FOAM STRUCTURE

The following key structural elements can be highlighted for aqueous foams (Weaire, et al., 2005):

- Bubbles which are pressed together to form the foam are separated by films or lamellae,
- Bubble films meet in a line or curve where an interstitial channel called a Plateau border is formed, and
- Several Plateau borders meet up to form nodes or vertices.

The complex structure is best illustrated by pictures and graphical representations. Figure 10 illustrates the aforementioned structures individually as well as identifying these structures in a real foam. Figure 11 shows a very detailed photograph of a foam where the complex structure is clearly visible.

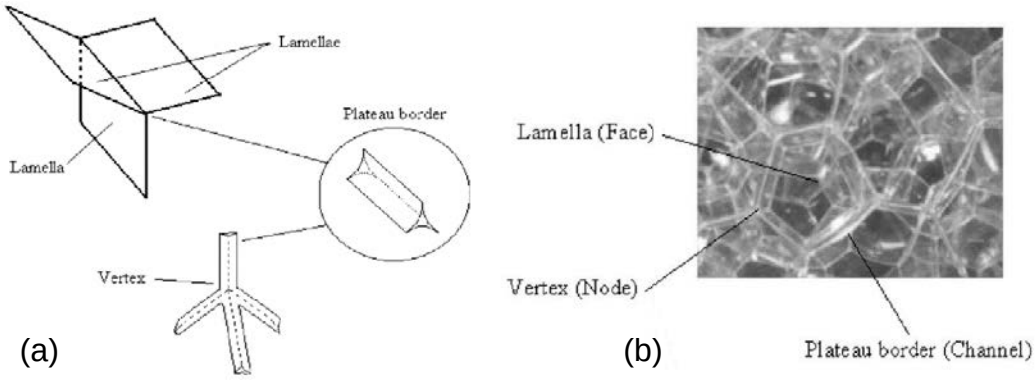

Figure 10: Illustration of structures occurring in an aqueous foam, (a) showing a graphical representation of lamella, plateau border and vertex structures,

and (b) identifying these structures in a real aqueous foam (Ventura-Medina & Cilliers, 2002)

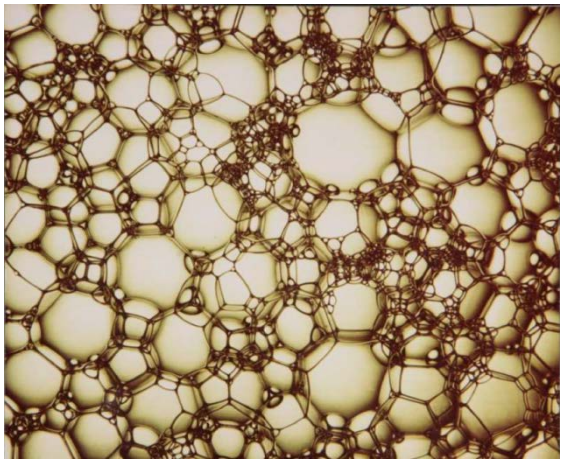

Figure 11: The structure of an aqueous foam (Weaire, et al., 2005)

This structure was first recorded in 1873 by the blind Belgian physicist Joseph Plateau who stated that certain rules must be satisfied (called Plateau`s rules) for a dry foam in equilibrium (Weaire, et al., 2005; Teixeira & Fortes, 2007):

- Only three films may meet at a Plateau border at equal angles of 120°, and
- Only four Plateau borders may meet at a node at equal angles of $\cos^{-1}(-1/3)$.

2.1.3.2. PROCESSES OCCURRING WITHIN A FOAM

This paragraph will serve as a brief introduction into the processes occurring within a 2-phase aqueous foam. Aqueous foams are made up of numerous bubbles pressed together; in turn the bubbles are made of a gas phase enclosed by a liquid film. This process can only occur in the presence of a surfactant which lowers the liquid surface tension enough for a bubble to form (Farrokhpay, 2011). A graphical representation of the surfactants` surface active role at the gas-liquid interface is shown in Figure 12.

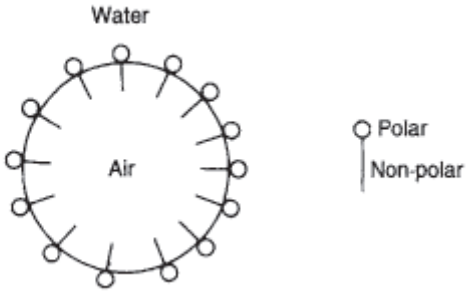

Figure 12: Graphical representation of a bubble clearly illustrating the role of the surfactant at the gas-liquid interface (Wills & Napier-Munn, 2006)

As the bubbles are pressed together in the foam; the films meet in Plateau borders (as discussed in Section 2.1.3.1). The curvature of the Plateau borders causes a capillary

force on the liquid present in the bubble films, which then causes the liquid to drain from the bubble films into the Plateau borders. Once the liquid has entered the Plateau border it will drain out of the foam under the force of gravity. The drainage of liquid from foams is a very complex subject and has been the subject of numerous literature studies (Durand, et al., 1999; Kruglyakov, et al., 2008; Koczo & Racz, 1987; Koehler, et al., 2000). In summary, two drainage regimes have been observed, namely: (1) Plateau border dominated flow and (2) node dominated flow. In Plateau border dominated flow all the viscous dissipation occurs along the Plateau border, i.e. the Plateau borders provide a non-slip condition and Poiseuille flow occurs. In node dominated flow all the viscous dissipation occurs in the nodes and plug flow occurs in the Plateau borders.

While the liquid is draining from the foam film thinning continues to occur due to capillary forces until a sufficiently thin bubble film is obtained (Wang, 2015). After this is achieved surface forces usually take over in the form of the disjoining pressure (Derjaguin & Landau, 1941; Verwey & Overbeek, 1948). In summary, the disjoining pressure consists of an attractive force and a repulsive force and the balance between these forces determines whether bubble coalescence will occur.

Coalescence, however, is not the only mechanism responsible for bubble growth. Foam coarsening or Ostwald ripening is the diffusion of gas from small bubbles (high capillary pressure) to large bubbles (small capillary pressure), i.e. large bubbles increase in size at the expense of small bubbles decreasing in size (Kostoglou, et al., 2015). That being said, Ventura-Medina & Cilliers (2002) noted that foam coarsening occurs over a substantially longer time frame than coalescence and therefore coalescence will dominate in a flotation froth.

2.1.3.3. FROTH STRUCTURE

Froth usually refers to a structure consisting of 3-phases, e.g. gas, liquid and solids. The structure (Section 2.1.3.1) and processes (Section 2.1.3.2) occurring within a froth are essentially similar to those of a 2-phase foam. Nonetheless, the addition of solids has dramatic effects on the bubble film stability and drainage (Johansson & Pugh, 1992).

Research on the effect of particles on foams and emulsions has been very prominent in literature. Two theories of how particles stabilise foams have found traction within the field. The first is the particle detachment energy theory. This states that the more energy required to remove a particle from its equilibrium position into the bulk liquid, the more stable is the froth. The second theory states that particle packing, size and contact angle will affect the maximum capillary pressure required for coalescence (Hunter, et al., 2008; Kaptay, 2006). That being said, the effect of solids can be intuitively thought of as the retardation of film thinning and coalescence, and the viscous dissipation of the slurry within the Plateau border and node network.

Figure 13 indicates possible particle arrangements between two liquid films. The issue of retarding film thinning will be addressed later and this figure serves as a visual aid to the reader.

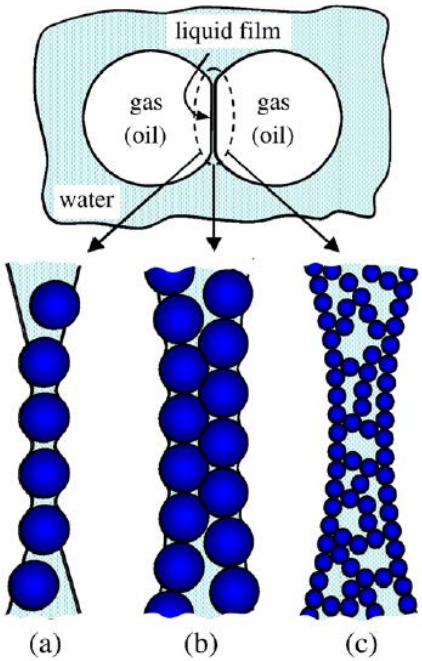

Figure 13: Possible particle arrangements between two liquid films: (a) monolayer of bridging particles, (b) a bilayer of closely packed particles and (c) a network of particle aggregates (Horozov, 2008)

From Figure 13 the decrease in coalescence events due to the addition of particles can clearly be seen as the particles, even in a monolayer, act as a barrier between the two films (Hunter, et al., 2008). However, particle hydrophobicity, roughness and shape could lead to foam destabilisation in some cases (Johansson & Pugh, 1992). Another scenario that can be thought of intuitively from Figure 13 is the fact that the fluid and detached particles present in the Plateau borders will drain slower due to increase in viscosity and the viscous dissipation at the Plateau border interface (Kumagai, et al., 1991).

In Section 2.1.3.2 film thinning was discussed and it was mentioned that the rate of film drainage was heavily dependent on Plateau border curvature. Thus the flow rate would be proportional to the pressure difference between the film and Plateau border (Kumagai, et al., 1991):

$$\Delta \mathbf{P} = \boldsymbol{P_{film}} - \boldsymbol{P_{PB}} \qquad \textbf{Equation 4}$$

Figure 14 shows a comparison between films and Plateau borders with and without hydrophobic particles attached.

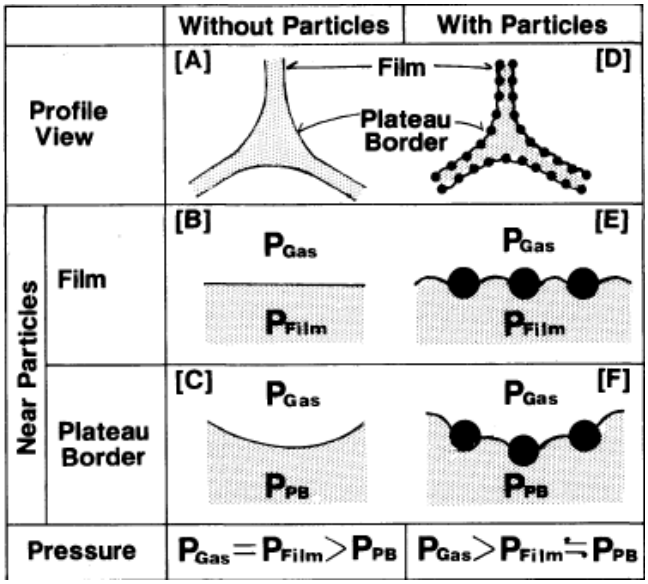

Figure 14: Effect of hydrophobic particles on the pressure difference between bubble films and Plateau borders

The addition of hydrophobic particles modifies the gas-film and gas-Plateau border curvature. This causes a minimisation in film thinning rate as well as the fact that the hydrophobic particles would resist liquid flow (Kumagai, et al., 1991). The result is a film that drains less readily resulting in a more stable foam.

In summary, numerous particle stabilisation mechanisms can be found in literature which goes together with data sets that support the stabilisation effect. A comprehensive data set by Achaye, et al., (2015) shows that smaller particles of similar hydrophobicities stabilise the froth and this is consistent with the mechanisms discussed above. Nonetheless, there are also data sets that show a destabilisation effect. It is thought this is mainly due to hydrophobicity, particle roughness and shape effects (Johansson & Pugh, 1992).

2.1.4. SCALE-UP PARAMETERS

2.1.4.1. COLUMN DIAMETER

Review of Studies in Foam/Froth Literature

Literature on column diameter is limited within foam literature. In addition, these studies are often very fundamental and therefore can be prone to depart from a realistic flotation froth. Table 1 highlights the specifics of all the articles found within literature that dealt with column diameter. The McFadzean (2013) data set presented in Section 1.2 will be referred to during this discussion and it should be noted that this data set has yet to be published and was generated by the Centre for Minerals Research.

Table 1: Detailed description of studies where column diameter was investigated

Author Name	Foam Generation Method	Average Bubble Size	Surfactant	Measuring Technique	Column Sizes
Ambulgekar, et al., 2004.	In-situ, sparger	1 – 3 mm	SLS	Micro-manometer, foam weighing	25.4, 32 and 75 mm
Brannigan & De Alcantara Bonfim, 2001.	In-situ, sparger	Not mentioned	Dawn soap	Visual observations and timing of front velocity	18, 25 and 37.5 mm
Papara, et al., 2009	External foam whipping	90% passing 250 – 500 µm	Protein based	Global volumetric estimations. Electrical resistance	40, 70 and converging (150mm top to 80mm bottom)

Numerous authors in literature have noted a relationship between foam drainage and stability (Koehler, et al., 2000; Kostoglou, et al., 2015; Kruglyakov, et al., 2008). Therefore, it can be assumed that the dependence of stability on column diameter stems from different drainage kinetics within the different column diameters. In small diameter columns the wall film and wall Plateau border area may become substantial when compared to the interstitial Plateau border area (Papara, et al., 2009). Wall films and wall Plateau borders could drain up to seven times faster in a Plateau border dominated foam (Papara, et al., 2009). Thus, the increase in the ratio of wall surface area to interstitial Plateau border area in small columns can lead to substantially faster drainage kinetics.

Figure 15 (b) displays the static foam decay as determined by Ambulgekar, et al., 2004. It is interesting to note that the trend represented in this data is very similar to the industrial data of McFadzean, 2013. A decrease in foam column diameter leads to a decrease in apparent froth stability. As mentioned previously this was proposed to be due to different drainage kinetics present in the different column diameters. Figure 15 (a) displays the liquid drainage velocity determined by Ambulgekar, et al., 2004, and it is important to note that this data is in direct agreement with the proposed

hypothesis. That is, as the foam stability decreases with decreasing column diameter. An increase in drainage can be seen with decreasing column diameter.

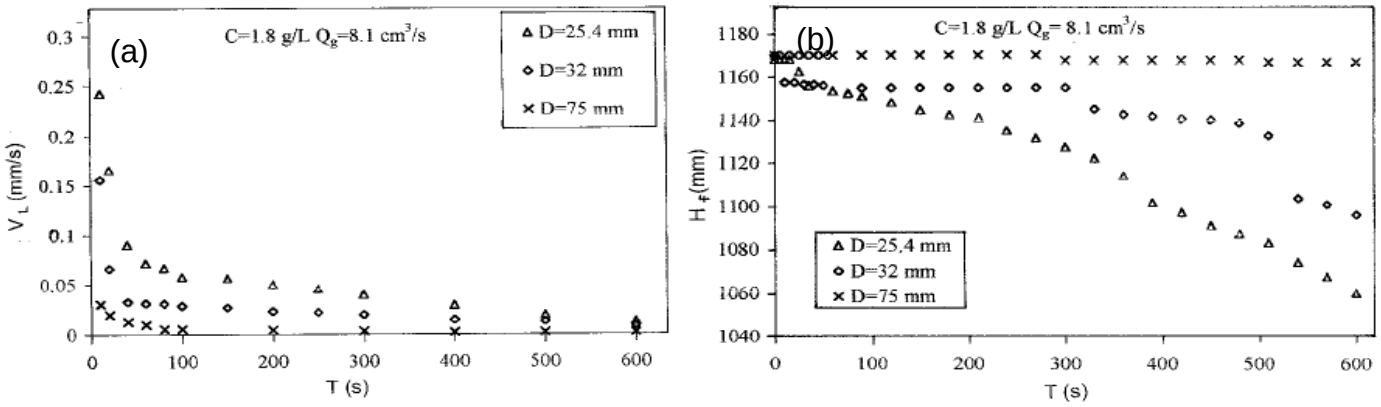

Figure 15: Effect of column diameter as characterised by (a) liquid drainage velocity, and (b) foam collapse rate (Ambulgekar, et al., 2004)

Figure 16 displays global liquid fraction evolution, as determined by still photographs, for different column diameters with hydrophobic and hydrophilic column walls. The formation of a thin liquid film on the wall of the container will always occur even when the wall surface is hydrophobic (Papara, et al., 2009). However, it is expected that this liquid film will be substantially thicker for hydrophilic walls. This, coupled with viscous dissipation occurring in the Plateau borders, can lead to substantial wall effects.

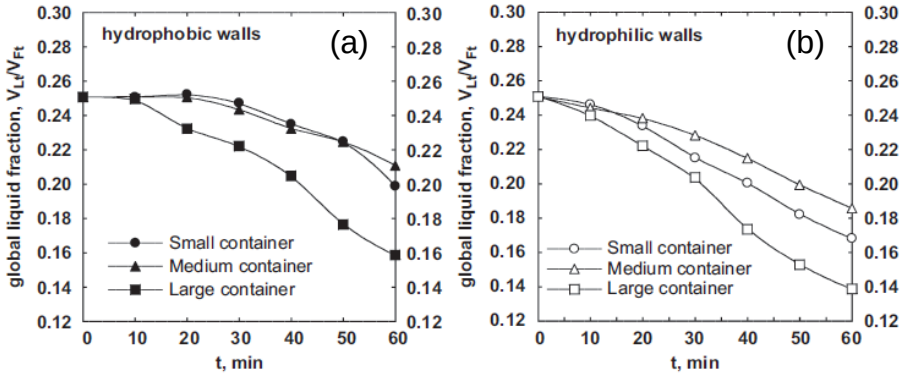

Figure 16: Global liquid fraction (V_{Lt}/V_{Ft}) evolution as determined by volumetric measurements for (a) hydrophobic walls, and (b) hydrophilic walls (Papara, et al., 2009)

This can be seen in Figure 16 as the hydrophilic walls show faster drainage kinetics. The effect of the hydrophilic walls diminishes as the container diameter increases due to the fact that in large containers interstitial Plateau border area far outweighs the wall film or wall Plateau border area (Papara, et al., 2009). Figure 17 shows similar data to that of Figure 16. However, the measurement technique has been changed from volumetric estimation to electrical resistance. The effect of hydrophobic and hydrophilic column walls remains the same: as the diameter increases the difference between the drainage kinetics diminishes.

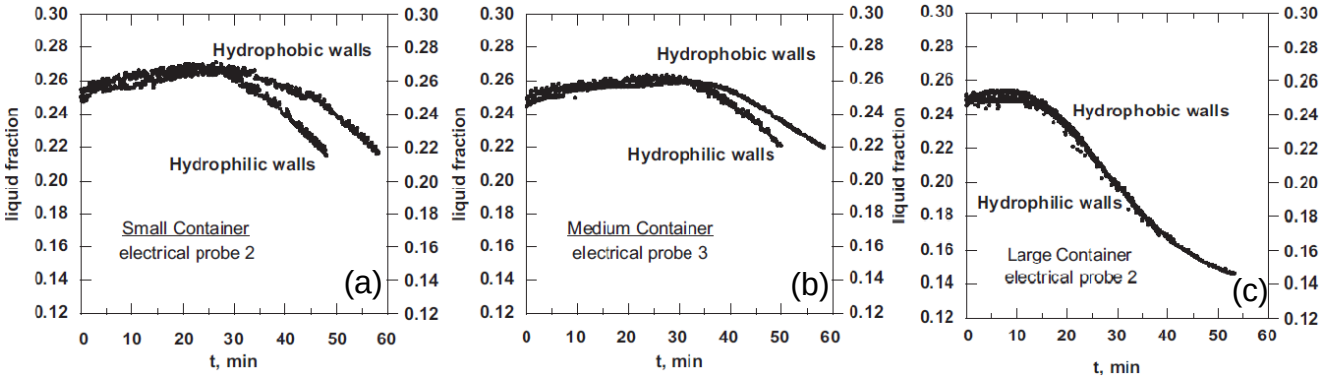

Figure 17: Liquid hold-up evolution at constant electrode position as determined by electrical resistance measurements for (a) small container, (b) medium container, and (c) large container diameter (Papara, et al., 2009)

The important observation from both Figure 16 and Figure 17 is the fact that the trend for column diameter is not the same as shown by Ambulgekar, et al., 2004. Papara, et al., 2009, shows that the largest column has the fastest drainage kinetics followed by the small and then medium column. This trend is the same for two different measurement techniques (Figure 16 and Figure 17) and therefore it is assumed to be due to the true behaviour of the system and not experimental error. On observation of Table 1 a key difference can be put forth; the Papara, et al., 2009, study used external foam whipping which generated a homogenous small bubble size foam. Both the Ambulgekar, et al., 2004, and McFadzean, 2013, data sets used in-situ foam generation which would lead to a heterogeneous bubble size foam. A homogenous foam is often used for the simplifications it provides. Therefore, it can be said the responses of these system may be very different. Nonetheless, the Papara, et al., 2009, data set still provides valuable insight as the differences seen between hydrophobic and hydrophilic column walls proves the effect of the wall can be substantial and suggests that the ratio of wall film area to Plateau border area may be significant.

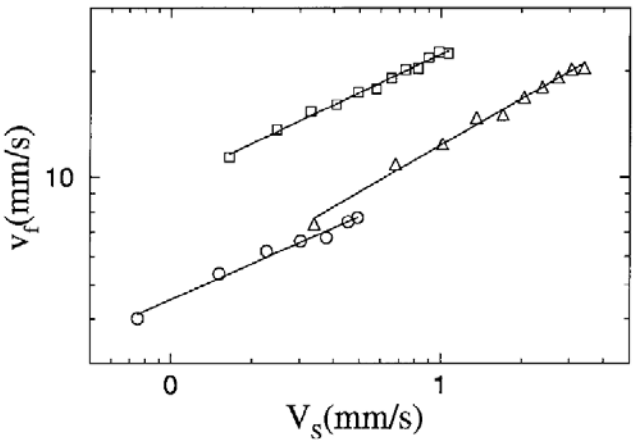

Figure 18: Liquid propagation velocity (v_f) as a function of superficial velocity (V_S), for column diameters of 18.0 mm (Δ), 25.0 mm (□), and 37.5 mm (o) (Brannigan & De Alcantara Bonfim, 2001)

Brannigan & de Alcantara Bonfim (2001) performed forced drainage experiments on a foam generated from a soap solution. Forced drainage experiments involve a stable static foam, which is then fed by varying soap liquid flow rates from the top and the liquid propagation velocity is then measured. Figure 18 shows that the large column had the smallest liquid propagation velocity followed closely by the small and medium column, respectively. Brannigan & de Alcantara Bonfim (2001) then used a correction factor based on column diameter to normalise the data. Figure 19 shows the relatively good correlation obtained from this normalised data. This correlation uses column area and a fitting parameter, σ, which is thought to be a function of bubble size. This is a highly debated statement and Brannigan & de Alcantara Bonfim (2001) stated that there is no proof of this and suggests, based on other work (Koehler, et al., 1999), that it should be a function of column area only.

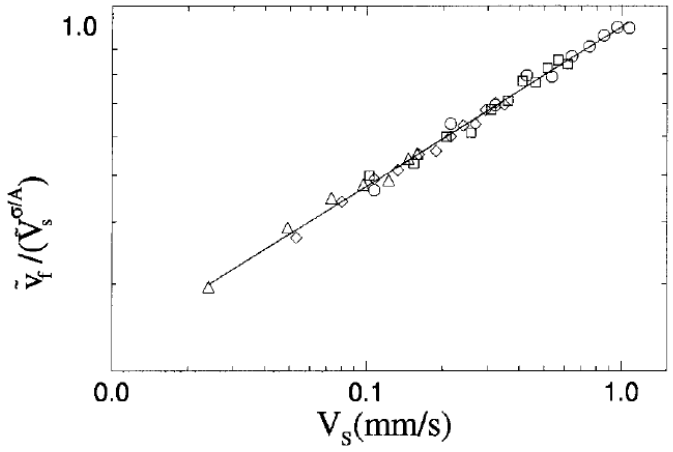

Figure 19: Liquid propagation velocity (v_f) as a function of superficial velocity (V_S), for column diameters of 18.0 mm (Δ), 25.0 mm (□), and 37.5 mm (o) using normalised values (Brannigan & De Alcantara Bonfim, 2001)

Wall Effects in General Literature: Head Loss in a Piping System

The previous section was only focussed on what foam literature had to say regarding the effect of column diameter. However, several other areas within literature also have to account for wall effects. Most notable of these areas would be head loss in a piping system as it has been well researched over the years. The Hagen-Poiseuille Law is very well known in fluid dynamics and is based on research done by G. Hagen (1797-1884) and J. Poiseuille (1799-1869) (Cengel & Cimbala, 2006).

$$\Delta P_{loss} = \frac{32\mu L v_{superficial}}{D^2} \qquad \textbf{Equation 5}$$

Where:

- ΔP_{loss} is the pressure loss (Pa);
- μ is dynamic viscosity (kg/m·s);
- L is the pipe length (m);

- $v_{superficial}$ is the superficial fluid velocity (m/s); and
- D is the pipe diameter (m).

It is important to note from Equation 5 that wall effects are accounted for by the reciprocal of pipe diameter squared, i.e. the area of the pipe. This is very similar to the argument made by Brannigan & de Alcantara Bonfim (2001) in the previous sub-section. However, it should be noted that a fluid flowing in a pipe is a substantially different system to foam/froth rises within a column for the simple reason that bubbles are present. Nonetheless, it certainly seems like the column area will have an impact.

Wall Effects in General Literature: Bubble Column Reactors

Another area within literature where wall effects are important is bubble column reactor scale-up. Bubble columns are widely used as multiphase contactors and/or reactors in the chemical, biochemical and petrochemical industry (Kantarci, et al., 2005). These reactors usually consist of a cylindrical vessel with a gas sparger at the bottom. Gas is sparged into the system where it contacts and/or reacts with a pure liquid phase or a solid-liquid phase (Kantarci, et al., 2005).

The area in literature has specifically been highlighted due to the presence of bubbles within these systems. It can be said that a froth growing in a column is not the same system as bubbles rising through liquid constrained by the column walls; and this is very true. However, both systems experience wall effects in the presence of a 2-phase solution while pipe friction had no bubbles present.

Figure 20 displays an example of the wall effects present within these system; as the column diameter decreases an increase in bubble rise velocity is seen.

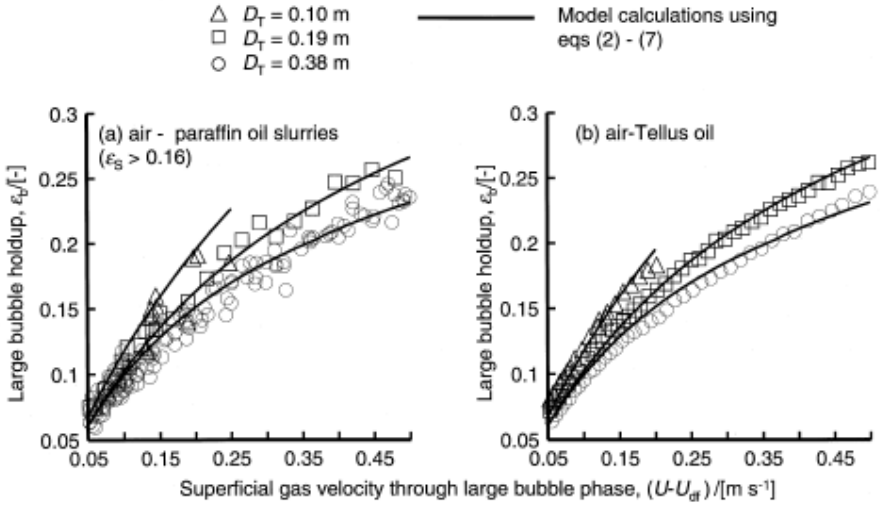

Figure 20: Influence of column diameter on the hold-up of large bubbles in (a) paraffin slurries and (b) Tellus oil (Krishna & S.T., 2000)

Numerous studies have endeavoured to account for the wall effects seen in Figure 20 and this is usually achieved by using some form of bubble size to column diameter. Head loss in a piping system has no bubbles to account for and therefore a straight column area correlation is acceptable. Brannigan & de Alcantara Bonfim (2001) mentioned that a correlation in foam should be based solely on column area which is very similar to head loss. However, this is a debatable statement and observing the bubble column literature it is suggested that a correction factor might be a function of both bubble and column diameter.

2.1.4.2. BUBBLE SIZE

In contrast to the column diameter section, the effect of bubble size on foam stability with special attention to drainage kinetics is well documented in literature (Lemlich, 1978; Kostoglou, et al., 2015; Magrabi, et al., 1999; Koehler, et al., 1999; Saint-Jalmes & Langevin, 2002). Literature agrees with one another that a large bubble foam displays significantly faster drainage kinetics. Figure 21 and Figure 22 display drainage data collected from a forced drainage experiment.

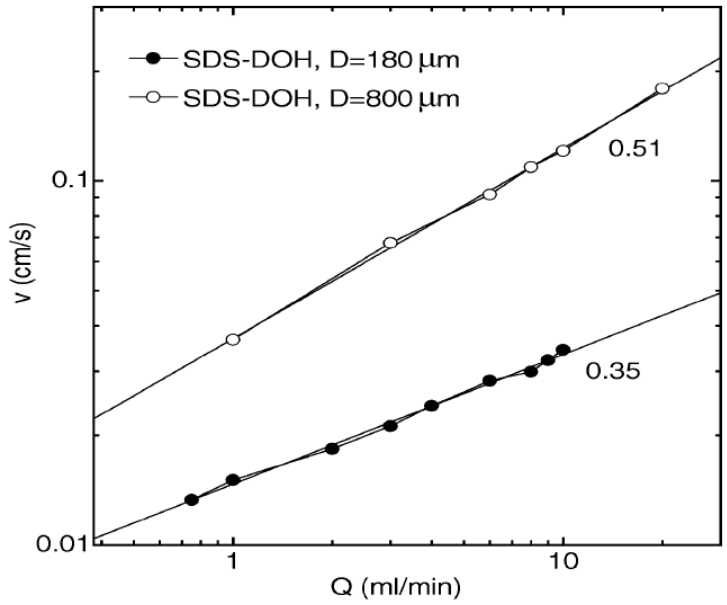

Figure 21: Liquid propagation velocity as a function of applied volumetric liquid flow for two different average foam bubble sizes (Saint-Jalmes & Langevin, 2002)

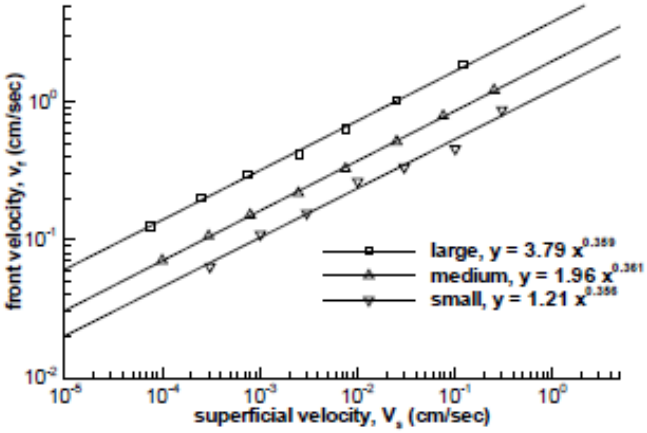

Figure 22: Liquid propagation velocity (front velocity) as a function of applied superficial liquid velocity for three different foam bubble sizes (Koehler, et al., 1999)

Both the data sets show that the liquid propagation velocity, or front velocity, is higher for foams with bigger bubble sizes, i.e. drainage is occurring faster in foams with bigger bubble sizes. So, from the fundamental studies shown it can be said that foams will decrease in stability at larger average foam bubble sizes. This section will discuss three key attributes of large bubbled foams/froths that can explain the behaviour seen throughout literature.

Plateau Border Area

Figure 21 and Figure 22 illustrated the dependence of drainage kinetics on the bubble size. It is proposed that this dependence arises from the fact that Plateau border area is heavily dependent on bubble size and in general foams with larger bubble sizes will have more Plateau border area. The Plateau borders are the interconnected network of “pipes” running through the foam/froth in which most of the water can be found. Therefore, if one increases this area the liquid will drain much faster, just like adding a bigger pipe to a pumping system.

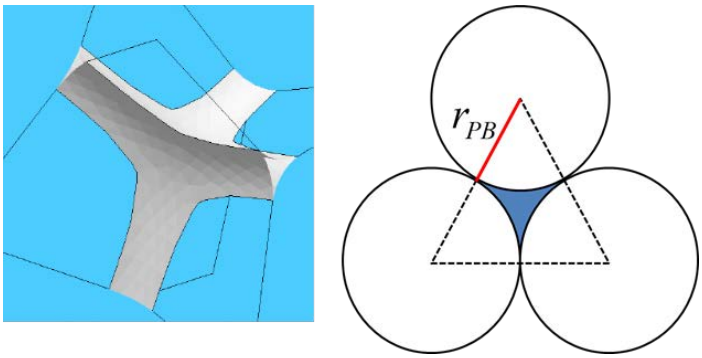

Figure 23: Visual representation of a Plateau border highlighting the radius of curvature

Figure 23 graphically illustrates the Plateau border curvature (r_{PB}). Please note that as it has been drawn in Figure 23 one could easily say that the Plateau border radius of curvature is the same as the bubble radius. The two values are closely linked, but usually are not the same thing especially when the bubbles have a complex structure such as a tetrakaidecahedron. The area of a Plateau border can be expressed by Equation 6.

$$A_{PB} = \left(\sqrt{3} - \frac{\pi}{2}\right) r_{PB}^2 \qquad \textbf{Equation 6}$$

It is not surprising that the area of a Plateau border is heavily dependent on the radius of curvature. However, as just mentioned, radius of curvature and radius of the bubble are not the same thing and therefore it is necessary to find a relationship between radius of curvature and bubble radius before conclusions on the bubble size and Plateau border area can be made.

$$r_{PB}^2 = 3.014(1 - \phi) r_{bubble}^2 \qquad \textbf{Equation 7}$$

Equation 7 displays the dependence of r_{PB} on the liquid hold-up of the foam/froth and the bubble radius (Hilgenfeldt, et al., 2008; Koehler, et al., 2000). Although there is an intimate relationship between bubble radius and liquid hold-up; it can be said that a larger bubble size could lead to a substantially larger Plateau border area.

Bubble Burst Rate and Bubble Size

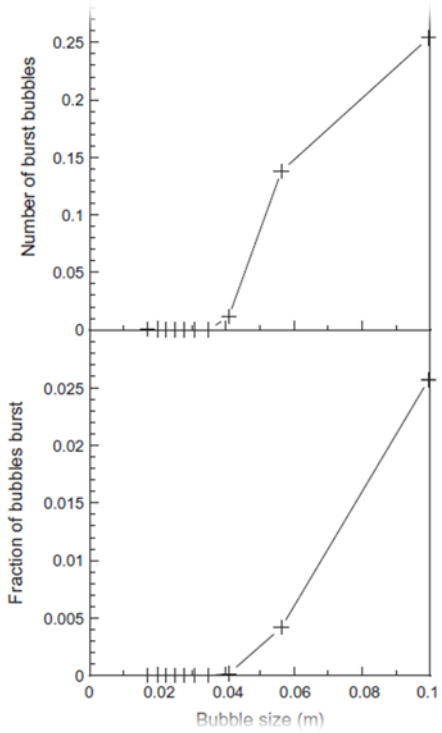

Figure 24: Bubble burst rate as a function of bubble size (Morar, et al., 2012)

Morar, et al., (2012) performed experiments on a copper and PGM pilot plant where image processing was used to determine the bubble burst rate. The experimental data is displayed in Figure 24 and it can be seen that as bubble size increases the number of bursting events captured increases. It is thought that this is caused by numerous competing effects, such as: large bubbles are drier and thus have less water to shield the bubble film and/or a large bubble has more surface area than a corresponding smaller bubble and therefore will experience a large applied force. Nonetheless, a foam/froth with on average more large bubbles will experience more bursting events, i.e. it should be less stable.

Amount of Material Transferred to Foam/Froth

Water is recovered to the froth phase by surfactant and solids attached to the bubble surface. A graphical representation of this is shown in Figure 12 where only surfactant is present; however, solids would have a similar arrangement on the bubble surface. A foam/froth with on average smaller bubbles will have more bubble surface area per volume of foam/froth compared to a large bubbled foam/froth. This increase in bubble surface area will lead to more water being transferred to the froth per volume of froth (Farrokhpay, 2011). This means that a froth with large bubbles will contain less water and therefore the films will be in close contact with one another, water and solids provide a barrier between films, thus making them more susceptible to bursting and/or coalescence.

2.2. GAPS IN LITERATURE REVIEWED

This section will highlight the current gaps within the literature reviewed in Section 2.1. The main objective here would be to clearly illustrate the reason this study was initiated seeing as it is the first of its kind in froth literature. The following key aspects can be highlighted:

1. Although Section 2.1.4.1 has highlighted numerous studies from foam literature where column diameter was investigated, no studies were found that focussed on mineralised froths.
2. All the foam studies referenced in Section 2.1.4.1 found that column diameter will have an effect; however, no real agreement was found between these studies.
3. In Section 2.1.4.2 the bubble size effects from literature were noted. This again follows mostly from 2-phase studies and limited studies have focussed on mineralised froths. Also, no studies have drawn a direct correlation between pulp bubble size and the effect thereof on measured dynamic stability.

From the highlighted points this study will address critical gaps within the literature regarding the practical implications of column diameter and pulp bubble size effects on measured dynamic stability of a mineralised system.

2.3. HYPOTHESES

Hypothesis 1: The measured dynamic froth stability will increase with increasing frothing column diameter. This is mainly due to the ratio of bubbles in contact with the wall compared to the bulk bubbles which decreases with increasing column diameter. This decrease leads to an overall lower drainage rate due to the substantial drainage difference between interstitial and wall Plateau borders, respectively.

Hypothesis 2: The measured dynamic froth stability will decrease with increasing pulp bubble size. This is due to (a) bigger Plateau border area for bigger bubbles leading to increased drainage, (b) big bubbles readily deform and burst, and (c) on average smaller bubble froths carry more water which retards the coalescence process.

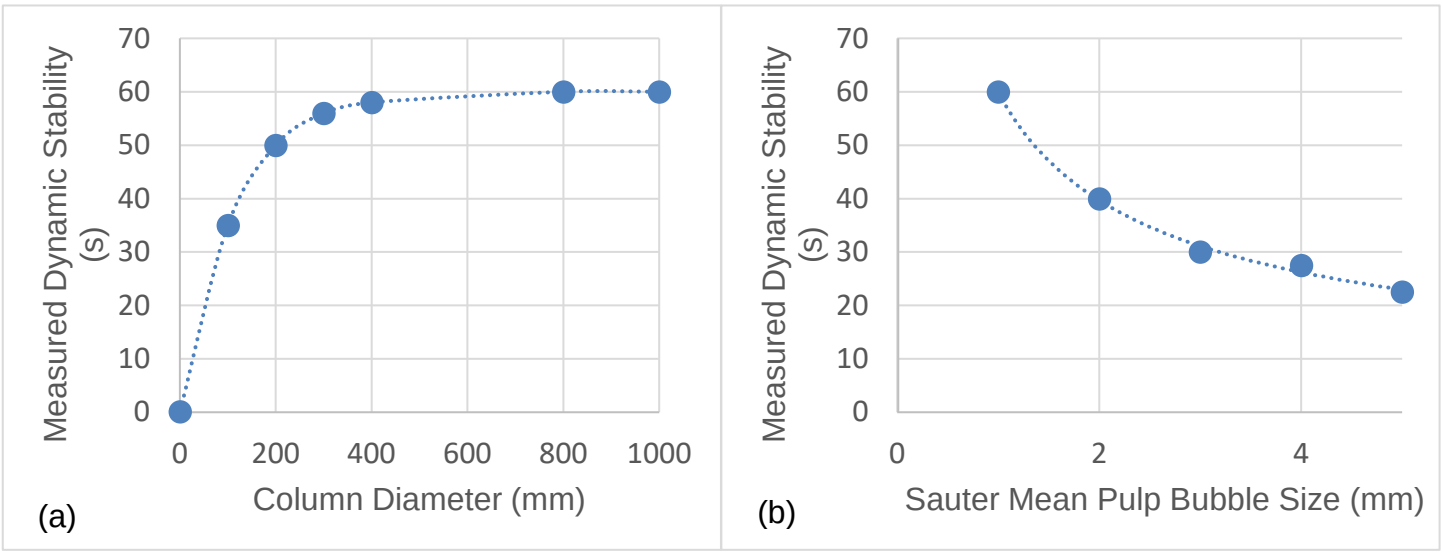

Figure 25: Graphical representation of (a) Hypothesis 1, and (b) Hypothesis 2

2.4. KEY QUESTIONS

This section will identify the key questions that will be answered by this research. It will be divided into three distinct sub-sections, namely: column diameter, bubble size and general.

2.4.1. COLUMN DIAMETER

The following key questions will be addressed by the column diameter experimental study:

- Foam literature has shown that a column diameter effect will be present; however, the overall trend is still unclear. Is there any evidence of this random variance in the data set or does the data follow a logical trend as described by Hypothesis 1?
- The current column diameter range (50 mm, 100 mm, 200 mm and 300 mm) was chosen based without any experimental evidence. Does the current

column diameter range explicitly cover the entirety of the wall effect, i.e. does it measure where the wall effect becomes insignificant?
- The experimental program will provide a unique opportunity as the same plant will be used. Does the froth behaviour change significantly across this time period?
- Is there a mechanistic reason behind using a ratio of bubble size to column diameter to describe the wall effect?
- If so, can an empirical relationship based on this ratio describe the experimental data collected?

2.4.2. BUBBLE SIZE

The following key questions will be addressed by the bubble size experimental study:

- Can the pulp bubble size be changed significantly by using the proposed geometric pore sized glass frits?
- Other than the collection zone efficiency does the air rate used significantly affect the resulting pulp bubble size?
- Can one perform a single characterisation on a specific pore size glass frit and use that as a standard or is a characterisation required on every new glass frit?
- Does the resulting pulp bubble size change due to aging effects of the glass frit?
- No published literature is available that explicitly shows the effect of decreasing pulp bubble size on froth stability. Is there a significant change and does this change follow a logical trend as described by hypothesis 2?
- Is there a constant trend between froth stability and pulp bubble size, even when the ore type is changed?

2.4.3. GENERAL

The following key questions will be addressed in general by this study:

- From the various froth stability experiments performed for this study, is there a list of optimum conditions for a froth stability test?
- Are there any experimental modifications that could provide more reliable experiments?
- Is there a method by which the dynamic froth stability test can be used independent of scale parameters?

CHAPTER THREE: EXPERIMENTAL METHODOLOGY

This study is quite unique with regards to the fact that both laboratory and plant scale experiments were done. The plant scale test work was completed at a PGM operation treating a Platreef ore (as discussed in Table 2). The laboratory scale test work was completed on three different PGM ore types, namely: Platreef, Oxidised PGM reef and a UG-2 reef. Although the ore type was changed, no changes were made to the reagent types used and this will be discussed further in section 3.1.2. Please note, all laboratory experiments used a similar ore preparation and milling technique.

Table 2: General comparison of the PGM ores used

	Platreef (Schouwstra & Kinloch, 2000; Schouwstra, et al., 2013)	Oxidised PGM reef (Becker, et al., 2014)	UG-2 (Jones, 1999)
Bulk Mineralogy	Dominated by pyroxenites, serpentines and calc-silicates. Negligible Chromite.	Dominated by pyroxenites (~34.9 wt%), alteration silicates (~40.4 wt%) and oxide/hydroxides (~11 wt%)	Dominated by Chromite (~ 60-90 wt%). Less silicate minerals pyroxene (~ 5-25 wt%) and plagioclase (~ 1-10 wt%)
BMS	Considerable concentrations of BMS (~ 1.5 wt%)	Lower BMS concentrations (~ 0.2 wt%)	Low BMS concentrations (~ 0.1 wt%)
Alteration Minerals	Moderate amounts of alteration minerals (~ 10-15 wt%)	Very high amount of alteration minerals (~ 40.4 wt%)	Sparse amount of alteration minerals (~ 2.5 wt%)

3.1. MATERIALS AND EQUIPMENT

3.1.1. ORE

As stated in the introduction to this section three different types of PGM ores were used, please refer to Table 2 for more information. For all plant scale experiments there was obviously no ore preparation and/or milling required as this is taken care of naturally by the plant. For all laboratory scale experiments the standard CMR ore preparation and milling procedures were used irrespective of the ore type. This section will highlight the standard ore preparation and milling procedure as well as the milling curves experimentally determined for the different ores.

3.1.1.1. ORE PREPARATION

Figure 26 graphically represents the standard CMR ore preparation methodology.

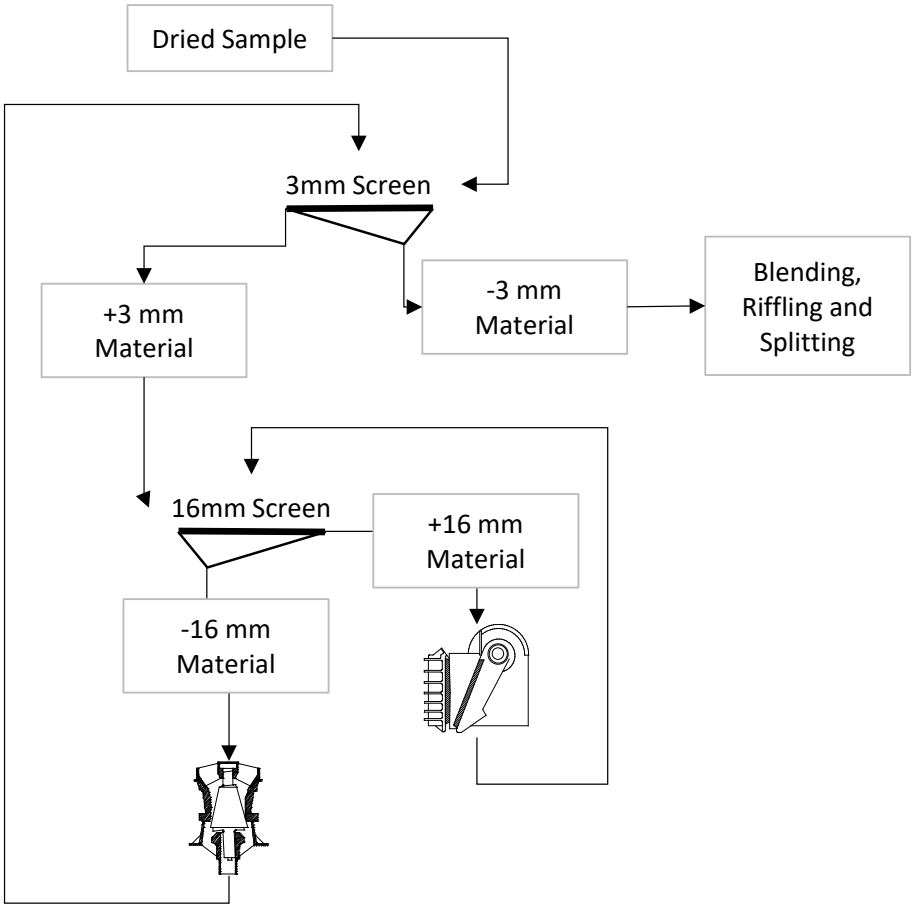

Figure 26: Schematic representation of standard CMR ore preparation procedure

All ore samples received by the CMR, regardless of total weight, undergoes a standard preparation procedure as follows (Figure 26):

- Sample is dried on a drying pan.
- Entire sample is screened over a 3 mm aperture screen; undersize is combined into buckets with lids for storage.
- The oversize from the previous step is screened over a 16 mm aperture screen.
- The oversize from the previous step is combined and then jaw crushed; while the undersize progresses to cone crushing.
- After jaw crushing that fraction of material is screened over a 16 mm screen to ensure that all material is passing 16 mm. All sub 16 mm material progresses to cone crushing while the 16 mm retained fraction is subjected to further jaw crushing until all material is sub 16 mm.
- The material that was originally sub 3 mm is combined with the jaw crushing product after which cone crushing is done. As was the case previously, all sub

3 mm material progresses while the retained material is subjected to cone crushing until 100 % is passing 3 mm.

- The crushed product is now combined with the material that was originally sub 3 mm. To ensure, as far as practically possible, that the entire sample is homogenous it is blended and then riffled.
- After the mixing process has been completed the sample is split using a rotary splitter into representative sample masses, usually 1 kg for milling purposes, which is individually bagged and labelled for further processing.

3.1.1.2. STANDARD MILLING PROCEDURE

The representative 1 kg sub-samples generated by the procedure described in the preceding section will require further size reduction. This is usually achieved by wet rod milling of the sample for a known time to achieve a defined % passing 75 µm. Regardless of the use of the sample (flotation, milling curve, etc.); the experimental equipment as well as the procedure used is always kept constant. Figure 27 shows the 1 kg laboratory scale stainless steel rod mill used for size reduction by milling.

Figure 27: Photograph of the 1 kg laboratory scale stainless steel rod mill

The mill is operated at a constant speed and is loaded with a standard set of 20 stainless steel rods. The standard set of stainless steel rods are usually made up of different diameter rods as follows: 6 x 12 mm, 8 x 16 mm, 6 x 21 mm. The following standard procedure is used:

- Inspect mill shell and rods to ensure it has been thoroughly cleaned to eliminate contamination. Also, ensure that speed setting on mill rollers has not been changed.
- Empty 1 kg sample directly into mill.

- All milling for this study was performed at 67 wt% solids. Therefore, after ore is introduced into the mill, 500 mL of synthetic plant water is added.
- Collector addition for this study was done in the mill. Therefore, if the sample is intended for flotation, a defined amount of collector will be added. Usually the volume of collector is not significant and therefore the amount of synthetic plant water added remains constant regardless if collector added or not.
- The lid of the mill must now be fastened and the mill must be positioned correctly on the rollers. Care should be taken to ensure the lid is fastened correctly before the mill is started.
- The mill can now be started while a stopwatch is used to time the duration. As soon as the total time has passed the mill can be stopped.
- 3 500 mL wash bottles filled with synthetic plant water are used to empty the mill contents into a bucket or the flotation device. All flotation tests were conducted at 33 wt% solids and therefore care should be taken not to use more water than is required.

3.1.1.3. MILLING CURVES

Due to the varying hardness and feed size distribution of the three different PGM ores used it is necessary to determine how long each sample must be milled. It has been shown previously that the % passing 75 µm is linear as a function of milling time. Three samples of each ore will be exposed to milling for a predefined amount of time (Table 3) using the procedure discussed previously. The resulting product was then filtered, dried and screened using a 75 µm aperture screen to determine to amount, as a %, passing 75 µm.

Table 3: Defined milling intervals for milling curve as a function of ore type

	Platreef	UG2	Oxidised PGM Ore
Interval 1	10	5	5
Interval 2	15	15	15
Interval 3	25	25	35

Figure 28 displays the experimental results for the milling characterisation done on all three ores. Please note that the curve for Platreef and UG2 are quite similar which is an interesting observation as it is expected that UG2 will be much softer. That being said, this is probably due to the vastly different feed size distributions as it can be said that the UG2 feed was in general coarser. Nonetheless, the experimental results still follow the expected linear trend and therefore no further investigation is advised. A 50% passing 75 µm value was used for all the laboratory scale experiments - this was chosen as to limit the amount of milling time but still achieve reasonable liberation. Table 4 shows the linear equations used and the milling times required. This was now

the standard milling time for that particular ore for the duration of the experimental program.

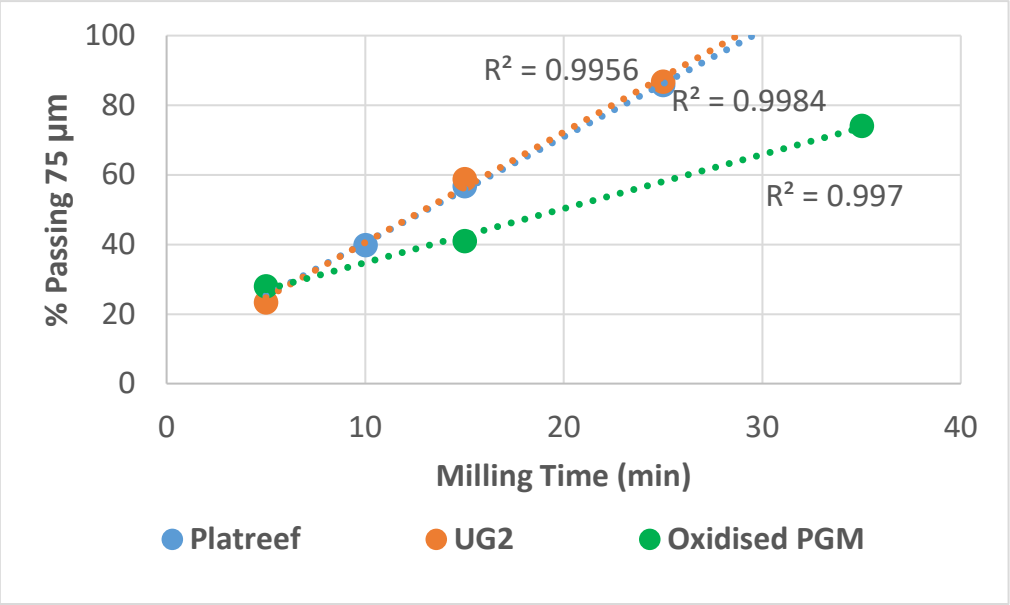

Figure 28: Milling curves for Platreef, UG2 and Oxidised PGM Ores

Table 4: Calculated required milling time for 50 % passing 75 µm

	Equation	Time Required (min)
Platreef	3.04x + 10.08	13.1
UG2	3.17x + 8.83	13.0
Oxidised PGM	1.55x + 19.24	19.8

3.1.2. REAGENTS

3.1.2.1. COLLECTOR

Sodium Isobutyl Xanthate (SIBX), commonly used by PGM operations, was used as a collector for all the laboratory scale experiments. SIBX is a yellow powder and a 1 w/v% solution was prepared by adding 1 g of SIBX powder per 100 mL deionised water. The solution was freshly prepared every three days and was stored in the reagent refrigerator overnight. A dosage of 100 g SIBX per ton of ore, or 10 mL collector solution, was added to each 1 kg sample to be milled. This dosage remained constant throughout the experimental campaign regardless of the ore type.

3.1.2.2. DEPRESSANT

Norilose 6064 is a carboxyl methylcellulose (CMC) depressant supplied by Senmin (Pty) Ltd and was used as the depressant for all the experimental work. Norilose 6064 was supplied in powder form and a 1 w/v% solution was prepared by adding 1 gram Norilose 6064 per 100 mL of deionised water. The solution was freshly prepared every

three days and stored in the reagent refrigerator overnight. Irrespective of the ore type a constant dosage of 100 g Norilose 6064 per ton of ore was used. The depressant was added into the feed tank of the frothing column with a conditioning time of 5 minutes.

3.1.2.3. FROTHER

The frother used for the experimental work was Senfroth 516 and was supplied by Senmin (Pty) Ltd. Senfroth 516 is a frother blend consisting of polyglycol ether and an alcohol; the exact proportions are proprietary. Senfroth 516 is supplied as a pure liquid and therefore no solution preparation was required. A constant dosage of 100 ppm, or 100 µL Senfroth 516 per 1L of synthetic plant water, was maintained throughout the experimental campaign. The dosage was chosen to be above the critical coalescence concentration (CCC) of DowFroth250, another PPG frother, reported by Zhang, et al., (2012).

3.1.2.4. SYNTHETIC PLANT WATER

Synthetic plant water was made by adding certain chemical salts to deionised water. The recipe, displayed in Table 5, is based on a study by Wiese, et al., (2005) and mimics the concentrations of key ions typically found in flotation circuits on industrial plants.

Table 5: Synthetic plant water composition

Chemical compound	Molecular Formula	Mass (g) in 20 L	Concentration (mol/l)
Magnesium sulphate heptahydrate	$MgSO_4.7H_2O$	24.60	0.00250
Magnesium nitrate hexahydrate	$Mg(NO_3)_2.6H_2O$	4.28	0.000417
Calcium nitrate tetrahydrate	$Ca(NO_3)_2.4H_2O$	9.44	0.000999
Calcium chloride dihydrate	$CaCl_2.2H_2O$	5.88	0.00100
Anhydrous sodium chloride	NaCl	14.24	0.00609
Anhydrous sodium carbonate	Na_2CO_3	1.20	0.000283

3.1.3. EQUIPMENT

3.1.3.1. LABORATORY SCALE FROTH STABILITY COLUMN

The principle of the plant and laboratory scale columns is the same, a tube that contains the froths that is transparent so that growth can be tracked, however, the laboratory scale column must include a method for generating bubbles.

Air Feed and Glass Frits

The air feed taps into the main air supply of the laboratory after which it passes through a regulator which decreases the pressure to around 2 bar. The regulated air now passes through an on/off valve and a rotameter before entering the column and passing through the glass frit. The size of the rotameter is usually determined by the size of the column, a 200 mm diameter column requires nearly 25 L/min while a 100 mm diameter column requires 6 L/min for the same superficial gas velocity, but usually varies from 0 to 25 L/min. Figure 29 shows a typical glass frit and it can be seen that it is basically a thin perforated glass disc.

Figure 29: Photograph showing a typical glass frit

The geometric mean pore size of the perforations, coupled with the air rate, will define the bubble size produced by the column. The glass frits are classified in terms of the geometric mean pore size as defined in Table 6.

Table 6: Glass frit properties as supplied by GlassTech (Pty) Ltd

Frit ID	Geometric Mean Pore Size (μm)	Thickness (mm)	Diameter (mm)
POR0	200	5	60
POR1	126		
POR2	63		
POR3	25		
POR4	13		

Columns

The main design consideration of the frothing column is easy tracking of froth growth, therefore the entire column inclusive of the base is made from transparent acrylic. Figure 30 shows a photograph of all three diameter (200, 100 and 50 mm) frothing columns. The standard column has a diameter of 100 mm and has been used in numerous studies to quantify froth stability. However, scale-up behaviour has long

been debated and therefore a 200 mm was designed for the purposes of this study. One major concern with increasing the diameter of the column is the layout of the bubble generating section. This is because the glass frits previously discussed comes in a maximum diameter of 60 mm and therefore as column diameter is increased, larger volume of air is required for the same superficial gas velocity, more than one frit is required. This can clearly be seen from Figure 30 as the 100 and 50 mm columns have one frit while the 200 mm column has four glass frits.

Figure 30: Photo of the 20, 10 and 5 cm frothing columns

Table 7 displays the most important technical data of the three different columns in terms of geometry.

Table 7: Froth column technical data

Column ID	Inside Diameter (mm)	Wall Thickness (mm)	Column Length (m)	Frit #	Frit Area (cm^2)	Column Area (cm^2)	A_{Frit}/A_{Column}
50 mm Column	**46**	**2**	**0.5**	**1**	**19.6**	**19.6**	**1.0**
100 mm Column	**94**	**3**	**1**	**1**	**19.6**	**69.4**	**0.3**
200 mm Column	**194**	**3**	**1**	**4**	**78.5**	**295.6**	**0.3**

Overall Setup

The frothing column requires auxiliary equipment to perform the experiments. The following equipment is required for optimal performance of the frothing column:

- An overhead stirrer within the column to prevent the settling of solids onto and/or into the pores of the glass frits;
- Feed tank and overhead stirrer to keep the bulk feed slurry in solution, and;
- A feed pump to transfer material between the column and the feed tank.

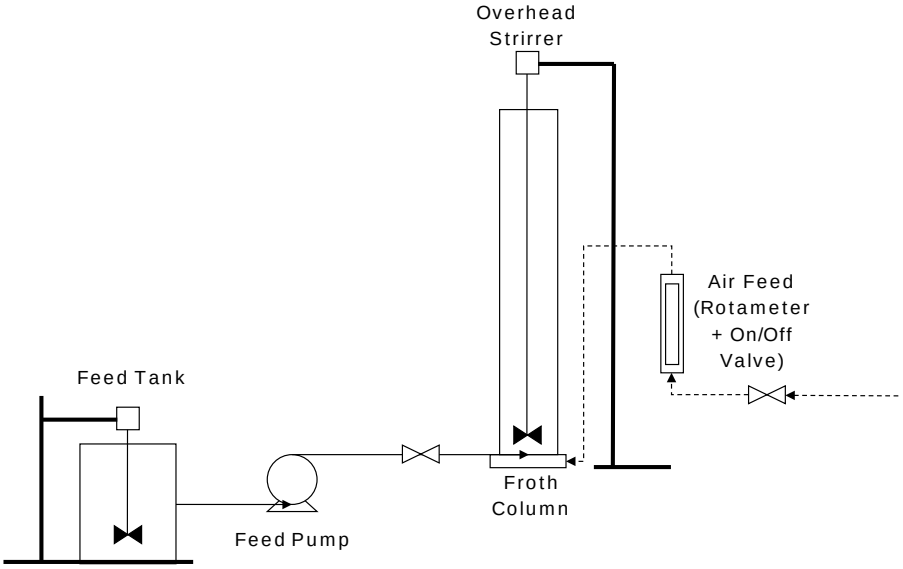

Figure 31: Schematic representation of frothing column setup

Figure 32: Photo showing frothing column and auxiliary equipment for (a) hot-float application on plant, and (b) laboratory setup

3.1.3.2. PLANT SCALE FROTH STABILITY COLUMN

The plant scale column setup is quite simple with regards to equipment because the flotation cell takes care of generating bubbles and particles. This section will highlight the column dimensions and setup used.

Columns

As is the case with the laboratory scale froth columns; the main concern is easy tracking of froth growth. For this reason, the material of construction is fairly similar to the laboratory column, i.e. highly transparent acrylic, however the wall thickness is significantly thicker to make the column more robust. Also, clearly marked heights are required on the side of the column as can be clearly seen from Figure 33. The columns also need to be exceptionally long to enable the correct placement of the column within the pulp phase of the flotation cell.

Figure 33: 200 mm Plant scale froth stability column (Dr McFadzean for scale)

Table 8 highlights the most important dimensions for the frothing columns used. As mentioned previously the column walls are substantially thicker to make the column robust.

Table 8: Plant scale forth stability column dimensions

Column ID	Inside Diameter (mm)	Wall Thickness (mm)	Length (m)	Column Area (cm^2)
50 mm	**40**	**5**	**2**	**12.6**
100 mm	**90**	**5**	**2**	**63.6**
200 mm	**190**	**5**	**2**	**283.5**
300 mm	**290**	**5**	**2**	**660.5**

Setup

The plant scale froth stability column does not require any auxiliary equipment as bubble generation and feed conditioning is taken care of by the flotation cell. Due to the wall thickness used coupled with the length of the column, each column is quite heavy and therefore a device is needed to hold the column in place. This back-board is very simple in design and simply hooks over the handrails above the cell, an example of the setup is shown in Figure 34 and Figure 35.

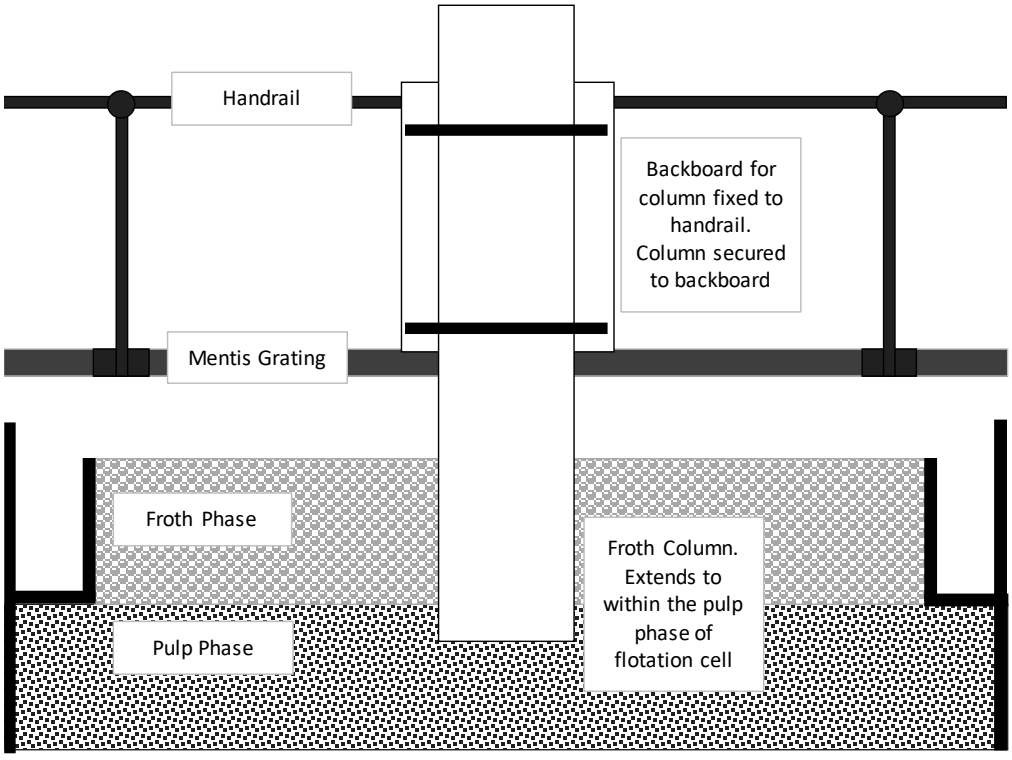

Figure 34: Schematic representing froth column setup used for plant scale experiments

Figure 35: Photos showing the 300 mm plant scale froth column setup in operation

3.1.3.3. ANGLO AMERICAN PLATINUM BUBBLE SIZER (APBS)

Overview

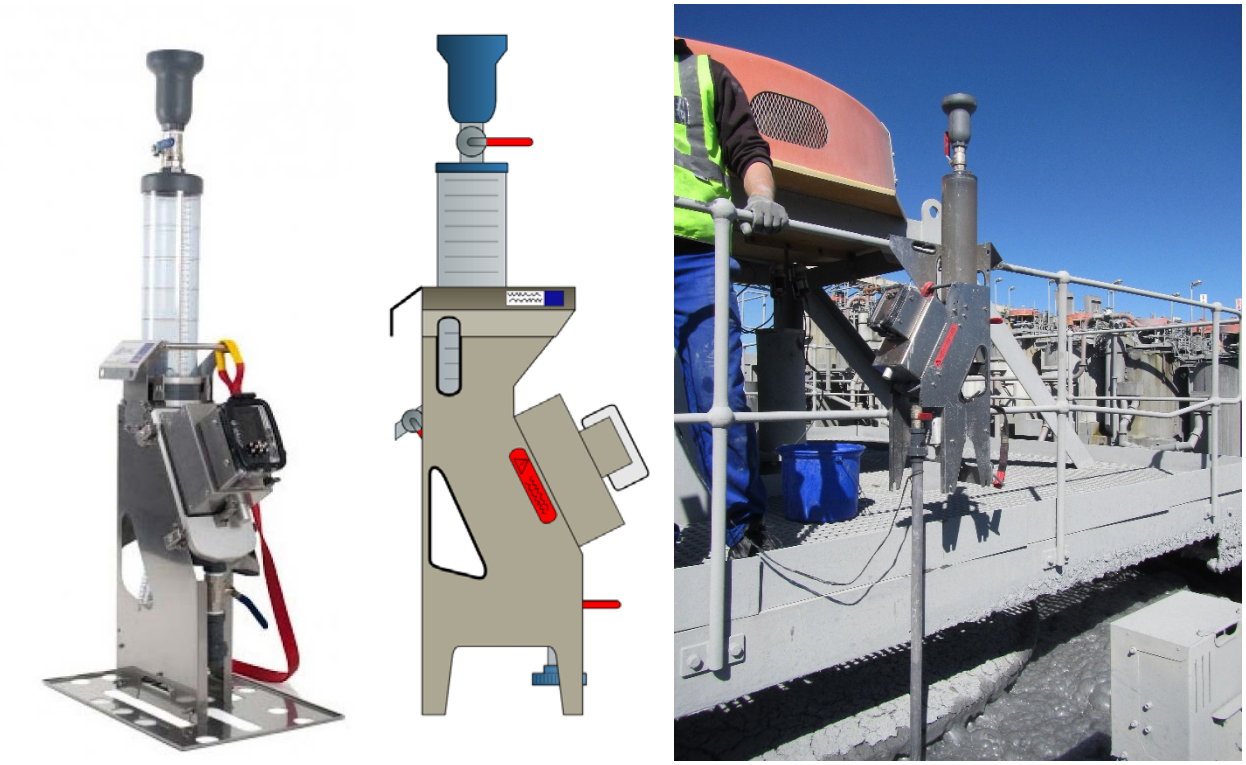

Figure 36: Photos showing the Anglo American Platinum Bubble Sizer unit

The Anglo American Platinum Bubble Sizer (APBS) is the current device used in practice to measure bubble size distributions and superficial gas velocity. The device

was developed for Anglo American Platinum by Stone Three Technology and operates on the same principle as the bubble viewer, however, significant improvements have been made to make it more user-friendly and robust for everyday plant use. The device operates using the following key principles:

- A body of water, closed off to atmosphere by closing certain valves and extending the downpipe to within the pulp phase, is displaced by rising bubbles.
- The rising bubbles are passed through a viewing chamber where the bubbles are photographed and sized using image analysis.
- The superficial gas velocity is measured by the rate at which the water in the water reservoir is displaced by rising bubbles.

A schematic of how these key principles are achieved from a design perspective is displayed in Figure 37.

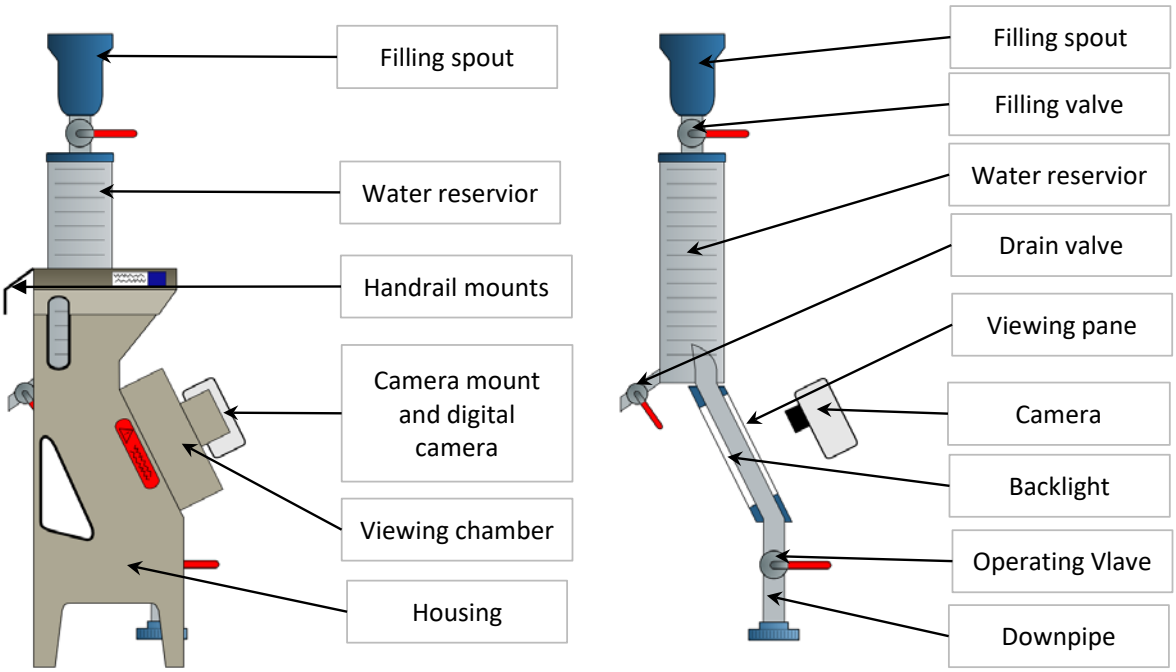

Figure 37: Schematic of APBS assembly with and without housing highlighting key operating points of the assembly

Plant Scale Setup

There are various concerns with measuring superficial gas velocity and bubble size in a flotation cell. For instance, a pressure correction factor is required to correct for the pressure difference between the viewing chamber and the collection point within the pulp phase of the flotation cell. Also, the position of the collection point is of critical concern as Gorain, et al., (1995), has shown that it varies as a function of position within the pulp phase. It has been shown that the global average bubble size distribution occurred halfway between the cell rotor and cell wall (Gorain, et al., 1997).

Taking the above mentioned considerations in account it can be seen that the position of the bubble sizer within the flotation cell crucial. Various measurements must be made of the bubble sizer in the measuring position to ensure the calculation of pressure correction factor; however, this will be discussed later. This section will only show the ideal position of the bubble sizer with the flotation cell.

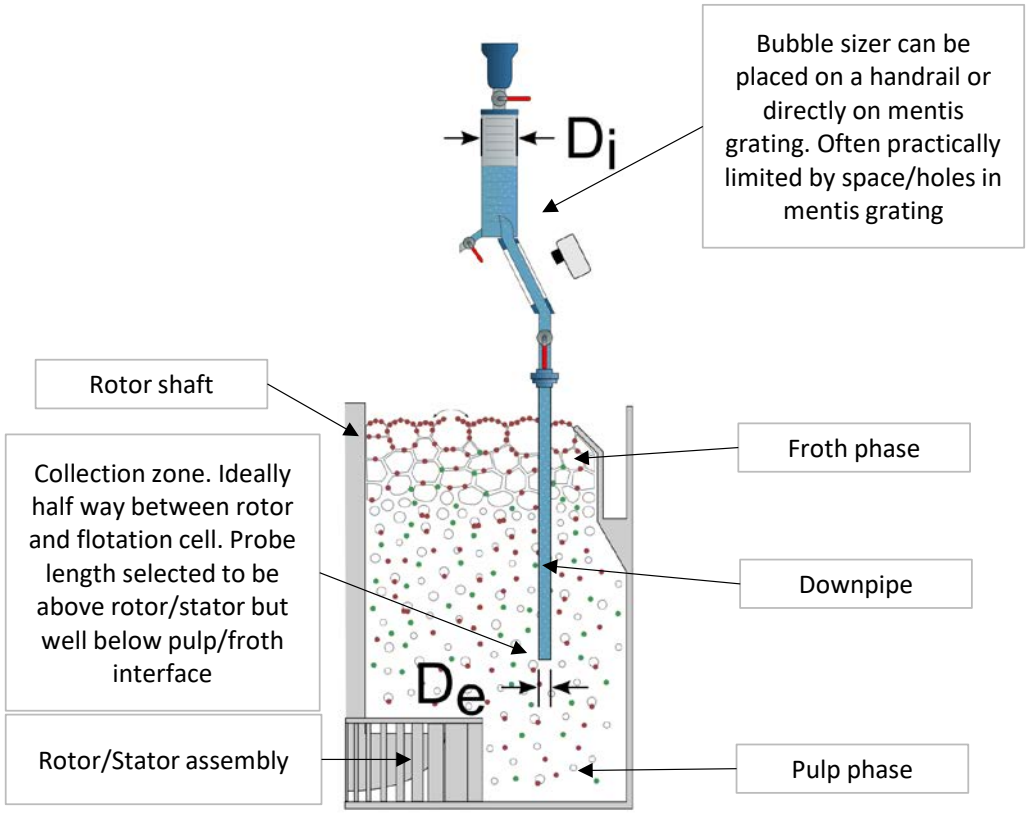

Figure 38: Schematic representation of plant scale experimental APBS setup

Laboratory scale setup

For the purposes of this study it was crucial to measure the bubble size produced by the various glass frits introduced in Section 3.1.3.1. A bubble size study has never been done on a frothing column, however, usually the UCT bubble sizer is used to analyse bubble size distributions of laboratory scale equipment. For this study a different approach was taken to limit the time spent in bubble size characterisation and therefore instead of using the UCT bubble sizer, the APBS was employed. Although this sounds trivial, a new setup had to be conceptualised to enable the use of the APBS on a laboratory scale froth column. Figure 39 shows photos of the experimental setup of which particular note must be made to the stand used to mount the APBS, the plant water reservoir filled with synthetic plant water and 100 ppm Senfroth 516, and a peristaltic pump used to empty and control the level of the frothing column.

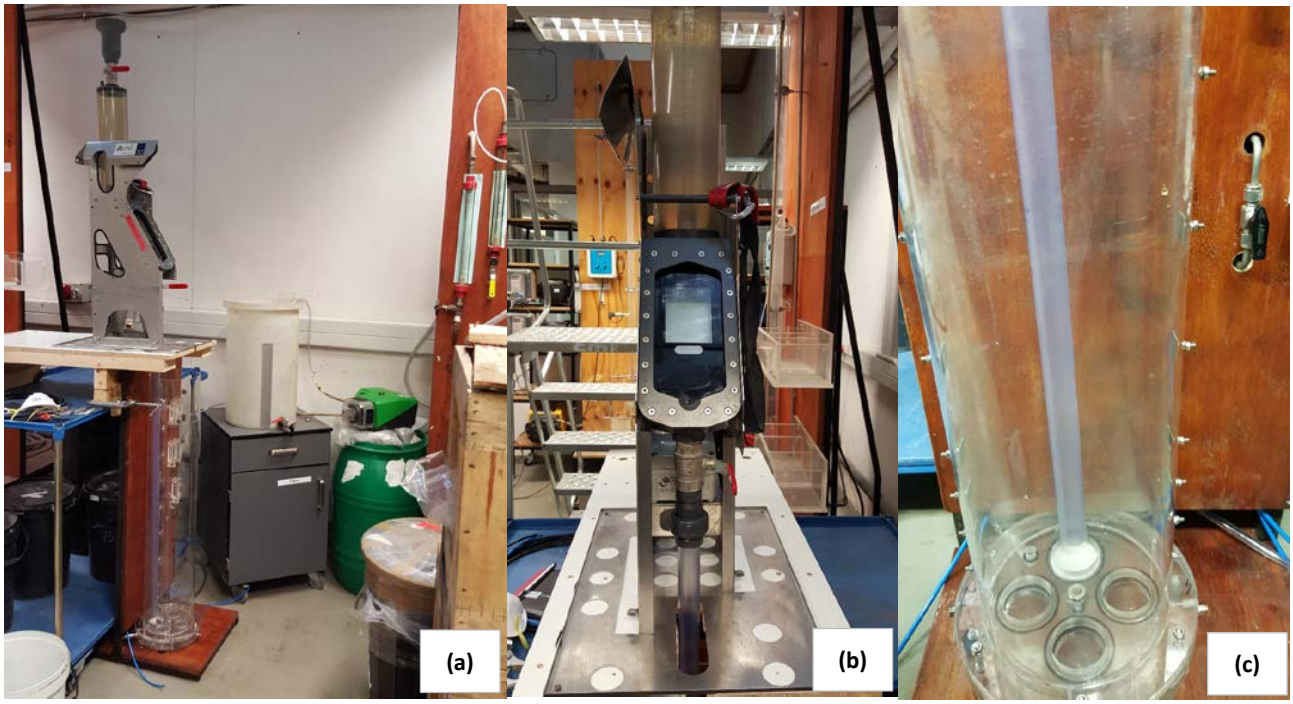

Figure 39: Photos of the laboratory scale APBS setup showing (a) the overall setup, (b) the APBS mounted on the baseplate and stand, and (c) the position of collection zone

3.2. EXPERIMENTAL PROCEDURES

In Section 3.1 of this document the reader has been introduced to all the experimental materials and equipment. This section will build on the previous section by describing the procedures used to acquire the various experimental data sets.

3.2.1. LABORATORY SCALE FROTH STABILITY

The measurement of froth stability was by means of the dynamic method for the entire study. Section 3.1.3.1 highlighted the various column sizes and glass frits that can be used to investigate the scale-up behaviour of the measurement; however, the procedure for obtaining growth data is always the same regardless of the experimental setup. Two techniques were used for this study and both will be described in the following sections.

3.2.1.1. TECHNIQUE 1: MANUAL FROTH GROWTH

Technique 1 is the standard procedure of froth growth data gathering which is by means of making manual marks on the column at set time intervals which is then measured afterwards. The overall procedure is as follows:

- The milled slurry is added to the feed tank and the feed tank stirrer is switched on to maintain a homogenous mixture. The collector is introduced into the laboratory rod mill while the rest of the reagents are introduced into the feed tank and given the appropriate conditioning time. Section 3.1.1.2 highlights the

standard milling procedure and states that a 33 wt% slurry was used for all the tests.

- Before the slurry is introduced into the frothing column, one must ensure that the rotameter is set to the correct flow-rate. Therefore, at this point in time the on/off air valve is opened and the rotameter is adjusted after which the shutoff air valve is closed again.
- The feed valve to the column is opened and the feed pump is started. The frothing column is filled to a standard level of 20 cm before the pump is turned off and the feed valve is closed. The 20 cm pulp level is marked on the column with a permanent marker.
- During the filling process it is vital to turn on the columns overhead stirrer to prevent settling of the solids.
- A set time interval is chosen beforehand at which froth height measurements will be made. Usually an interval of 2 seconds provides enough data to quantify the shape of the froth growth curve while not overwhelming the user.
- The air shutoff valve can now be opened. At the same time the stopwatch is started.
- Every 2 seconds for the first two minutes a mark is made on the column where the current froth level is. Usually steady-state, i.e. maximum froth height, would be reached in this time period; however, if the froth is still growing after two minutes additional measurements should be made in intervals of 30 seconds up until equilibrium has been reached.
- Air flow is now discontinued to the column by closing the air shutoff valve.
- Usually the froth decay is also noted; however, this was not the case for this study. Therefore, as soon as the air feed to the column has been closed, a measuring tape can be used to measure and record the markings on the side of the column.
- After the froth height data has been measured and recorded, Acetone is used to clean the column surface of permanent marker markings. Please note that it is advised that the column surface should be allowed to dry off any excess acetone before a repeat run is attempted.
- At this point a repeat run can either be attempted by repeating the above mentioned steps or the column can be drained and cleaned for the next run.
- To drain the column, the feed valve is opened and the pump is started in reverse and the material is returned to the feed tank.
- The location of the column draining point means that not all the slurry will be removed and therefore the pump discharge is removed from the feed tank and placed in a waste container. After this the column is filled with water to remove any remaining solids and also clean the column.
- Please note that the column overhead stirrer remains on for the duration of this procedure to prevent solids from settling on the glass frit as well as to help clean to column of solids.

- Lastly after all of the solids and water has been drained into the waste container, the overhead stirrer is switched off and removed. The column is removed from its stand and thorough cleaning, if required, is done offline.

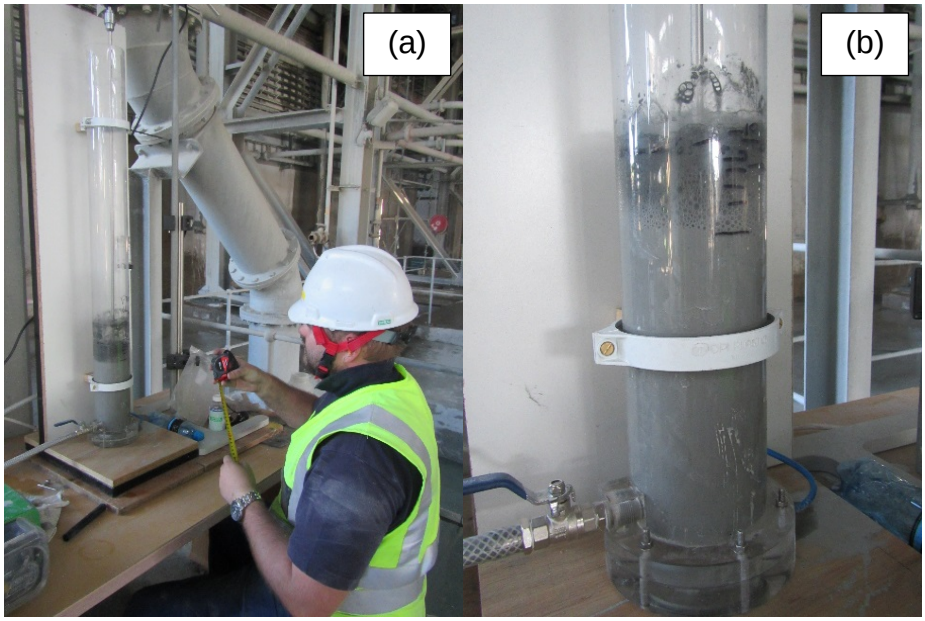

Figure 40: Photos of laboratory scale frothing column showing (a) using a measuring tape to record froth growth, and (b) the markings on the side of the column at set time intervals

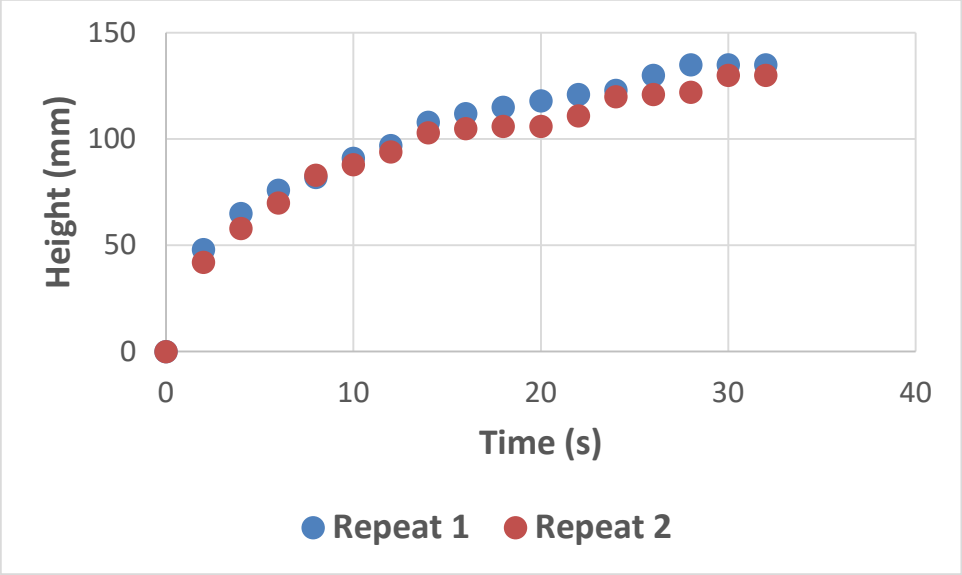

Figure 41: A typical height versus time plot generated by applying the above described methodology

3.2.1.2. TECHNIQUE 2: VIDEO OF FROTH GROWTH

Technique 2 is a method in which the froth growth is filmed and the froth growth data is collected afterwards from the video. The procedure is the same as the one presented in Section 3.2.1.1 but instead of manually taking measurements all the

measurements are done from the video afterwards. This does require a froth column that is clearly marked so that one can read off the heights from the video, this was achieved by adding transparent stick-on measuring tape to the frothing column. This methodology has numerous advantages over the manual method with the most pronounced being the fact that the pulp-froth interface can be actively tracked coupled with screenshots at any point in time that can be used for bubble sizing. The overall procedure is as follows:

- The milled slurry is added to the feed tank and the feed tank stirrer is switched on to maintain a homogenous mixture. The collector is introduced into the laboratory rod mill while the rest of the reagents are introduced into the feed tank and given the appropriate conditioning time. Section 3.1.1.2 highlights the standard milling procedure and states that a 33 wt% slurry was used for all the tests.
- Before the slurry is introduced into the frothing column, one must ensure that the rotameter is set to the correct flow-rate. Therefore, at this point in time the on/off air valve is opened and the rotameter is adjusted after which the shutoff air valve is closed again.
- The feed valve to the column is opened and the feed pump is started. The frothing column is filled to a standard level of 20 cm before the pump is turned off and the feed valve is closed. The 20 cm pulp level is marked on the column with a permanent marker.
- During the filling process it is vital to turn on the columns overhead stirrer to prevent settling of the solids.
- It is crucial to ensure the focus of the camera is set correctly so that the entire froth column can be tracked in experiments where the growth height is high. This has been the main problem with this method as a slight change to the light can affect the video quality.
- The video recording can be started at this point in time. After which the air shutoff valve can be opened.
- The froth is now allowed to reach equilibrium height which usually took about 5 minutes.
- The video recording can now be stopped.
- Air flow is now discontinued to the column by closing the air shutoff valve.
- At this point in time a repeat run can either be attempted by repeating the above mentioned steps or the column can be drained and cleaned for the next run.
- It is advised that the recorded video should be reviewed on a larger screen to ensure the focus remains good throughout the experiment. This can be quite time-consuming however it ensures that no experiments will need to be repeated due to bad video quality.
- To drain the column, the feed valve is opened, and the pump is started in reverse and the material is returned to the feed tank.

- The location of the column draining point means that not all the slurry will be removed and therefore the pump discharge is removed from the feed tank and placed in a waste container. After this the column is filled with water to remove any remaining solids and also clean the column.
- Please note that the column overhead stirrer remains on for the duration of this procedure to prevent solids from settling on the glass frit as well as to help clean to column of solids.
- Lastly after all of the solids and water has been drained into the waste container, the overhead stirrer is switched off and removed. The column is removed from its stand and thorough cleaning, if required, is done offline.

It must be emphasised at this point that the video quality was often poor during the experiments and due to the simple setup and camera this was only picked up after the experimentation was done. It helps a lot to do dummy runs before the actual experiment, which should then be viewed on a larger screen such as a laptop screen, to ensure the focus is good. That being said, changes to light during the experiments often resulted in changing optical conditions. It is advised that a better setup should be investigated as the overall concept is much better than the manual method.

Now that the general laboratory method has been discussed; a discussion regarding the video processing will be done. The method results in a video of the entire froth growth event and therefore time intervals can be chosen after experimentation is done. For the purposes of this study the following time intervals were used:

- Every 1 second for the first 5 seconds of froth growth,
- Every 2 seconds until the 20 second mark is reached,
- Every 10 seconds until the 100 second mark is reached, and;
- Every 30 seconds until 300 seconds has passed.

Three repeats were done per condition, i.e. three separate videos of the froth growth were made before the next experimental condition. For every video, the video was paused at the proposed time interval stated above and a screenshot was taken. From each screenshot a froth height and a pulp-froth height was recorded. Figure 42 shows the froth evolution captured by the video and indicates the measurements taken from each screenshot. The most important being delta time, or elapsed time, which indicates the time of froth growth and delta height, or froth height, which is calculated by taking the froth height minus the pulp height. Please note, that each individual repeat consists of 24 separate screenshots which must be analysed as indicated by Figure 42 and therefore it can be said that this method is quite time consuming.

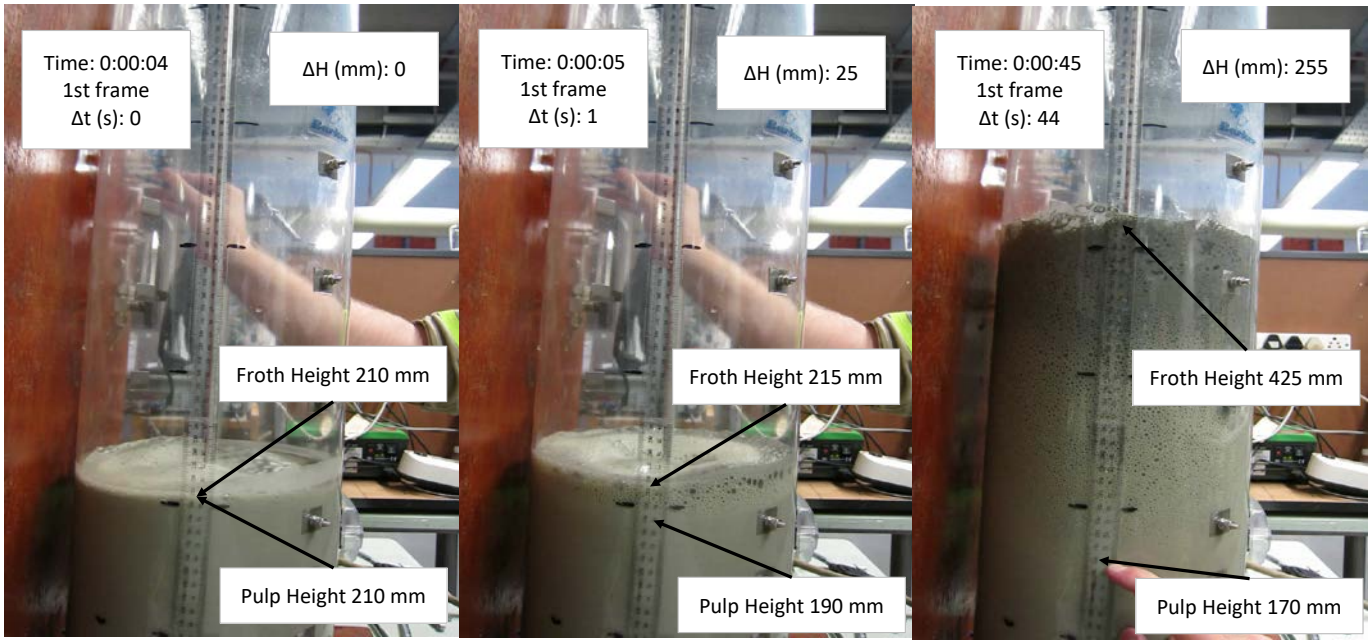

Figure 42: Various screenshots from the Platreef POR1 system indicating the analysis done on every screenshot

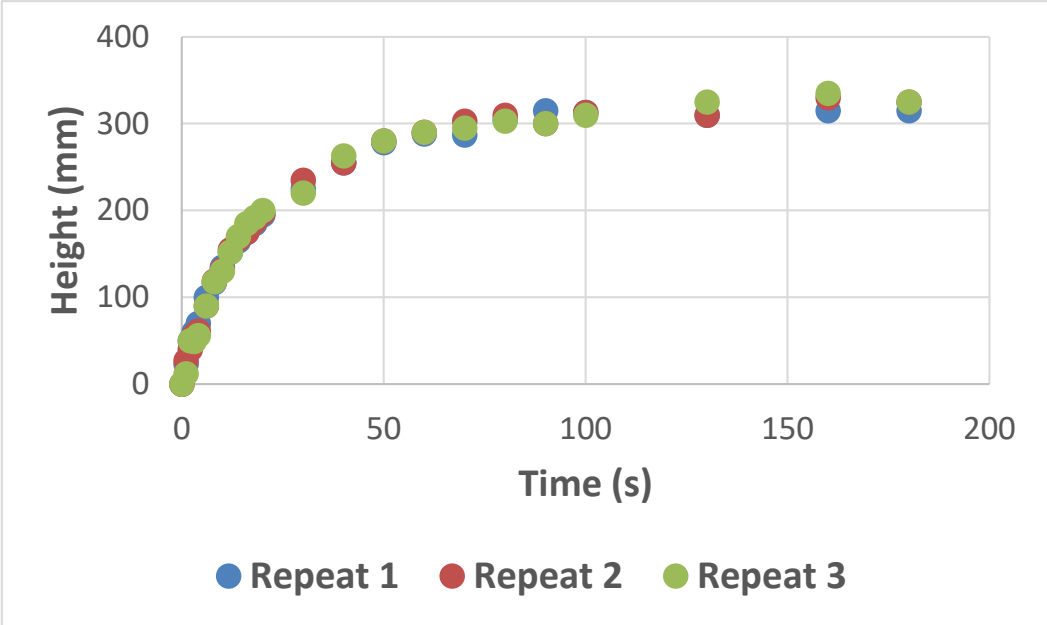

Figure 43: Resulting height and time plot for Platreef POR1 system showing good repeatability

Figure 43 indicates the resulting height versus time plot after all the screenshots have been processed. Firstly, the data in Figure 43 is indistinguishable from the data in Figure 41 even though different techniques have been used to collect it. Lastly, good repeatability can be observed for the experiment in question and it can be said that the shape of the curve is very well defined.

3.2.2. PLANT SCALE FROTH STABILITY

In essence the data gathered on the plant scale is very similar to that of the laboratory with one exception; time is now a dependent variable and a defined height interval is decided upon prior to the experiment. Please refer to Section 3.1.3.2 of this document for the experimental setup used. Regardless of what column diameter and/or flotation cell the procedure always remained constant as follows:

- The gap from the top of the handrail to the top-of-froth is measured coupled with a froth depth measurement. These measurements are used to position the column on the backing plate and a safety margin of 10 cm was always applied. Please note, the column must be inserted below the pulp/froth interface.
- As mentioned in Section 3.1.3.2 the column setup is quite heavy and therefore safety is of the utmost importance. The fixtures used to mount the column to the backboard should be tightened as much as possible; however, take care not to crack the column.
- Ideally two people must pick up the column assembly and lower it into the float cell.
- A set height interval must be decided upon before experimentation starts. An interval of 5 cm was used throughout this study.
- The starting value can be calculated from the measurements taken first and the experimental sheet can be prepared based on this. For example, if the starting value is 45 cm, an experimental sheet should be prepared as follows: 45, 50, 55, 60, etc.
- As soon as the column is in position, the stopwatch should be started. Every 5 cm the split function of the stopwatch is used to record the time.
- After a run, the column must be lifted out of the pulp and froth phase, and thoroughly cleaned with plant water. After which a repeat run can be done by following the same steps as mentioned above or the column can be removed.

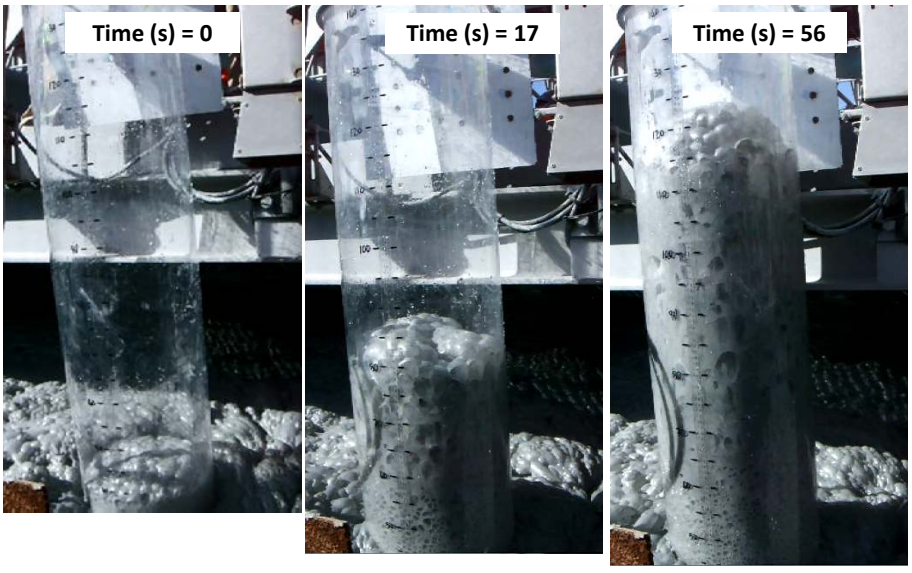

Figure 44: Photo showing the typical froth evolution seen and measured by the above discussed procedure

As was the case with the previous data sets ΔH is calculated by subtracting height zero from the specific height at that point in time. A typical example of the resulting plot is shown in Figure 45.

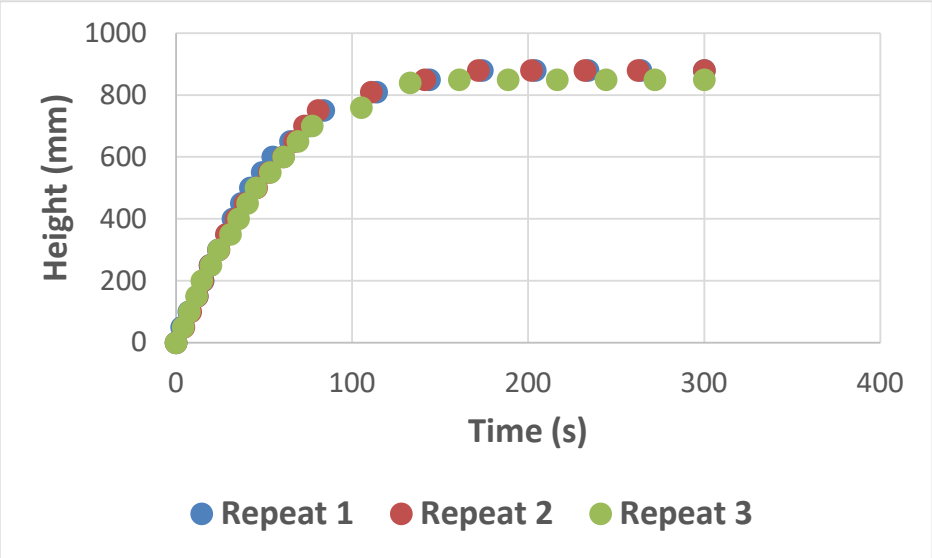

Figure 45: Resulting height versus time plot for the first rougher cell using a 30 cm column

It can be seen that the data presented in Figure 41, Figure 43 and now Figure 45 all looks similar even though the measuring methodology is vastly different.

3.2.3. BUBBLE SIZE MEASUREMENTS

Measurement of bubble size was of critical concern for this study. The APBS was always used to measure pulp bubble size irrespective if this was on plant or laboratory scale. Froth bubble sizing was usually manually done from either photos and/or videos collected during the experiments. This section will highlight the procedure for gathering bubble size data.

3.2.3.1. ANGLO AMERICAN PLATINUM BUBBLE SIZER

As mentioned in Section 3.1.3.3 of this document the APBS is usually used to measure both superficial gas velocity and bubble size. However, of particular importance for this document will be using the APBS for bubble sizing. The following standard bubble sizing procedure was used, please refer to Figure 37:

- Firstly, the APBS should be placed in position as was discussed in Section 3.1.3.3 for both plant and laboratory scale.
- A bucket of plant or synthetic plant water containing 100 ppm frother should be prepared.
- Ensure all valves are closed, except for the filling valve.
- Use the filling spout to fill the water reservoir.
- Close the filling valve.

- Connect the downpipe and ensure the o-ring is in place. Do not cross thread the downpipe as this will cause air leaks that can be mistakenly photographed as bubbles.
- Ensure that the viewing glass is clearly marked with the cell number and/or condition.
- Open the operating valve and fill the downpipe with water. Ensure that more prepared frother water is close by as the setup can use a lot of water based on the length of the downpipe.
- Close the operating valve as soon as the downpipe is filled.
- Open the filling valve and fill the water reservoir. This should be done as quickly as possible when doing plant scale measurements as air from the float cell will start to fill the downpipe.
- Close the filling valve and switch on the back light and camera.
- Open the operating valve.
- As soon as steady state flow is achieved, i.e. a steady flow of bubbles and not pockets of air bubbles at irregular rates, photographs can be taken of the bubbles.
- For plant experiments a typical number of 1000 bubbles are captured by each photo, whereas, this is decreased to about 400 for the laboratory scale experiments. Usually 15 to 20 photos, or 15000 to 20000 bubbles, are deemed representative for a normal plant scale measurement. Therefore, to sample the same amount of bubbles in the laboratory measurement, about 40 to 50 photos are required.
- Also, a reasonable space (about 5 seconds) should be allowed for between photos to ensure that the same bubbles are not sampled twice.
- After all the photos have been taken the operating valve can be closed. At this point in time a repeat run can be done by repeating the procedure or the bubble sizer can be moved and/or the experimental condition can be changed.

The following camera settings was used:

- Mode: Custom/Program
- Flash: Off
- Focus: Multi-focus and macro mode
- Exposure: High exposure (+1 2/3)
- Resolution: 2048x1536 pixels & fine jpeg quality
- Zoom: widest angle (zoomed out)
- Shutter speed: Faster than 1/500 (1/1000 recommended)

Figure 46 displays real photographs taken of bubbles for a plant and laboratory scale experiment. It can be seen that the plant photograph has a lot more bubbles present and therefore it reinforces the fact that less photos can be taken during a plant scale experiment. Also, a clear difference can be seen in the clarity of the two photos which

is mainly due to the suspended solids present in real plant water compared to synthetic plant water.

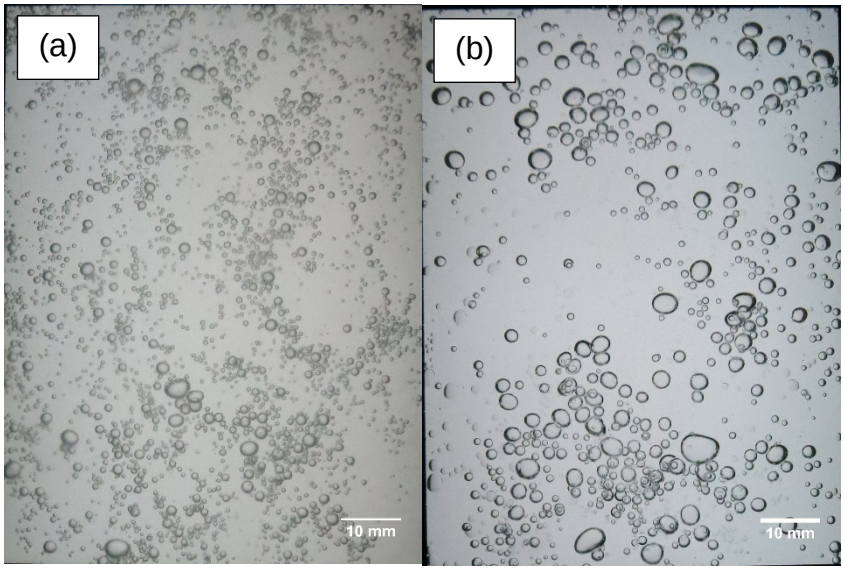

Figure 46: Example of bubbles photographed by the APBS for (a) second rougher cell of a PGM operation, and (b) POR2 glass frit at 6L/min

These photographs are now fed to the APBS software which uses image processing to segment the bubbles and subsequently size them. This process is fully automated and a batch of photos are fed to the software which then calculates a global average and a histogram of the bubbles.

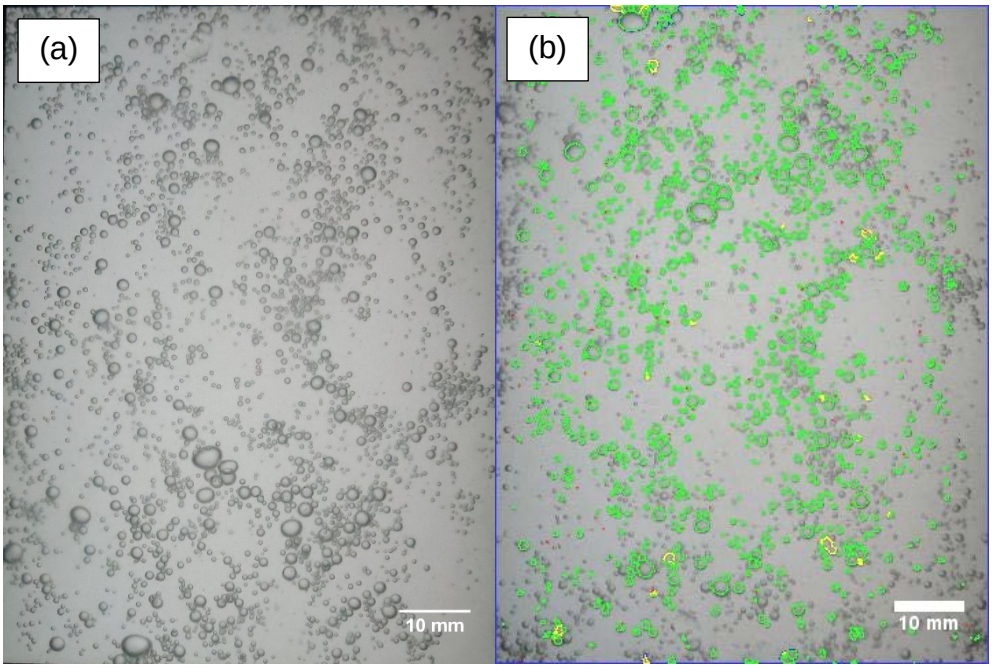

Figure 47: Photograph showing (a) the experimental bubble photo, and (b) segmentation of that photo by the APBS software

As mentioned before the software produces a histogram of the total accepted bubbles counted (green bubble in Figure 47) from the batch and produces a csv file with all the data. The interval classes for the software are programmed into the algorithm and therefore cannot be changed. However, the interval classes' ranges from 33 - 44 µm to 22.6 – 32.0 mm and therefore most normal operating bubble sizes are covered.

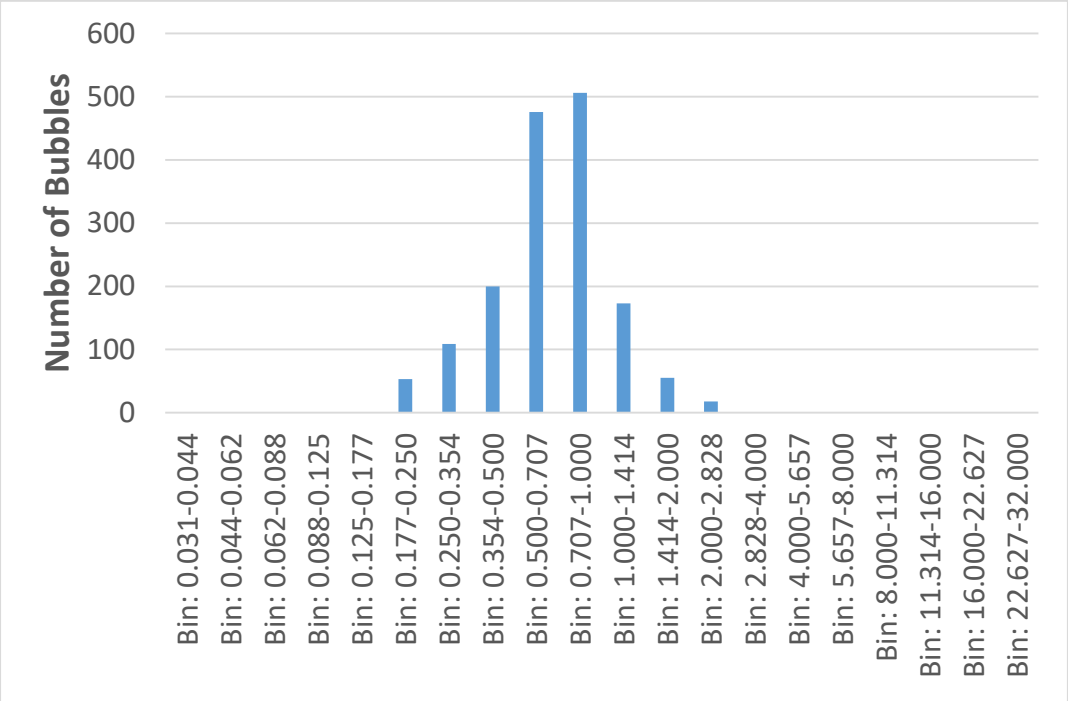

Figure 48: Example of APBS software generated histogram for the image displayed in Figure 47

3.2.3.2. MANUAL BUBBLE SIZING

Although the APBS software is excellent for pulp bubble sizing, it does struggle with froth bubbles mainly due to the size and the irregular nature of the bubbles. For this reason, manual bubble sizing was done where froth bubble sizing was required. Manual bubble sizing is done by taking a screenshot and/or photo of the froth and then using a free program called ImageJ to physically measure each bubble. It is very time consuming and for that reason a maximum of 400 bubbles per experimental condition was measured. This is much less than the 15000 to 20000 bubbles sampled by the APBS software, however, it is thought that it gives a good indication of the bubble size although it might not be statically robust.

Figure 49 gives an example of how the screenshot is cropped and then used for measurement of top-of-froth bubble size. Please note the ImageJ software requires the user to input the scale which is easily done as a measuring tape on the side of the column provides a continuous scale reference. For each screenshot about 100 bubbles were counted and therefore a total of four screenshots per experimental condition resulted in a total of 400 measured bubbles.

Figure 49: Example of how a screenshot is used to determine the top-of-froth bubble size by manually measuring the bubbles

The manual data can then be used to produce the exact same data as that of the APBS software, just with much less data points. The classical way of looking at bubble size distributions is a frequency plot and an example of this is displayed below in Figure 50

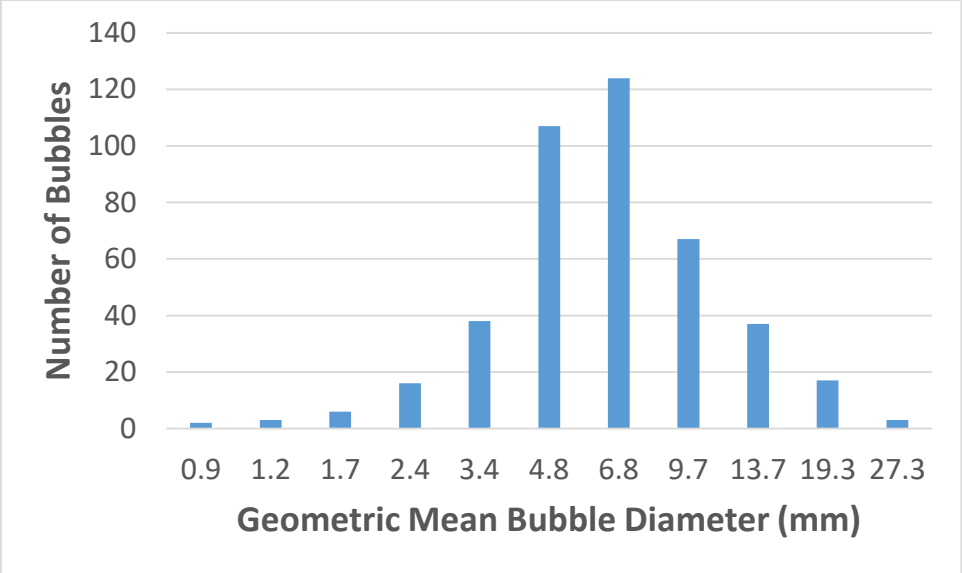

Figure 50: Example of a histogram produced by manually measuring the bubbles

Please note the geometric mean bubble diameter is based on the class intervals of the APBS software output.

3.3. DATA ANALYSIS

Section 3.2 explained in detail how the raw data was gathered. This section will focus on further processing and calculations done to the raw data.

3.3.1. FROTH STABILITY

Dynamic froth stability is often presented by displaying a dynamic stability and/or tau parameter. Dynamic stability can be calculated by using Equation 1 from section 2.1.2.2 of this document and is presented below for the readers' convenience (Barbian, et al., 2003).

$$\boldsymbol{\Sigma = \frac{V_f}{Q} = \frac{H_{max} * A}{Q}} \qquad \textbf{Equation 8}$$

Where:

- ∑ is the dynamic foam stability (s),
- H_{max} is the equilibrium foam height (cm),
- A is the cross-sectional area of the foam column (cm^2), and
- Q is the volumetric feed flow rate of air (cm^3/s).

The equilibrium height is often determined experimentally, however, Barbian, et al., (2005) presented an exponential equation which fitted the equilibrium height and therefore eliminated various experimental variations. This equation was presented in Section 2.1.2.2 as Equation 2 and is presented below for convenience (Barbian, et al., 2005).

$$\boldsymbol{H(t) = H_{max}\left(1 - e^{-\frac{t}{\tau}}\right)} \qquad \textbf{Equation 9}$$

Where:

- H(t) is the foam height at time t (cm),
- H_{max} is the equilibrium foam height (cm),
- t is time (s), and
- τ is the average bubble life time, a measure of froth stability (s).

Equation 9 is fitted to the raw data as described in Sections 3.2.1.1, 3.2.1.2, and 3.2.2 by means of a weighted sum of square errors. This allows the user to be in full control of the weighting of various points, for instance, less weighting can be given at the start of the experiment where the growth is rapid and more weighting can be given towards the end of the experiment. Solver is then used to minimise the weighted sum of square errors by adjusting the H_{max} and τ in Equation 9

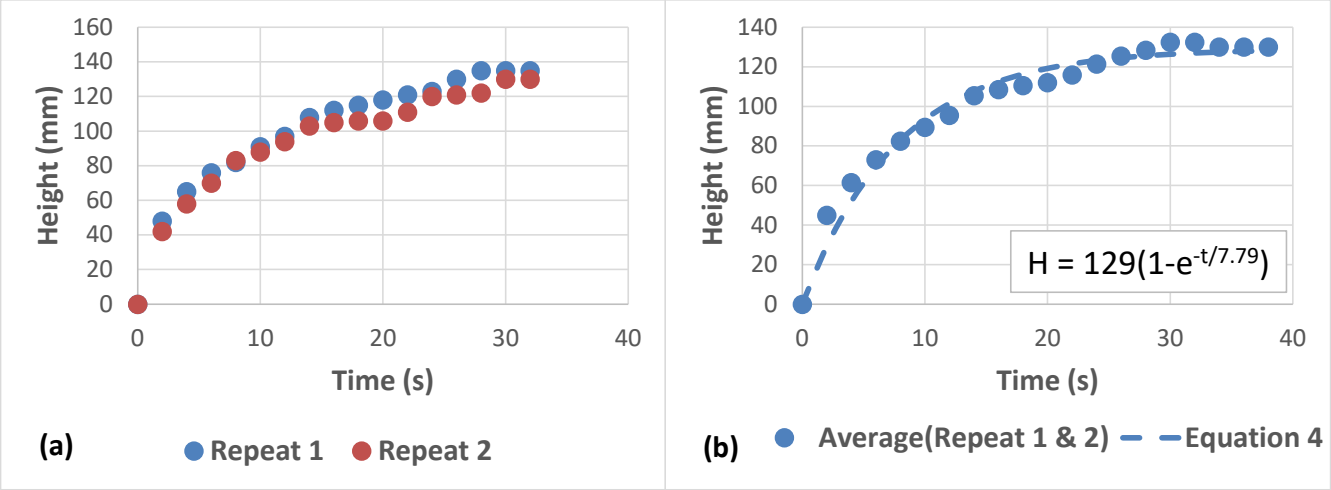

Figure 51: Froth stability data showing (a) the experimental data presented in Figure 41, and (b) how Equation 9 is fitted to get H_{max} and τ

Figure 51 shows how the raw data presented in Sections 3.2.1.1, 3.2.1.2, and 3.2.2 is processed to get H_{max} and τ values. The equilibrium height value is then inserted in Equation 8 together with a superficial gas velocity, either measured by the APBS or controlled if it is a laboratory experiment, to calculate the dynamic stability.

3.3.2. BUBBLE SIZE

3.3.2.1. SAUTER MEAN BUBBLE DIAMETER

The bubble size distribution is quite often presented as a Sauter mean bubble diameter value. It is similar, at least in concept, to taking an average however it better describes the volume to surface area ratio and therefore is primarily used in flotation. The Sauter mean bubble diameter was calculated using Equation 10.

$$d_{32} = \frac{\sum_{i=1}^{N} d_i^{\,3}}{\sum_{i=1}^{N} d_i^{\,2}} \qquad \textbf{Equation 10}$$

3.3.2.2. PRESSURE CORRECTION FACTOR

As mentioned in Sections 3.1.3.3 and 3.2.3.1 it is often required to do a pressure correction on the bubble size measured by the APBS due to the pressure change between the viewing chamber and the collection point.

$$PCF\,(d_{32}) = \sqrt[3]{\frac{P_{atm}+\rho_p g H_p(1-\epsilon_g)-\rho_w g H_w(1-\epsilon_g)}{P_{atm}+\rho_p g H_p(1-\epsilon_g)}} \qquad \textbf{Equation 11}$$

Where:

- d_{32} is the Sauter mean bubble diameter
- P_{atm} is the atmospheric pressure (Pa),
- ρ_p is the pulp density without bubbles (kg/m^3),
- ρ_w is the density of water (kg/m^3),

- g is the gravitational constant (m/s^2),
- ε_g is the gas hold-up of the pulp,
- H_w is the distance from the end measuring mark to the end of the APBS probe (m),
- H_p is distance from the pulp surface to the end of the APBS probe (m).

The calculated correction factor is often very small for normal plant scale operations and typically changes the measured diameter by about 1%. The correction was not used for the laboratory data as it was assumed that the pressure change will be negligible.

CHAPTER FOUR:COLUMN DIAMETER EFFECTS

4.1. INTRODUCTION

This section will display and discuss data collected to quantify the effect column diameter has on measured dynamic stability. Most of the column diameter data was collected using the industrial scale column setup as discussed in Section 3.1.3.2 and 3.2.2. Bubble size data will also be discussed in this chapter and this was collected using the experimental methodologies discussed in Section 3.2.1.2 and 3.2.3.2. The layout of this chapter will be as follows:

- Section 4.2 – Measured dynamic froth stability as a function of column diameter. It is important to note that all the data was collected on the same PGM processing plant; the McFadzean (2013) data was collected on the third rougher in 2013 while the 2015 data was collected on both the first and third rougher cell.
- Section 4.3 – Correcting for column diameter. This section will propose an empirical relationship that can be used to correct for column diameter.
- Section 4.4 – Towards a scale independent methodology for froth stability. This section will present bubble size data gathered on a laboratory scale in two different column diameters and discuss the implications of the observed behaviour.

Dynamic stability is extracted from growth data as discussed in the experimental methodology chapter. The growth data will not be directly displayed in the discussions of this chapter; however, it will be presented in full in the appendix of this document.

4.2. MEASURED DYNAMIC STABILITY AS A FUNCTION OF COLUMN DIAMETER

Figure 52 displays the McFadzean (2013) data set that was first introduced in Section 1.2 of this thesis. Please note, this data set is unpublished and was gathered by the Centre for Minerals Research This data set represents the first indication of the column diameter effect and therefore has been used extensively to motivate this study. There are some interesting observations to be made from Figure 52, such as:

- The overall trend of the data follows what is expected from literature, which is: an increase in measured dynamic stability with an increase in column diameter (Ambulgekar, et al., 2004).
- The 50 mm and 100 mm column achieved a similar dynamic stability.
- Lastly, the dynamic stability difference between the 200 mm and 300 mm column is fairly large, which is indicative of the presence of a wall effect even up to the 200 mm column. This is much larger than the 37.5 mm quoted by Papara, et al., (2009), however this was based on a 2-phase system.

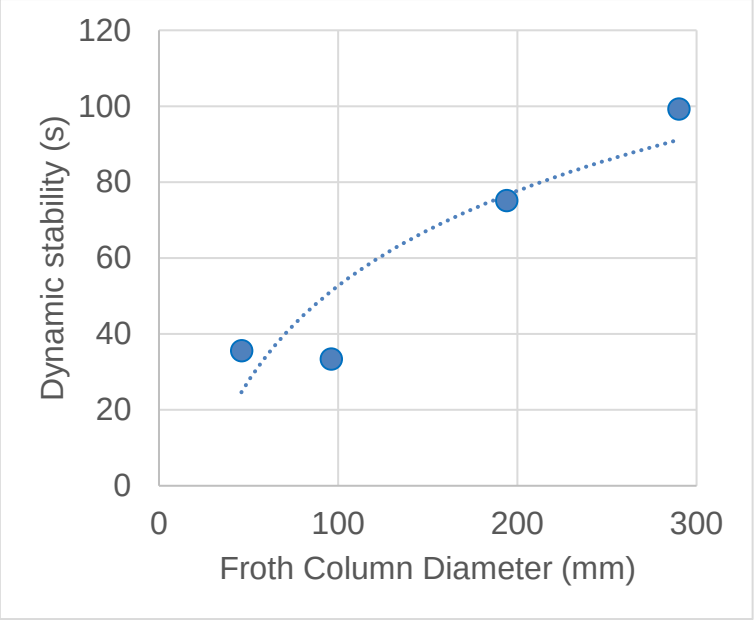

Figure 52: Dynamic stability as a function of column diameter for the third rougher cell of a PGM operation (McFadzean, 2013)

The choice of column diameters (50, 100, 200 and 300 mm) was not given much thought except for which diameter column was readily available. Figure 52 therefore highlights some key observations as the data suggests that below 100 mm no real change is observed and therefore the use of the 50 mm column can be questioned. Moreover, significant changes in dynamic stability is present even up to 300 mm and therefore a larger column diameter could be useful. Figure 53 displays the first of the new data sets that was collected in 2015 on the first rougher.

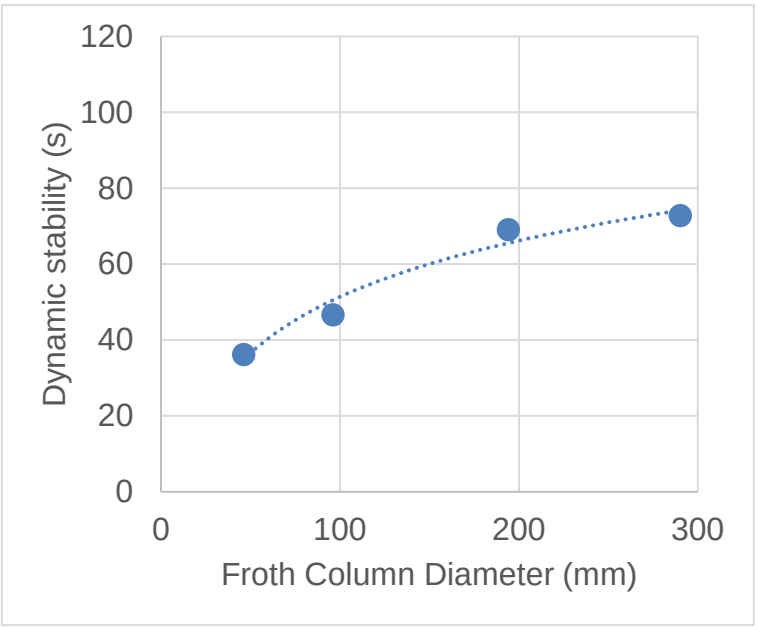

Figure 53: Dynamic stability as a function of column diameter for the first rougher cell of a PGM operation

Firstly, the overall trend of the data confirms what was seen in Figure 52, i.e. an increase in column diameter results in a subsequent increase in measured dynamic stability. The increase in measured dynamic stability for the 50 mm, 100 mm and 200 mm columns are quite rapid whereas only a slight increase is seen for the 300 mm column. This behaviour highlights some key differences to that of the data displayed in Figure 52, which is:

- The use of the 50 mm column is justified as there appears to be a significant dynamic stability difference.
- Also, the difference in dynamic stability for the 200 mm and 300 mm column is very small which indicates that wall effects have become negligible. This is encouraging to see as it suggests that a 300 mm column closely approximates an infinitely large system, which is beneficial due to the fact that the measurement columns do not have to be larger to find a reasonable approximation to full scale froth stability.

Figure 54 displays the second and last of the 2015 data sets and it was collected on the third rougher cell.

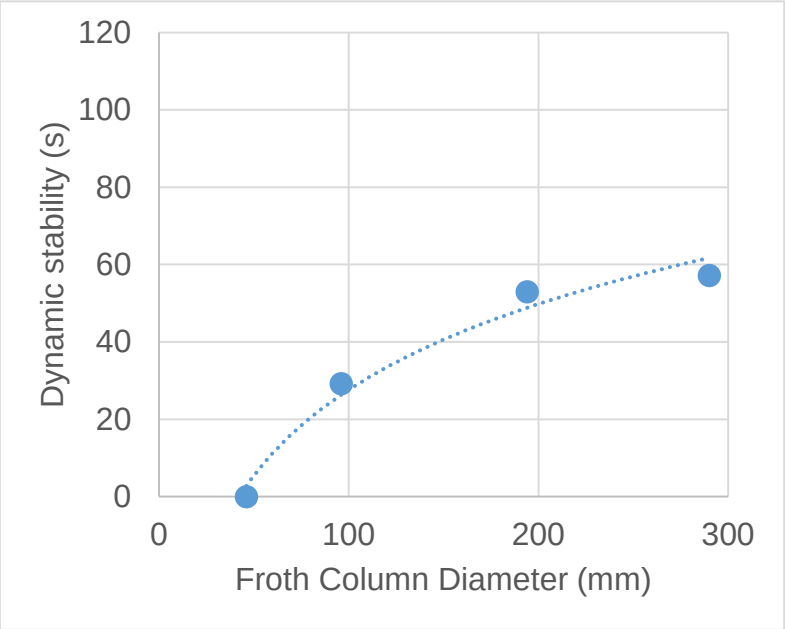

Figure 54: Dynamic stability as a function of column diameter for the third rougher cell of a PGM operation

Firstly, the general trend in the data displayed in Figure 54 is similar to both of the previous data sets. An increase in measured dynamic stability is seen with increasing column diameter due to a decrease in the global drainage of the froth in larger columns as less of the froth is in contact with the wall. This observation has been consistently seen throughout all the experimental results and it is in close agreement with literature (Ambulgekar, et al., 2004; Papara, et al., 2009). The data represented in Figure 54 also indicates that a suitable experimental range for the column diameter was chosen.

This is a valuable insight as the 2013 data, displayed in Figure 52, suggested that a larger column diameter might be required to experimentally determine the point at which wall effects become insignificant.

Secondly, the data displayed in Figure 52 and Figure 54 are for exactly the same flotation cell operating at a similar superficial gas velocity but for two different years, namely 2013 and 2015. If the dynamic stabilities are directly compared it can be said that the froth was significantly more stable in 2013 compared to 2015. This observation is highlighted as a side note to illustrate the step change that occurred within the froth of the same plant within 2 years. This may be due to an ore change, difference in grind or solids concentration, or a change in frother dosage or type. This is the long-term goal that this research seeks to address as changes like this need to be incorporated in the control strategy; however, due to lack of measurement it can easily go unnoticed.

4.3. CORRECTING FOR COLUMN DIAMETER

4.3.1. DEFINING AN EMPIRICAL RELATIONSHIP

In general, the experimental data displayed in Section 4.2 follows a similar trend. This section will endeavour to develop a relationship that can be used to account for a change in column diameter. There are significant drainage differences between Plateau borders and bubble films in contact with the wall compared to the interstitial Plateau borders (Papara, et al., 2009). Therefore, it is thought that at the heart of the correction for wall effects would be a ratio of bubble surface area in contact with the wall to the overall bubble surface area.

The surface of the column in contact with froth, A_c, can be calculated by Equation 12.

$$A_c = \pi D_c H_{max} \quad \textbf{Equation 12}$$

The total surface area of the bubbles contained within that section of the column, assuming spherical bubbles and a constant bubble size with height, can be calculated by Equation 13.

$$A_b = N_b\left(\pi D_b^2\right) \quad \textbf{Equation 13}$$

Where, N_b, is the number of bubbles which can be calculated by Equation 14.

$$N_b = \frac{V_{Total\ Froth}}{V_{Bubble}} = \frac{3D_c^2 H_{max}}{2D_b^3} \quad \textbf{Equation 14}$$

Combining Equation 13 and Equation 14 results in Equation 15.

$$A_b = \frac{3\pi D_c^2 H_{max}}{2D_b} \quad \textbf{Equation 15}$$

The ratio of A_c to A_b, or the ratio of the wall surface to the bubble surface is then easily calculated from Equation 12 and Equation 15.

$$\frac{A_c}{A_b} = \left[\frac{\pi D_c H_{max}}{1}\right]\left[\frac{2D_b}{3\pi D_c^2 H_{max}}\right] = \frac{2D_b}{3D_c} \propto \frac{D_b}{D_C} \qquad \textbf{Equation 16}$$

Equation 16 is a simplification compared to a real system where bubbles are not spherical and bubble size will not be constant with froth height. Nonetheless, the basic concept will remain similar. The surface of the column was taken to approximate the area of the Plateau borders and films in contact with the wall, while the total bubble surface area represents the interstitial Plateau border area. The ratio of these two will define the differences in drainage experienced by the foam/froth if only column diameter is changed. Figure 55 displays the hypothetical response of the ratio of bubble size to column diameter as a function of column diameter.

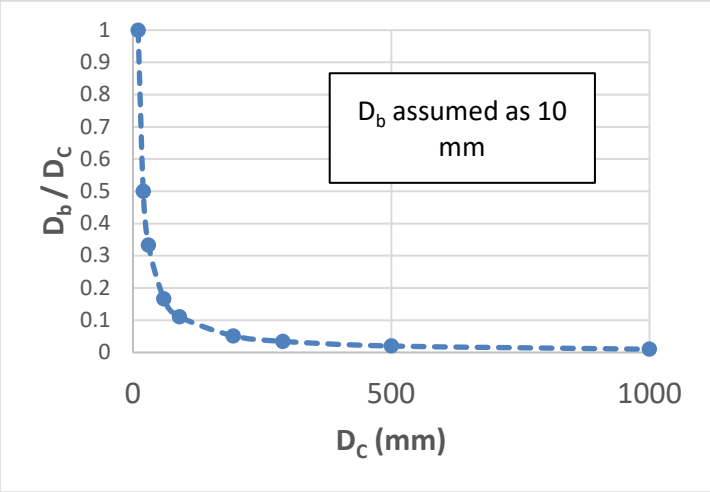

Figure 55: D_b/D_c as a function of column diameter

A constant bubble size has been assumed and therefore the shape of the curve is simply defined by the inverse of column diameter. Assuming a constant bubble size is based on the fact that the material presented to the bubble films remains constant and therefore the size at which failure of a bubble occurs should also remain unchanged; however, this will be discussed in more detail in Section 4.4. Two boundary conditions exist for the ratio of bubble size to column diameter and these are discussed below.

1. $D_b/D_c \rightarrow 1$. The measured froth stability will tend to zero as the area of the wall approaches the bubble area. In other words, even though the slurry will have a theoretical stability, no stability can be measured in the specified system.
2. $D_b/D_c \rightarrow 0$. The measured froth stability will tend towards the theoretical limit as the wall area becomes insignificant to the bubble area.

The boundary conditions described above can quite easily be represented in an equation.

$$\Sigma_{measured} = \Sigma_{\infty}\left(1 - \left(\frac{D_b}{D_c}\right)\right)$$ **Equation 17**

Equation 17 relies on two empirical fitting parameters which can be described as follows:

- $\sum_{\infty}$ represents the dynamic stability in an infinitely large system. This parameter is quite easy to engage with as it is simply the measured dynamic stability at which wall effects become insignificant. The experimental data has shown that the dynamic stability reaches a maximum between the 200 mm and 300 mm column and therefore the experimental data should help define a realistic value.
- D_b represents a bubble size dependent variable. The dependence of wall effects on the bubble size has been clearly illustrated within the simple derivation of Equation 16. Bubble size does change with froth height therefore mechanistically this parameter is probably best represented by a global average; however, this will be discussed in more detail in the next section.

In summary it can be said that the curve generated by Equation 17, as shown in Figure 56, appears to follow the general trend of the experimental data quite well.

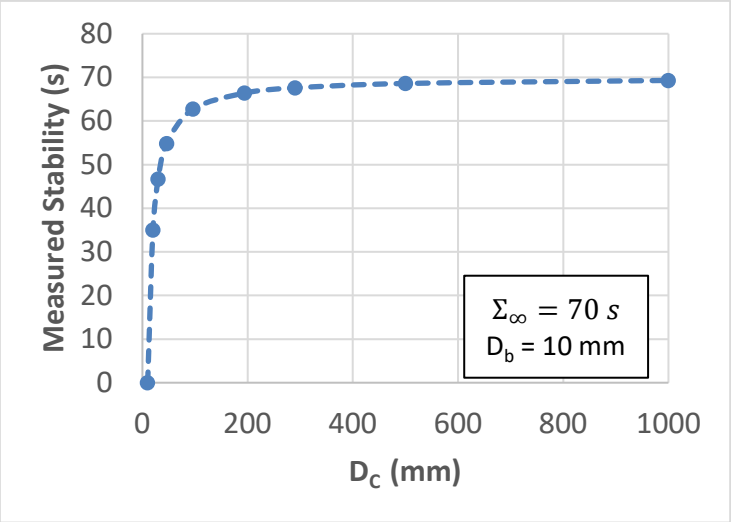

Figure 56: Hypothetical response of Equation 6 as a function of column diameter

4.3.2. EVALUATING THE PORPOSED EMPIRICAL RELATIONSHIP

The significance of the empirical relationship proposed in Equation 17 can only be determined by the robustness it provides when describing experimental data. This section will evaluate the proposed relationship by fitting it to the experimental data sets previously displayed in Section 4.2.

The McFadzean (2013) data set provides a unique challenge to fit due to the behaviour of the 50 mm and 100 mm column in combination with the fact that a maximum

dynamic stability is never reached. Figure 57 displays the resulting fit obtained from the experimental data.

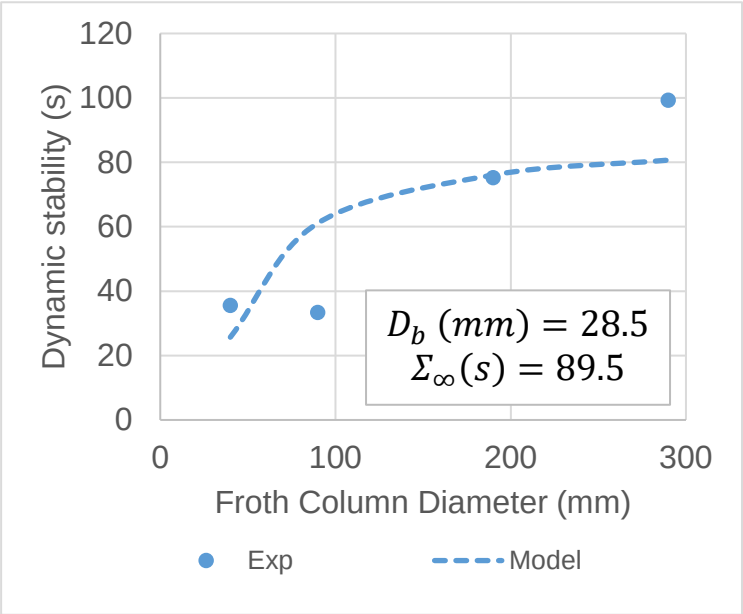

Figure 57: Measured and predicted dynamic stability as a function of column diameter for the third roughing cell of a PGM operation (McFadzean, 2013)

The fit of the model is relatively poor when compared to the other data sets, but this, in combination with an analysis of the other data sets, simply casts doubt on the accuracy of the McFadzean (2013) data set. Figure 58 displays the fit obtained for the first of the 2015 data sets and it can be said that Equation 17 describes the data very well.

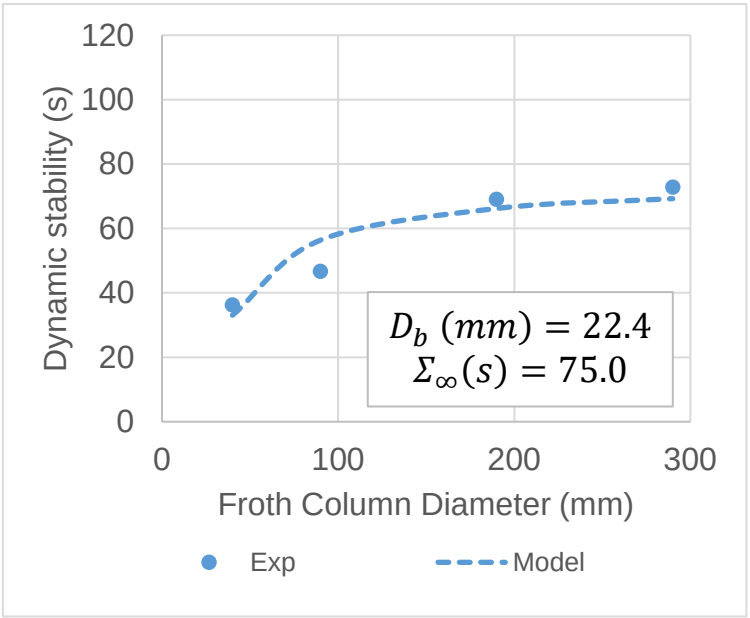

Figure 58: Measured and predicted dynamic stability as a function of column diameter for the first roughing cell of a PGM operation

Comparing the fitted parameters to those obtained from the 2013 data set; the following can be said:

- The fitted maximum dynamic stability is larger for the 2013 data (89.5 s vs 75.0 s) which is to be expected as higher experimental values were seen. However, the data displayed in Figure 58 does reach a noticeable maximum whereas the 2013 data does not.
- The fitted bubble size is significantly larger for the 2013 data set (28.5 mm vs 22.4 mm); however, both values fit quite easily into a normal operating range of bubble size at the top-of-froth surface for an industrial plant.

Figure 59 displays the data collected on the third roughing cell during the 2015 campaign.

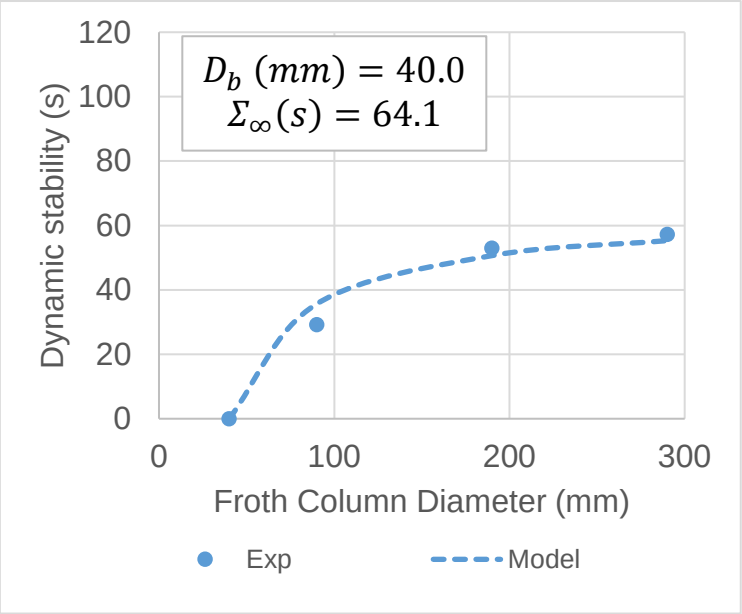

Figure 59: Measured and predicted dynamic stability as a function of column diameter for the third roughing cell of a PGM operation

There was no froth growth in the 50 mm column and therefore the dynamic stability has been set to zero in Figure 59. Following from Equation 17 zero dynamic stability can only be achieved when the ratio of bubble size to column diameter is equal to one. For this reason, the bubble size parameter was set to 40 mm as this is the inside diameter of the 50 mm column. Even with this assumption it can be said that Equation 17 describes the data very well and the following observations can be made:

- In general, for all the data sets the proposed empirical relationship is a good description of the shape of the behaviour.
- Equation 17 has proven to be robust and reliable and therefore it can be useful to analyse data sets where wall effects are suspected. This will, however, rely on assumption of the fitted parameters and therefore caution should be exercised.

- Lastly, the fitted parameters seem reasonable and follow the trends present in the data. For instance, the fitted maximum dynamic stability decreases in order of how stable the systems are in general, i.e. the third rougher cell has a lower maximum dynamic stability (64.1 s) than the corresponding first rougher cell (75.0 s).

Lastly, the bubble size parameter should be observed in more detail. For the experiments performed in 2015 on the first and third rougher cells; a series of top-of-froth photographs were taken throughout. These photographs can be used to extract a Sauter mean top-of-froth bubble size for the two respective flotation cells and this is then plotted against the fitted D_b parameter in Figure 60.

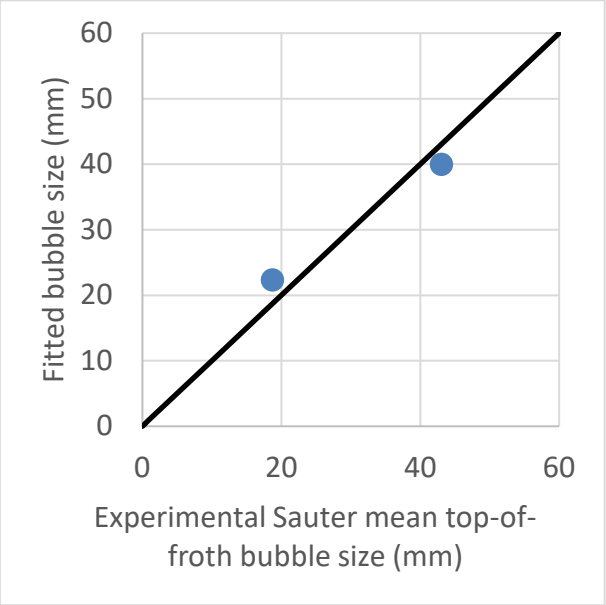

Figure 60: Experimental Sauter mean top-of-froth bubble size plotted against fitted D_b for the first and third rougher cell (or the data represented in Figure 58 and Figure 59)

Figure 60 shows that there is excellent correlation between the experimentally measured Sauter mean top-of-froth bubble size and the fitted D_b. Even though it only has two data points one can argue that the correlation suggests that the fitted D_b is a top-of-froth dependent variable. From the derivation of Equation 17 the D_b parameter arises from the fact that it represents the total surface area of the bubbles in the froth and therefore mechanistically there seems to be no reason that D_b should be a top-of-froth variable. It should rather be best approximated by a global area of the entire froth. Sauter mean has long been used to approximate bubble size within flotation processes due to the excellent representation it gives to surface area. However, the calculation of the Sauter mean is heavily biased towards large bubble sizes and therefore a global average Sauter mean bubble size for a froth would be close to the size obtained for the top-of-froth.

4.4. TOWARDS A SCALE INDEPENDENT ANALYSIS OF FROTH STABILITY

Section 4.2 illustrated that there is a significant difference in measured dynamic stability at different column diameters. This is mainly attributed to drainage differences and in Section 4.3 it was shown that dynamic stability can be corrected for if these drainage differences are accounted for. The dynamic froth stability test is dependent on both drainage and film stability changes which are combined to quantify a froth stability number. This section will propose a manner in which the data can be viewed independently of drainage differences and therefore can be used to determine froth stability, independent of scale.

A fundamental 2-phase foam study by Kostoglou, et al., (2015), clearly illustrated the dependence of the global bubble size distribution within a coarsening and coalescing foam on the amount of surfactant present within the system. This is not a new observation and numerous other authors have stated that bubble size change as a function of height within the foam is highly dependent on the frothing solution used (Chang, et al., 1956; Marrucci, 1969; Saint-Jalmes & Langevin, 2002). In 3-phase froth systems where the presence of solids heavily affects the stability it has been found that various physical properties of the particles affect the rate of coalescence (Ata, et al., 2003; Dippenaar, 1982). Therefore, from the above mentioned observations it can be said that the rate of bubble size change up the froth is heavily dependent on the material loaded on the bubble surface. This behaviour was confirmed by Morar, et al., (2012), who used machine vision techniques to analyse the top of various flotation froths and found that bubble burst rate is solely dependent on top-of-froth bubble size and solids loading. In a system where the quality and amount of material presented to the bubble is constant, such as a system where the column diameter change is the only variable, one would expect the loading of the bubble surface to remain constant. Hence a certain terminal bubble size will be stable and this will remain constant regardless on the change in column diameter.

4.4.1. TOP-OF-FROTH BUBBLE SIZE AS A FUNCTION COLUMN DIAMETER

This experimental work used a 100 mm and 200 mm laboratory scale froth stability column and employed a series of photographs to determine the top-of-froth Sauter mean bubble size. A thousand bubbles were sampled from various photographs for each column diameter.

Figure 61 displays the experimentally determined top-of-froth bubble size distribution determined for the 100 mm and 200 mm column. In general, it can be said that there appears to be a slight difference in the distributions; with the 200 mm column having a larger fraction of bubbles above 2 mm. The distributions do peak at a very similar bubble size of around 2.5 mm. In addition, if the Sauter mean is calculated it gives a

value of 4.3 mm or 4.9 mm, for the 100 mm and 200 mm column respectively. Thus, for a halving in column diameter, there is a small difference observed in bubble size distribution. The data presented in Figure 61 illustrates that the assumption of a constant terminal bubble size, as discussed previously, is possible.

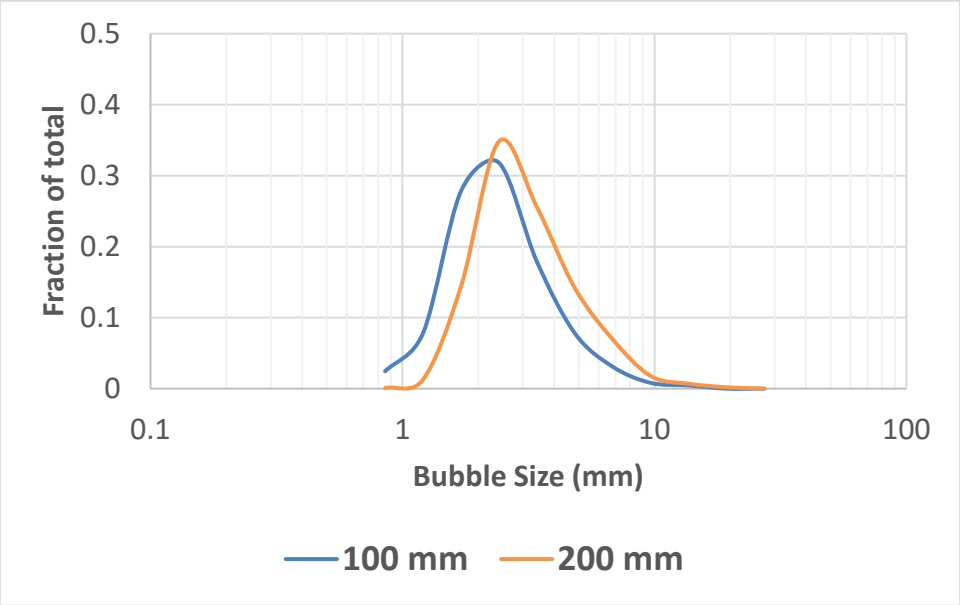

Figure 61: Top-of-froth bubble size distribution as a function of column diameter using Platreef ore and operating at 6 L/min

4.4.2. SIDE-OF-FROTH BUBBLE SIZE AS A FUNCTION OF COLUMN DIAMETER

The column diameter experiments were done at various pulp bubble sizes as well as the two defined column diameters. As a result of this there is a vast range of maximum froth heights present within the data set.

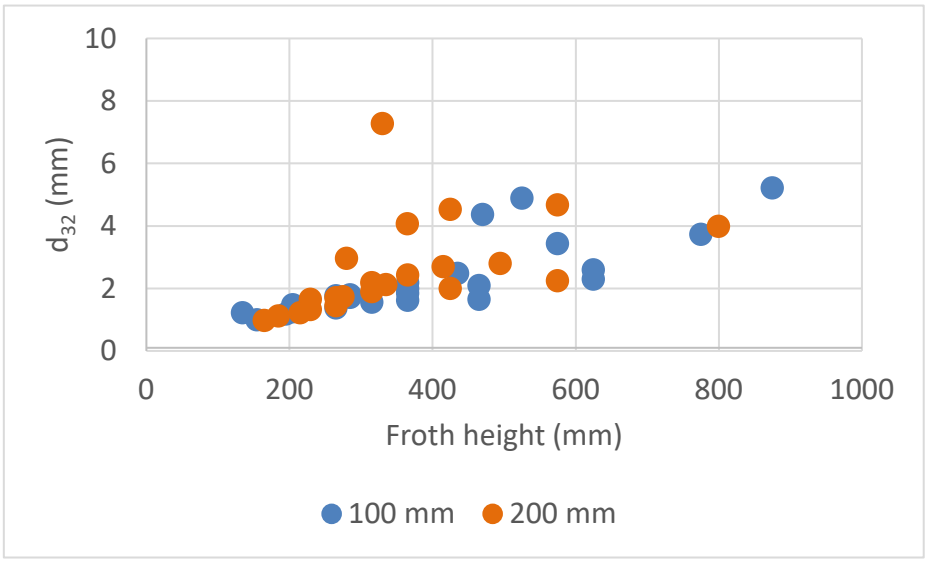

Figure 62: Experimental Sauter mean bubble size as function of froth height for the 100 mm and 200 mm column

Figure 62 displays the experimental Sauter mean bubble size as a function of experimental froth height and it can be seen that the data set contains large amounts of scatter. Therefore, the froth heights were normalised by dividing by the associated maximum froth height attained under each condition (Equation 18).

$$CFH = \frac{H_i}{\Sigma * J_g} = \frac{H_i}{H_\infty} \qquad \textbf{Equation 18}$$

Where:

- CFH is the corrected froth height;
- H_i is the froth height at which the bubble size was determined;
- J_g is the superficial gas velocity;
- $\sum$ is the measured dynamic stability, and;
- H_∞ is the equilibrium froth height.

Figure 63 highlights the resulting plot if Equation 18 is applied to the data displayed in Figure 62.

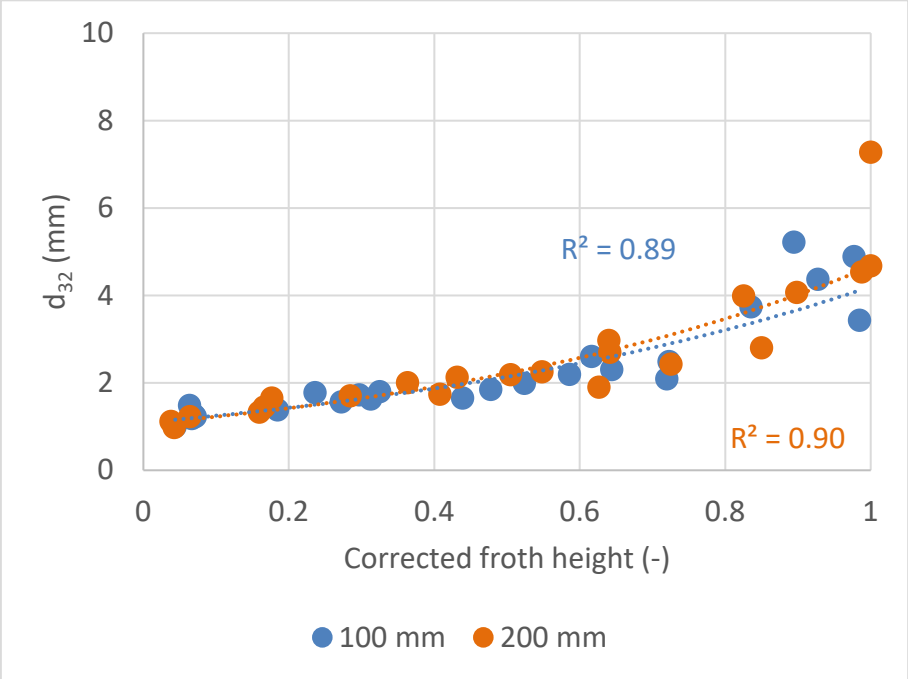

Figure 63: Sauter mean bubble size as a function of corrected froth height for the 100 mm and 200 mm froth column

There are numerous discussion points regarding the data presented in Figure 63; however, the most striking observation is that the bubble growth rate as a function of corrected froth height is the same for the 100 mm and 200 mm column. Both data sets, the 100 mm and 200 mm, follow a well-defined exponential increase in Sauter mean bubble size as a function of the froth height. This exponential type behaviour with froth height has been seen previously by Ata, et al., (2003), and is attributed to the froth being drier as you progress in froth height and therefore the bubbles are more

susceptible to coalescence. However, the striking new observation is the fact that both the 100 mm and 200 mm column data collapse onto one common relationship once a correction for froth height has been made. This is attributed to the fact that bubble growth is controlled by the material loaded onto the bubble film which remains unchanged between the 100 mm and 200 mm column. Froth height, in this case, is only dependent on drainage and therefore if high drainage occurs a low froth height would be experienced and vice versa. However, the film stability remains unchanged and therefore it collapses onto one common characteristic relationship.

Slight differences in the exponential trend line of the 100 mm and 200 mm column data do exist as is shown in Figure 63 and the difference is more prominent towards the top of the froth. This is an interesting observation as it has been shown in Section 4.4.1 that there are differences, albeit very slight, between the top-of-froth bubble size distributions of the 100 mm and 200 mm column. It was unclear whether this observation was due to the fact that there is a real difference or if this observation was simply experimental error. That being said, Figure 63 shows large variance occurring in the Sauter mean bubble size towards the top of the froth. For each individual point in Figure 63 only 200 bubbles were sampled for size and therefore, seeing as there is no mechanistic reason, it highlights that possibly more bubbles should be sampled to eliminate the natural variance that occurs at the top of the froth. As one moves to lower froth heights in Figure 63 the variance is much less, and the 100 mm and 200 mm data sets definitely collapse onto one. This highlights an important point regarding the comparison of the top-of-froth and the side-of-froth methodology. A measure of the growth of the bubbles throughout the froth is more representative than observing a boundary condition such as the top of the froth.

CHAPTER FIVE: PULP BUBBLE SIZE EFFECTS

5.1. INTRODUCTION

This section will display and discuss data collected with regards to the effect of pulp bubble size on measured froth stability. Figure 64 illustrates the normal operating ranges of superficial gas velocity, J_g, and bubble size, d_b, for various industrial and laboratory scale flotation cells and their resultant bubble surface area flux, S_b. Figure 64 shows a substantial difference in operating regimes between industrial and laboratory scale.

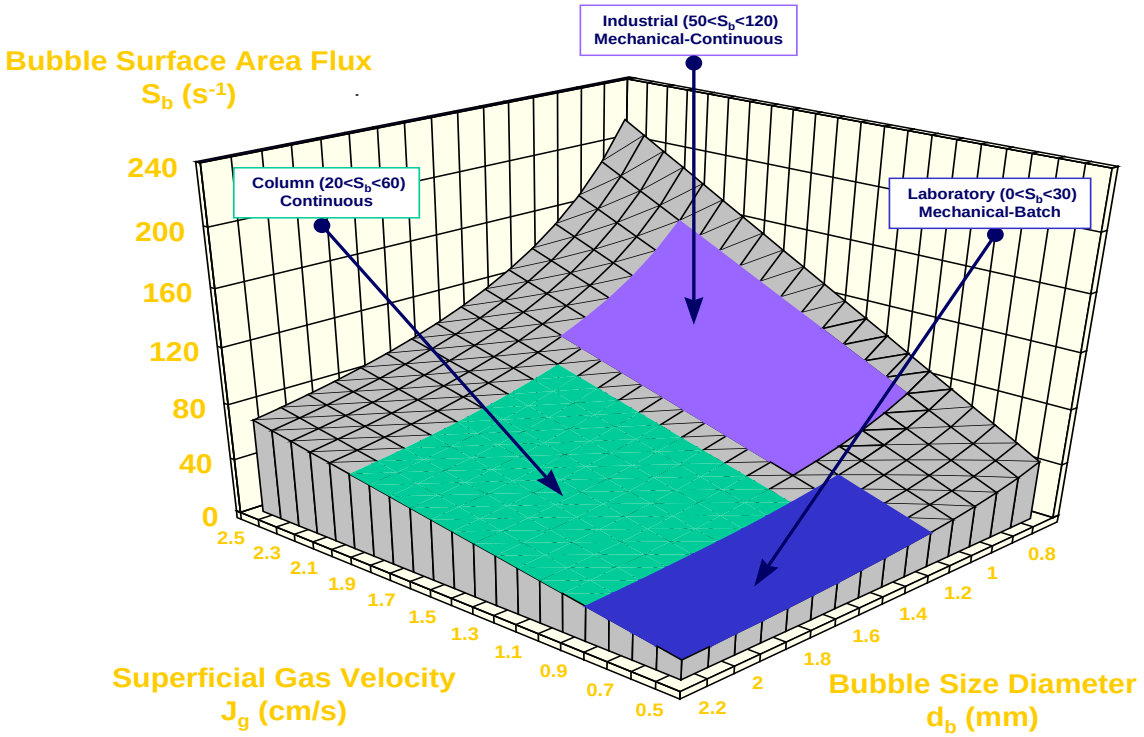

Figure 64: Bubble surface area flux as a function of both superficial gas velocity and bubble size – illustrating the normal operating region of industrial and laboratory flotation cells

Using the bubble surface area flux methodology applied to flotation modelling one can easily correct for these differences in terms of pulp flotation kinetics (Deglon, et al., 1999; Gorain, et al., 1995; Gorain, et al., 1997). However, the effect of these parameters is less well known for the froth phase performance. Moreover, bubble size distribution is typically not measured and/or controlled in laboratory experiments. Therefore, to evaluate the scale-up behaviour of the froth stability measurement, one should be aware of the pulp bubble size and the effect it has on the measurement.

This chapter will be divided into three sub-sections, namely:

- Section 5.2 – Glass frit characterisation. Glass frits, as specified in Section 3.1.3.1, are used to generate bubbles instead of the typical rotor-stator

assembly. This section will endeavour to characterise the bubble size produced by these glass frits with respect to air flow-rate, pore size and frit age.

- Section 5.3 – Effect of pulp bubble size on measured froth stability. In this section 3 different PGM ores as well as a 2-phase system was studied. The classical froth height as a function of time data collected will be displayed and discussed.
- Section 5.4 – Top-of-froth and side-of-froth bubble size as a function of pulp bubble size. In conjunction with the typical froth height versus time data displayed in the previous section, all experiments are analysed with respect to bubble size.

Please note that the related experimental methodologies for collecting the data displayed in this chapter can be found in Chapter 3 of this thesis.

5.2. GLASS FRIT CHARACTERISATION

The froth stability column is quite unique with regards to the fact that glass frits are used to produce the pulp bubble size distribution, as opposed to the conventional rotor-stator assembly. The glass frits were introduced in Section 3.1.3.1 and can be visualised as a porous piece of glass through which air can be sparged. The glass frits use an identification number, e.g. POR0, POR1, etc., based on the geometric pore size which is clearly defined in Table 6 (Chapter 3) and will be used as identification throughout this section.

5.2.1. EFFECT OF AIR ADDITION ON BUBBLE SIZE

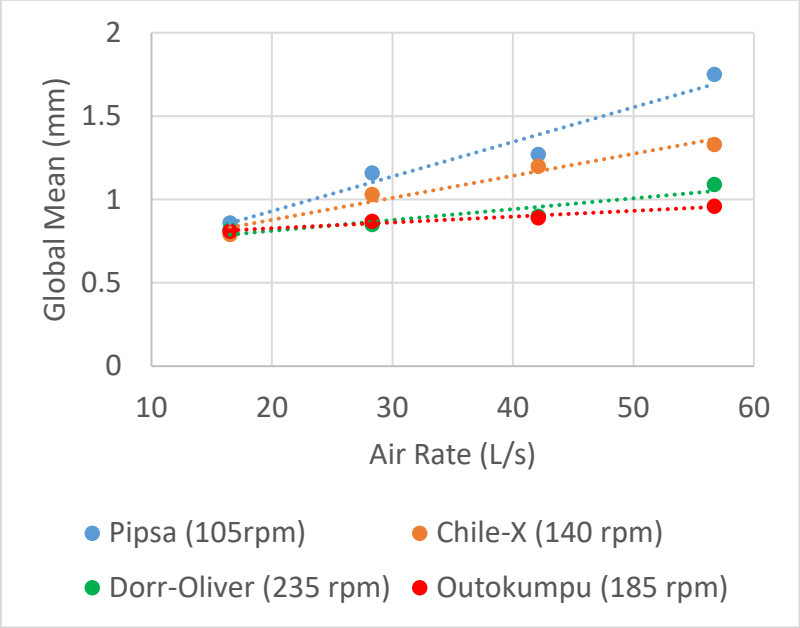

Figure 65: Mean bubble size produced by different rotor-stator types as a function of air addition rate (Gorain, et al., 1995)

Figure 65 highlights the effect of air addition rate on the global mean pulp bubble size produced by various rotor-stator assemblies. A well-defined linear increase in bubble size is seen with increasing air addition rate. Although the bubble generation mechanism is vastly different between a rotor-stator assembly and that of the glass frit; similar behaviour is expected where, in general, an increase in bubble size is expected with increasing air addition rate. An interesting observation from Figure 65 is the fact that even though different types of rotor-stator assemblies as well as varying tip speeds were used by Gorain, et al. (1995) a consistent minimum bubble size was seen. Also, it should be stated that currently air addition rate and the effect thereof on bubble size is not monitored during the froth stability experimental test. The effect of air addition rate on bubble size using conventional bubble generation is well known and therefore this exposes a limitation within the current froth stability methodology. Figure 66 displays the Sauter mean bubble size as a function of air addition rate for the five different pore size glass frits.

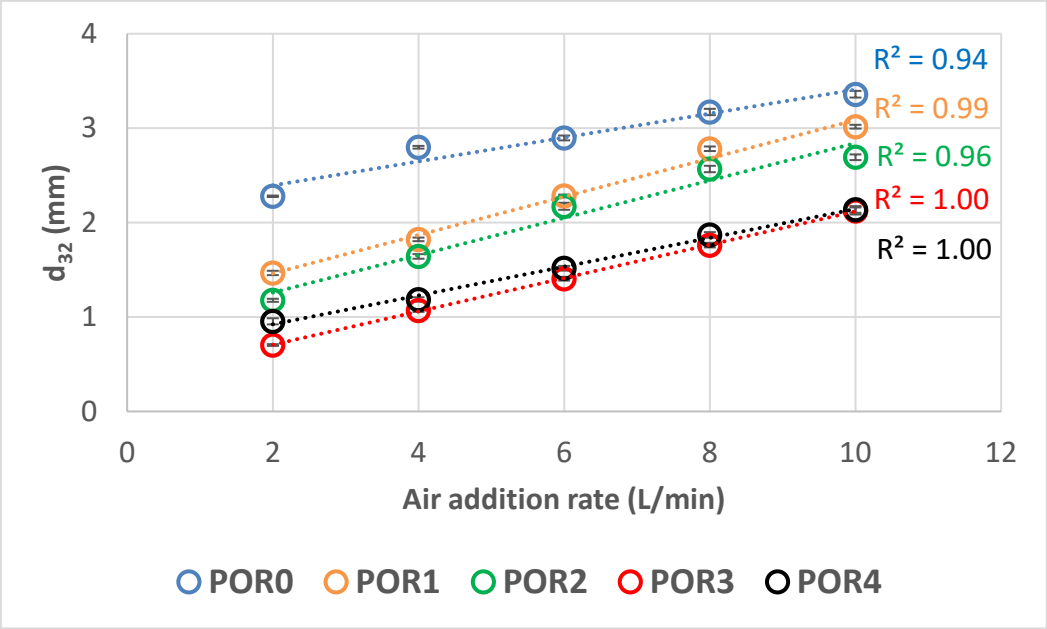

Figure 66: Sauter mean bubble diameter (d_{32}) as a function of air addition rate for 5 different geometric mean pore size glass frits

In general, the data presented in Figure 66 follows the expected linear trend that was indicated by the Gorain, et al., (1995), data set; i.e. Sauter mean bubble size increases linearly with increasing air addition rate. Moreover, the data follows a logical decrease in Sauter mean bubble size where the POR0 frit produces a larger bubble size than the POR1 frit for all air addition rates. The behaviour of the POR3 and POR4 glass frits are unexpected. In general, the POR4 produces either a similar or slightly larger Sauter mean compared to the POR3. It is thought that this behaviour is unfortunately inherent in the frits themselves and therefore unavoidable. The porous glass disc is fitted within a slot machined out of the Perspex stability column and O-rings are used to ensure a tight fit is achieved. Unfortunately, the porous glass frit will never be completely sealed against the solid surface of the stability column and therefore air

will escape at the side of the glass frit. As the porosity of the glass frit is decreasing, more resistance to flow through the glass frit is experienced which means that both the POR3 and POR4 will experience vastly more resistance than the POR0.

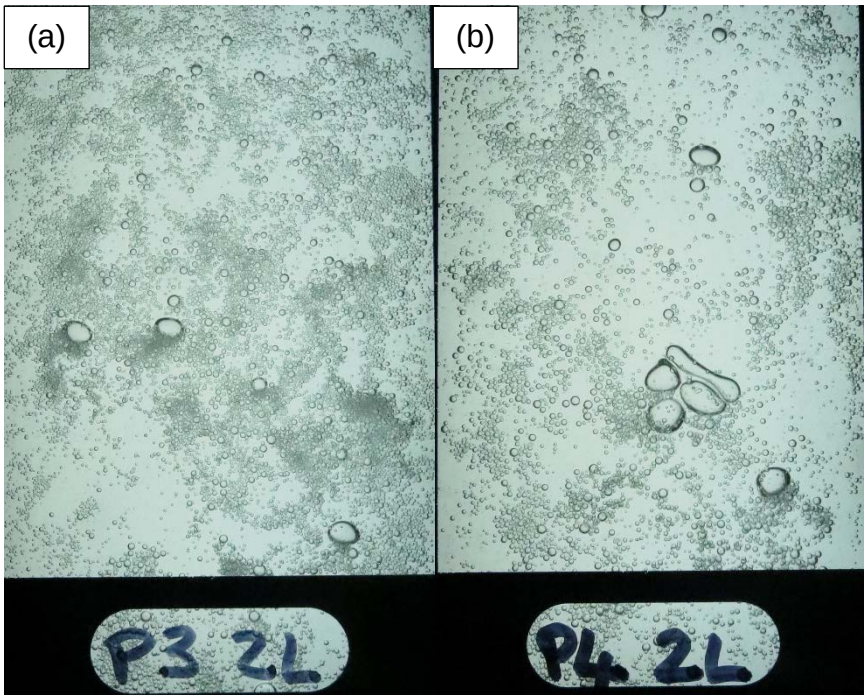

Figure 67: Photograph of sampled bubbles for (a) POR3 glass frit, (b) POR4 glass frit

It can be seen from Figure 67 that both POR3 and POR4 glass frits produce a few large bubbles, however, it is slightly worse in the POR4 frit as blooms of large bubbles are often seen passing by the sampling glass. These large bubbles are sampled by the bubble sizing software and can cause a large bias towards larger mean bubble sizes especially when using Sauter mean to approximate the population mean. As stated previously, this behaviour cannot be corrected for with a simple design modification and therefore this discussion rather highlights the fact that it does occur and operators should be conscious of it.

5.2.2. EFFECT OF PORE SIZE ON BUBBLE SIZE DISTRIBUTION

The main benefit of using glass frits is the fact that bubble size can be changed without significant changes to the hydrodynamic and/or mixing regime within the pulp phase. In a conventional rotor-stator setup, bubble size is usually changed by changing the geometry of the setup, rotational speed and/or air addition rate – all of which significantly affects the mixing and contacting regime within the pulp phase. The use of glass frits allows the froth stability column to be operated at a constant air addition and mixing rate while significant changes to the resulting bubble size is brought about by using a smaller pore size glass frit. Figure 68 highlights the fact that a linearly increasing trend is seen between Sauter mean bubble size and the geometric mean pore size.

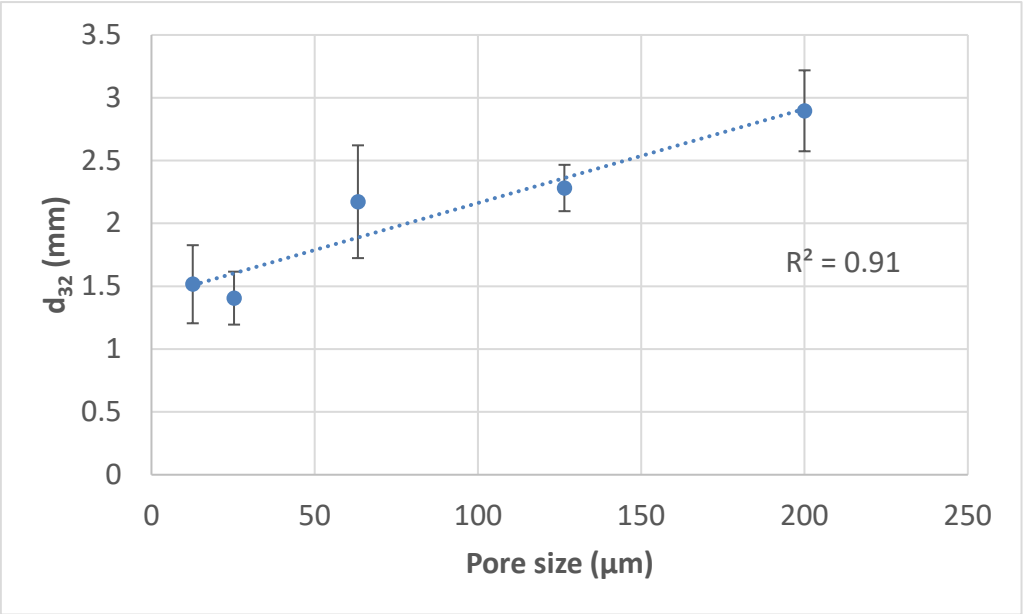

Figure 68: Sauter mean bubble size as a function of pore size operating at 6 L/min and 100 ppm Senfroth 516

In the previous section standard error was used to illustrate the confidence in the mean (which will be very high due to the vast number of bubbles sampled). Figure 68 displays the standard deviation of the measurements to illustrate the distribution of the data around the mean. This is done to highlight the fact that in general the distributions generated by the glass frits are quite wide and prone to random variation; whereas the bubble size distributions measured on plant are much more sharply defined and narrow. As was the case in the previous section, the bubble sizes produced by the POR4 and POR3 glass frits are somewhat unexpected with the smallest pore size glass frit (POR4) producing a slightly larger Sauter mean. A potential issue of bias for the Sauter mean was highlighted previously and therefore it will be valuable to have a look at the respective bubble size distributions as well.

Figure 69 shows the shape of the bubble size distribution for the different pore size glass frits. There are some interesting observations:

- The POR0 and POR1 distributions are very wide and show bimodal behaviour. Bimodal behaviour is usually seen when coalescence occurs due to lack of frother. In the case of these experiments the frother addition was in excess of the Critical Coalescence Concentration (CCC) and therefore the bimodal behaviour is a direct result of the bubble generation mechanism.
- The POR2 distribution is not bimodal, but it is very wide which was indicated by the large standard deviation in Figure 68
- As indicated by Figure 68 the POR3 and POR4 bubble size produced are very similar; however, the POR4 distribution peaks at a slightly smaller bubble size while also having a slightly larger fraction of small bubbles. Even though the Sauter mean suggests fairly similar behaviour between the POR3 and POR4

glass frits, the bubble size distribution suggests that there is a significant, albeit small, difference.

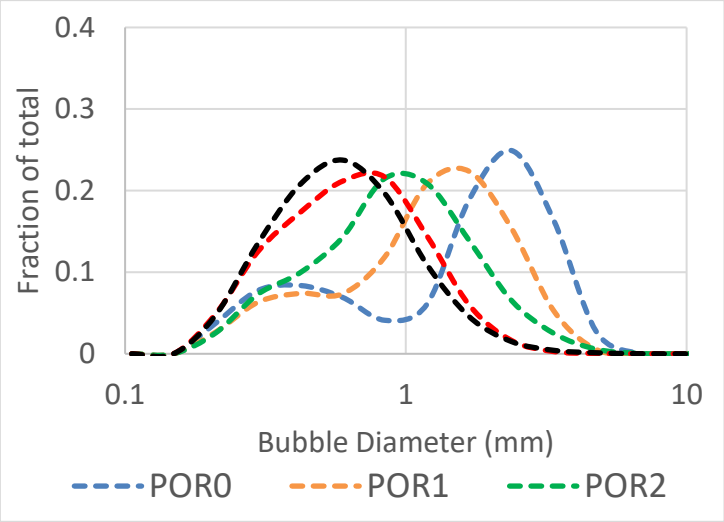

Figure 69: Bubble size distribution as a function of glass frit pore size at 6 L/min and 100 ppm Senfroth 516

5.2.3. EFFECT OF MANUFACTURING VARIANCE AND FRIT AGING ON BUBBLE SIZE DISTRIBUTION

The position of the glass frit in the stability column allows solids to settle onto it. Due to the porous nature of the glass frit, some solids might enter the disc and cause the pores to become blocked. Moreover, natural manufacturing variance will also lead to varied pore sizes even though it is labelled as a POR1 glass frit. Figure 70 displays the resulting Sauter mean produced by three independent and randomly selected new glass frits.

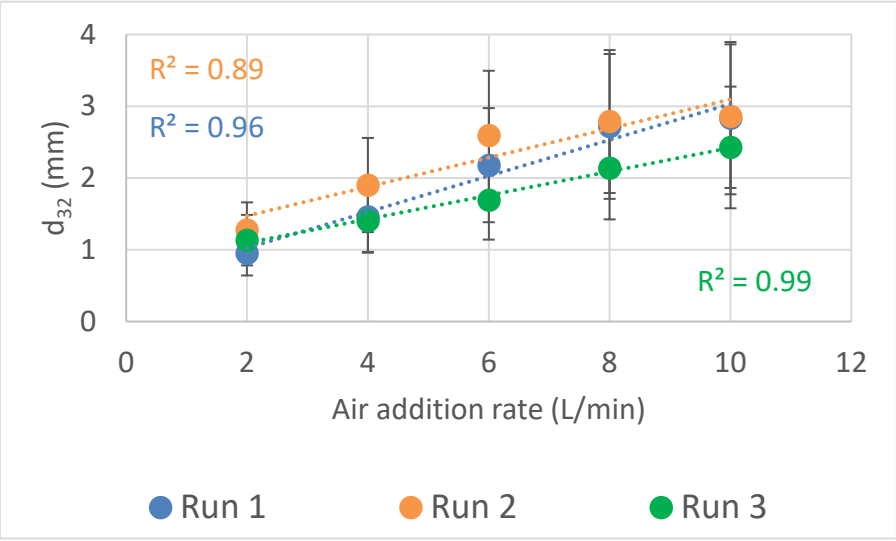

Figure 70: Sauter mean bubble size as a function of air addition rate where each run represents a new POR2 glass frit

The overall trend remains the same regardless of the run number, i.e. a linear increase in Sauter mean is seen with increasing air addition rate. That being said, it can be seen from Figure 70 that variation does occur in the Sauter mean produced depending on which frit was used, which indicates that random variation in the Sauter mean does occur between new glass frits which is most likely due to slight changes in pore size. The error bars displayed in Figure 70 are the standard deviations of the measured bubbles and therefore gives an indication of the distribution around the mean. For all the runs in Figure 70 this standard deviation range is overlapping indicating the individual distributions have similar width; however, as the Sauter mean indicates it would peak at slightly different bubble sizes.

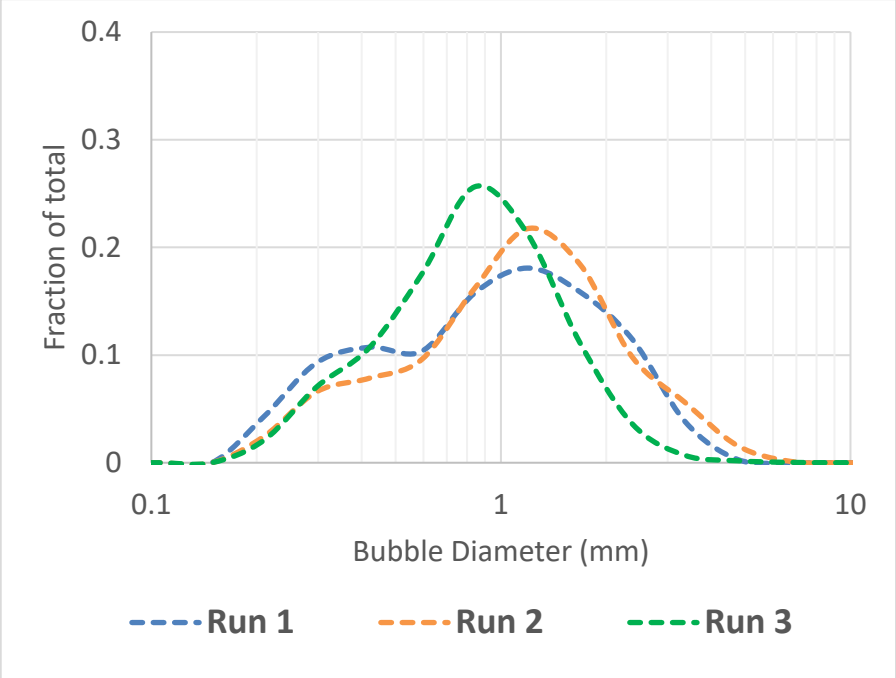

Figure 71: Bubble size distribution for three new POR2 glass frits operating at 6 L/min and 100 ppm Senfroth 516

Figure 71 highlights the behaviour mentioned above as it can be seen that all three glass frits produce a similar range of bubble sizes; however, significant changes in where this distribution peaks is present for all three. In particular the behaviour of run 3 should be highlighted as it peaks at a significantly smaller bubble size while also exhibiting unimodal behaviour whereas both the run 1 and 2 glass frits have bimodal behaviour. This difference does not appear to be that significant in Figure 70; however, it is thought that such a large fraction of smaller bubbles would dramatically affect the behaviour of the system. If each glass frit is characterised beforehand this type of difference should be clearly visible; however, if one POR2 glass frit is characterised and this is used to extrapolate similar pore sized glass frits it might lead to unexpected behaviour. Figure 72 displays the Sauter mean bubble size as a function of air addition rate for a new and used glass frit.

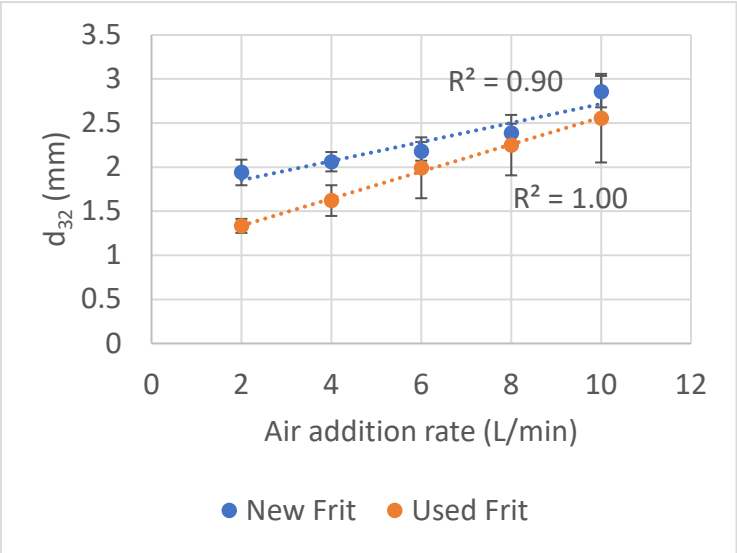

Figure 72: Sauter mean bubble size as a function of air addition rate for a new and used POR1 glass frit

The error bars displayed in Figure 72 are the standard deviations of the measurement and not the standard error. This is done to give an indication of the spread of data around the mean rather than an estimation of the confidence of the mean which would be rather good due to the large numbers of bubbles sampled. Figure 72 indicates that a shift in the Sauter mean bubble size produced by the frit has occurred; however, the distributions overlap from 6 L/min upwards indicating that this shift is not as pronounced and similar distribution shapes are present.

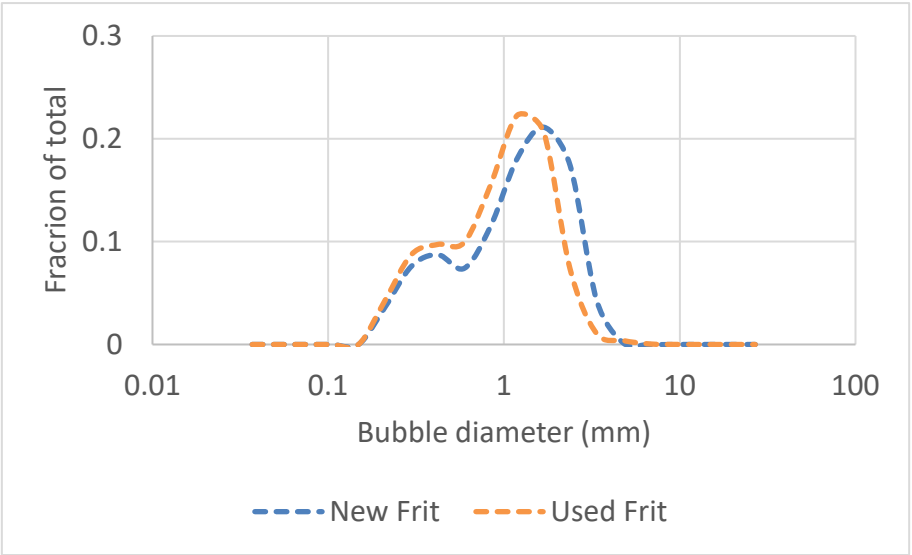

Figure 73: Bubble size distribution for a new and used POR1 glass frit operating at 6 L/min and 100 ppm Senfroth 516

Figure 73 displays the fact that the distribution shape is very similar between the new and used POR1 glass frit; with the major difference being that the distribution peaks at a slightly smaller bubble size for the used frit. Physically a smaller bubble size would be expected due to the relatively large pores of the POR1 frit; solids would easily enter

and block these pores and/or slightly obstruct the pores resulting in a net decrease in pore size. Whether this shift in bubble size is occurring due to aging effects and/or random variation in the pore size of the glass frits from manufacturing is unknown. The encouraging observation to take from the data displayed in Figure 72 and Figure 73 is the fact that even though shifts in the frit characteristics do occur; it appears to be statistically insignificant especially at air addition rates of 6 L/min and upwards.

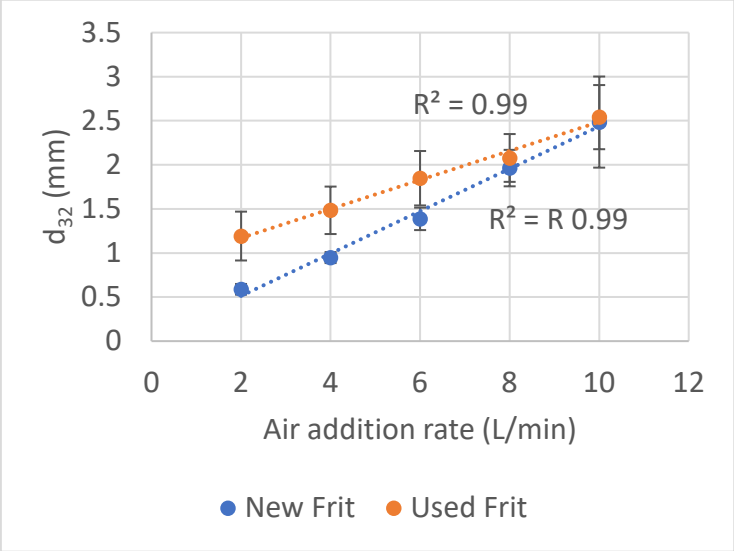

Figure 74: Sauter mean bubble size as a function of air addition rate for a new and used POR3 glass frit

Figure 74, much like Figure 72, shows a difference between the Sauter mean produced by a new and used glass frit; however, in this case the used frit produces on average larger bubbles. It is thought that the fact that larger bubbles are repeatedly produced at low air addition rates is an indication of the pores being blocked. As the pore open area decreases, an increase in resistance to flow through the glass frit is experienced and therefore this causes air to leak at the side of the frit. This mechanism has been described previously during the discussion of the comparison between a POR3 and POR4 glass frit and it does appear to be present throughout the data as the pore open area is decreased. Unfortunately, this means that care should be exercised when running small pore glass frits as these appear to be more susceptible to leaking. Figure 75 highlights the shift experienced in the bubble size distribution between a new and used POR3 glass frit operating at 6 L/min. It can be said that in general the range of bubble sizes produced remain similar; however, significant changes in the distribution peaks occur. It is thought that even though the distributions are only slightly different; the increase in the fraction of smaller bubbles for the new frit will have noticeable effects on the overall system in terms of froth stability.

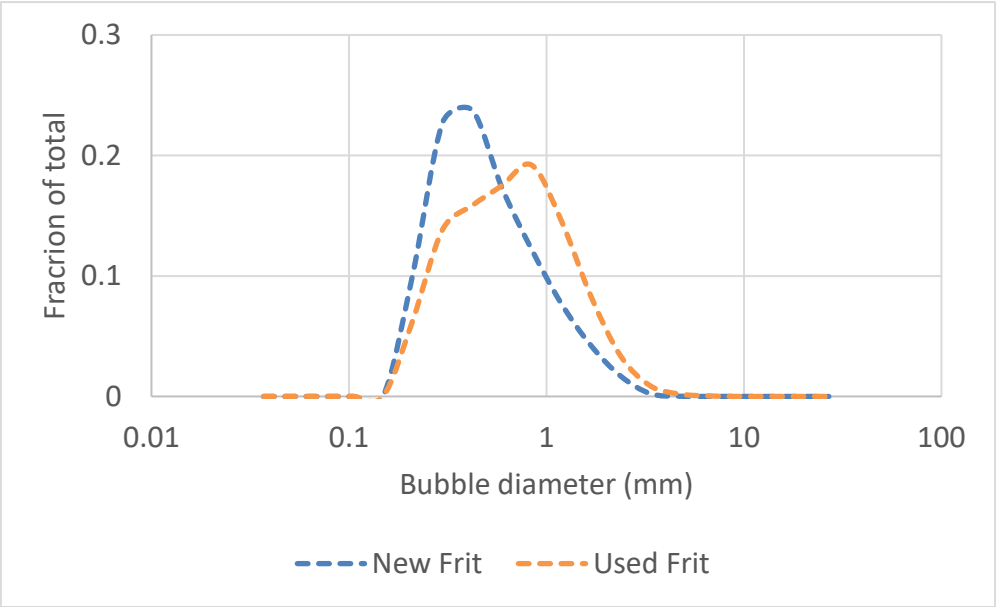

Figure 75: Bubble size distribution for a new and used POR3 glass frit operating at 6 L/min and 100 ppm Senfroth 516

In summary it has been shown that changes in the Sauter mean and bubble size distributions occur as a result of manufacturing variance and/or aging. This effect is most pronounced at air addition rates below 6 L/min and small pore sized glass frits. Ideally one would want an online measurement of the pulp bubble size; however, seeing as this will add to the experimental complexity it is advised that the operator should at least characterise each glass frit once. The current methodology where pulp bubble size is not characterised is probably not unheard of for studies where comparative results are required; however, concern must be expressed at the lack of measurement regarding the bubble size.

5.3. MEASURED DYNAMIC STABILITY AS A FUNCTION OF PULP BUBBLE SIZE

The characteristics of the glass frits used to generate the bubbles for the stability column have now been discussed. It was seen that numerous factors affect the Sauter mean and bubble size distributions produced by the glass frits. This section will focus on using the five different geometric mean pore sized glass frits to generate different bubble sizes while the other parameters are kept constant as far as possible. In addition to the five different pulp bubble sizes; three different PGM-bearing ores were used in the experimental campaign. It is important to note, as stated in Chapter 3, the solids percent passing 75 µm as well as the reagent addition were kept constant throughout this test work. The Platreef ore was used to perform a repeat with more than a year separating the experiments, the only difference being a baffle system was added to the stability column to ensure better mixing of the pulp phase. The dynamic stabilities for each experimental condition are presented in Figure 76 as this gives a

good platform for discussion of the results. The dynamic growth curves, used to determine the dynamic stability, can be seen in the appendix.

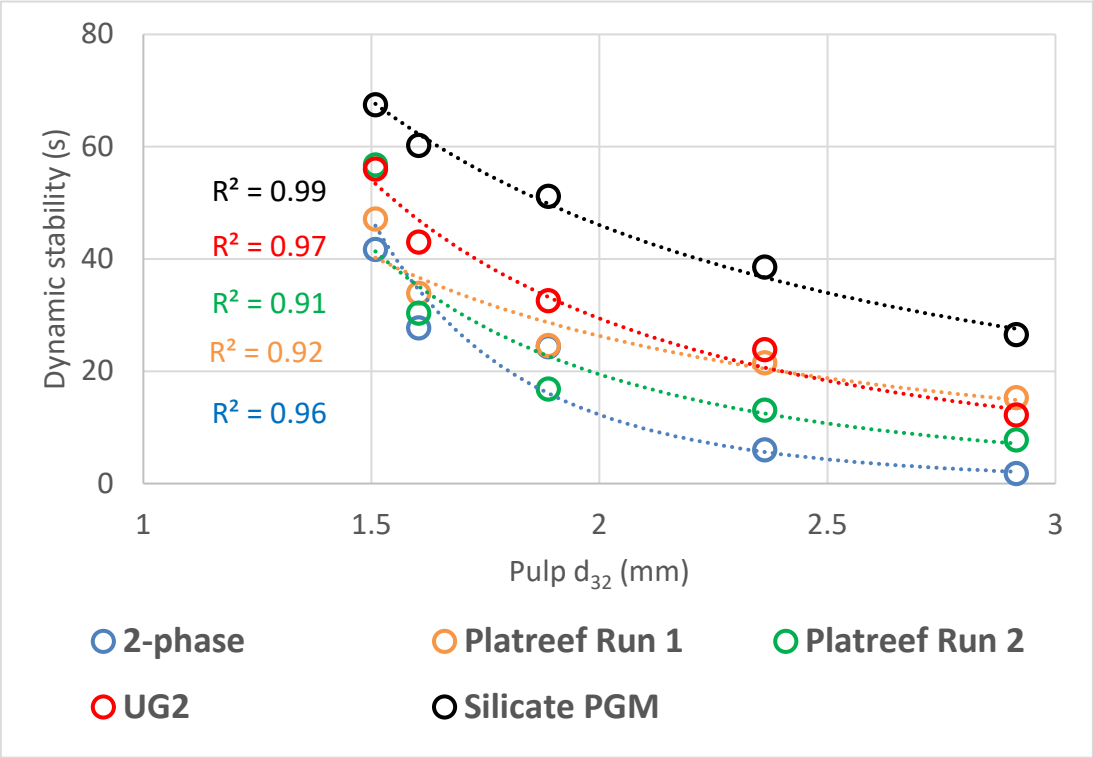

Figure 76: Dynamic stability as a function of pulp Sauter mean (d_{32}) bubble size for all experimental systems (2-phase and 3-phase)

The overwhelming observation from Figure 76, regardless of ore-type, is that the measured dynamic stability decreases with increasing pulp bubble size. This decrease in measured dynamic stability can be well described by a power law relationship regardless of the ore-type. This observation follows the original hypothesis and it is thought that the behaviour is seen due to the following mechanisms:

- An increase in the pulp bubble size results in an increase in the global average froth/foam bubble size which then significantly alters the drainage characteristics of the froth/foam (Kostoglou, et al., 2015).
- Large froth/foam bubbles will on average have less water per volume of froth/foam and hence the bubbles are more susceptible to coalescence (Farrokhpay, 2011). This has been experimentally proven by Morar, et al., (2012) who showed that large bubbles are more likely to burst.

Apart from the fact that the data conforms to what was expected there are other interesting secondary observations to be made from the data set. In general, it can be seen that the 3-phase systems achieved a higher dynamic stability than that of the 2-phase system. This highlights the stabilising effect solids have on the froth and this is present regardless of the starting pulp bubble size. From Figure 76 it can be seen that the repeat runs of the Platreef ore, a year apart, resulted in significantly different

dynamic stabilities. It is unclear whether this change in dynamic stability is due solely to the addition of baffles to the stability column or whether there have been changes in the pulp bubble size also. This highlights an important problem with the current froth stability methodology which deals with the lack of online pulp bubble size measurement. Section 5.2 has highlighted the fact that significant change in bubble size can occur solely based on the characteristics of the glass frit. This fact coupled with the poor scale behaviour of the dynamic growth method leads to experimental uncertainty which highlights the need for a scale independent measure. Lastly, the behaviour of the UG2 ore is quite surprising as it generates a similar or slightly higher dynamic stability than the Platreef ore. It is thought that the UG2 ore, which has much less naturally floatable gangue than that of Platreef, will result in a mostly barren and therefore less stable froth. Naturally floating gangue is thought to be closely related to the amount of altered silicates; however, the results in Figure 76 suggest that it might be heavily influenced by the bulk mineralogy as well. That being said, seeing as the particle size distribution of both ores are not fully characterised for this study the UG2 ore might be substantially finer than the Platreef while still meeting the 50 % passing 75 µm criteria. The aforementioned explanation does make sense as the milling time for both UG2 and Platreef were similar while it is known that a UG2 ore is substantially softer than a Platreef ore.

5.4. TOWARDS A SCALE INDEPENDENT ANALYSIS OF FROTH STABILITY

Foam literature highlights the differences in drainage that occurs due to bubble size changes, with foams of larger bubble size draining substantially faster (Koehler, et al., 1999; Saint-Jalmes & Langevin, 2002). The experimental results displayed in Section 5.3 indicate that there is a significant change in dynamic stability with changing pulp bubble size. This behaviour is thought to be as a direct result of drainage differences and not due to an actual change to the film stability. As has been discussed in Section 4.4, dynamic stability is a function of drainage as well as film stability. If parameters such as ore type, particle size distribution, reagent addition and/or reagent type, are considered; it can be said that such changes would result in significant changes in how the bubble films are loaded and subsequently drain. Therefore, changes as mentioned before will result in large changes in film stability. Changes to scale parameters, such as pulp bubble size, will not change the material presented to the bubbles and therefore the film should load in a constant manner, i.e. there should be a maximum terminal bubble size that can be stable at the current bubble loading. This will be the case even though it might occur across a much shorter height span due to the drainage differences induced by the change in pulp bubble size. This idea has proved valuable for the analysis of column diameter effects and therefore it will be extended to pulp bubble size.

5.4.1. TOP-OF-FROTH BUBBLE SIZE

Section 3.2.1.2 of Chapter 3 discussed a video technique for froth growth tracking. All laboratory scale experiments used this technique and therefore it is possible to get an estimate of top-of-froth bubble size for each experiment.

5.4.1.1. TOP-OF-FROTH BUBBLE SIZE AS A FUNCTION OF PULP BUBBLE SIZE

Figure 77 shows the top-of-froth bubble size distributions experimentally determined for the 2-phase system.

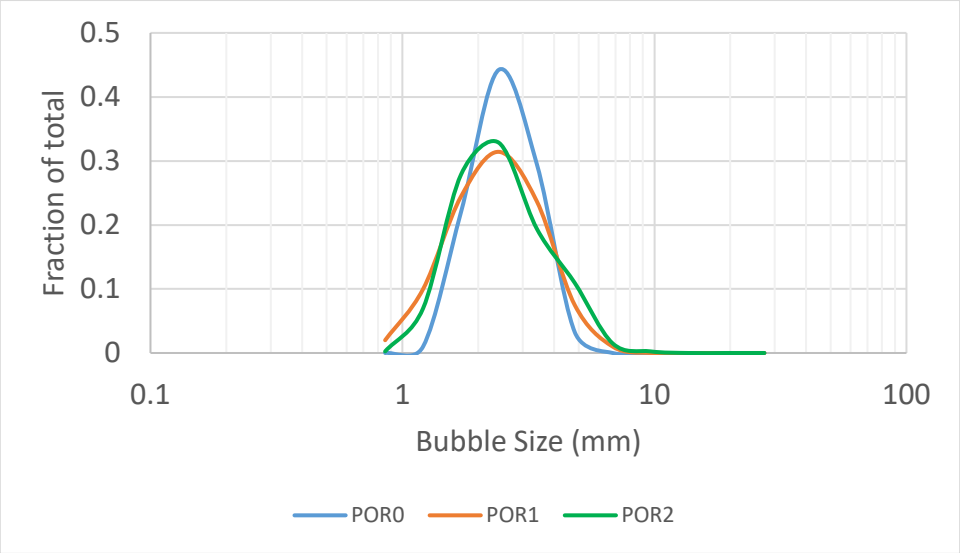

Figure 77: Top-of-froth bubble size distribution as a function of pulp bubble size for the 2-phase system

Figure 77 does not show the bubble size distributions for the POR3 and POR4 experiments due to the fact that bubble edges are difficult to identify as a result of the optical properties of the 2-phase system. Nonetheless, it can be seen from Figure 77 that the top-of-froth bubble sizes are very similar for all the experiments. The POR1 and 2 distributions are essentially the same; while the POR0 distribution has a very similar shape but some discrepancies in the absolute values. It should be noted that only 400 bubbles were measured to obtain the trend seen in Figure 77 and therefore absolute values are mostly irrelevant and the main observation should be the shape of the curve.

Figure 78 displays the top-of-froth bubble size distribution for the first run with Platreef ore. The shape of the individual distributions are remarkably similar and peak at a similar bubble size which is indicative of a constant top-of-froth bubble size, i.e. top-of-froth bubble size is independent of pulp bubble size.

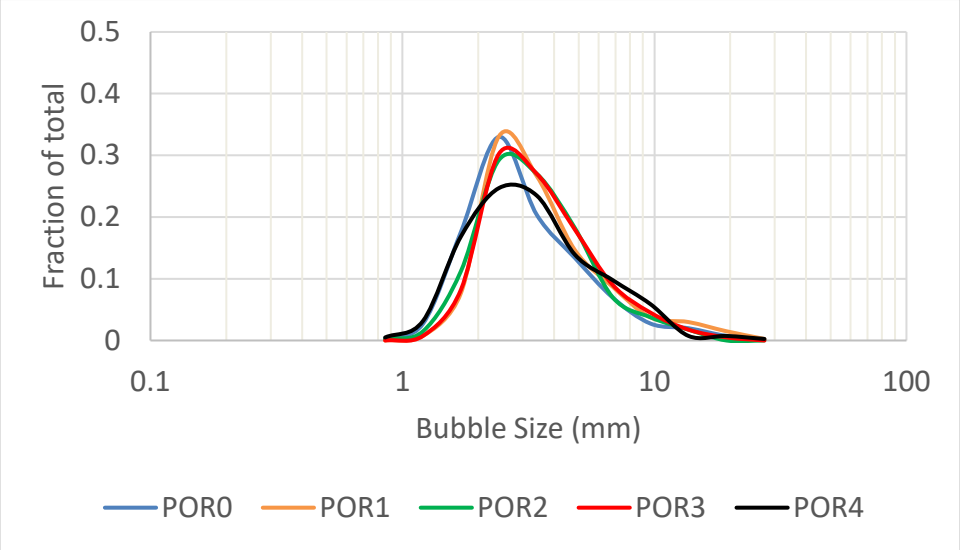

Figure 78: Top-of-froth bubble size distribution as a function of pulp bubble size for repeat one of the Platreef system

Figure 79 displays the experimentally determined top-of-froth bubble size distributions for the second Platreef run.

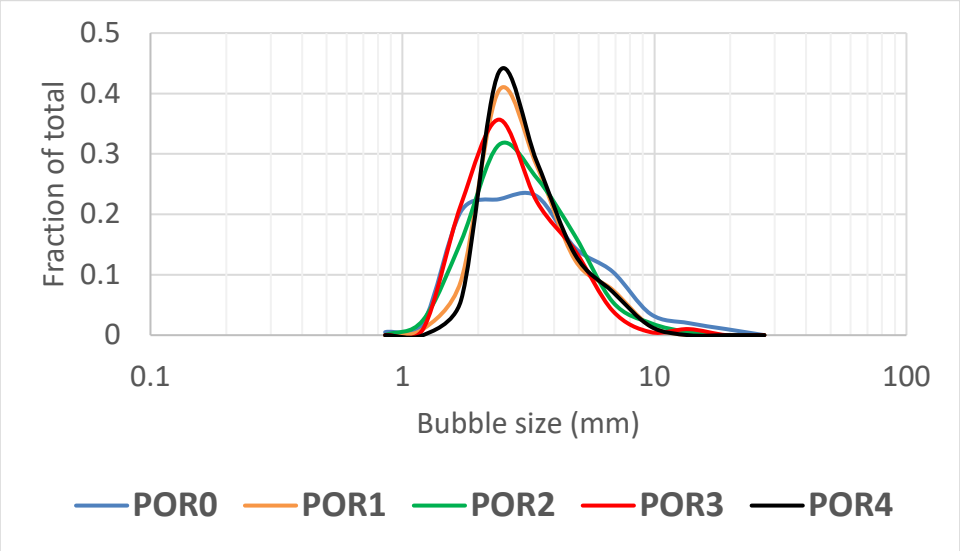

Figure 79: Top-of-froth bubble size distribution as a function of pulp bubble size for repeat two of the Platreef system

As was the case with the previous Platreef data, all the bubble size distributions have remarkably similar shapes and peak at a similar bubble size. If the dynamic stability data of Figure 76 is observed again, it can be said that significant differences were present for the dynamic stability of the entire pulp bubble size range of the two Platreef runs. This is not seen if Figure 78 and Figure 79 are compared as the distributions peak at fairly similar values as well as the fact that the shapes of the distributions are remarkably similar. However, more on the comparison of the different ore-types will be discussed later in Section 5.4.1.2. For the data displayed in Figure 79 only 200 bubbles were sampled for sizing which can be statistically challenging seeing as there

is large variance at the top-of-froth. Nonetheless, the repeatability between the different runs is good and it compares well with the previous Platreef data and therefore there is no evidence to suggest too few bubbles were sampled.

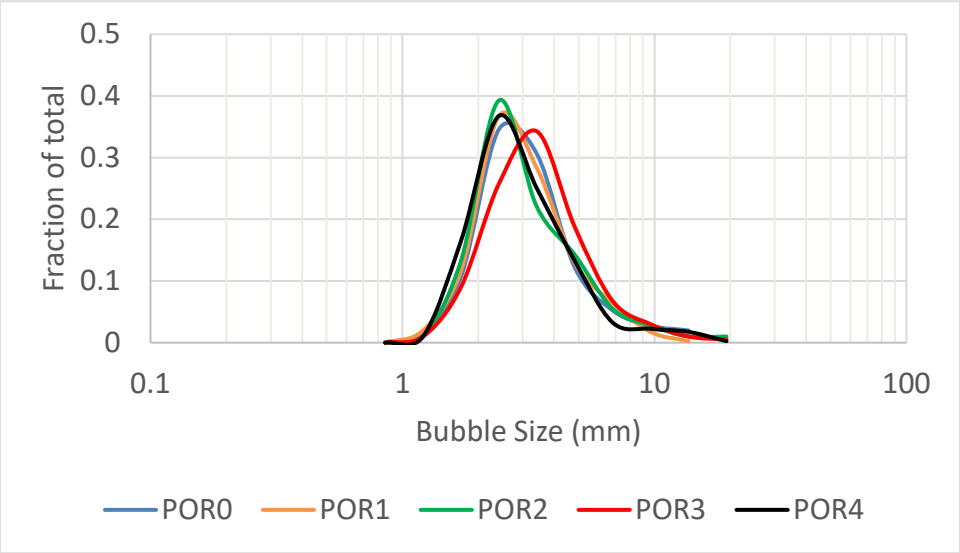

Figure 80: Top-of-froth bubble size distribution as a function of pulp bubble size for the UG2 system

The consistent behaviour of the top-of-froth bubble size distribution that has been seen throughout this section is repeated in Figure 80 for the UG2 system. Figure 81 displays the top-of-froth bubble size behaviour for the silicate-rich PGM ore.

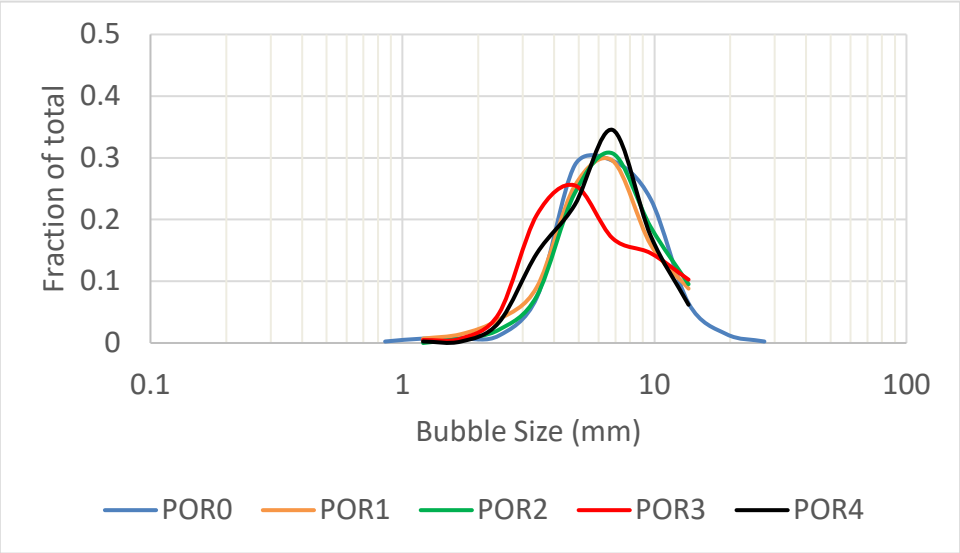

Figure 81: Top-of-froth bubble size distribution as a function of pulp bubble size for the silicate-rich PGM ore

The distributions are very similar, and this has been consistently seen for all other data sets. The POR3 distribution should be highlighted as it does have slightly different behaviour compared to the others. It is difficult to formally conclude whether this is an actual effect or if it is artificial due to the limited number of bubbles sampled.

In summary, a review of all the bubble size distributions indicates the consistent behaviour of the top-of-froth bubble size for the different pulp bubble sizes used. This can be further summarised by stating that for a particular experimental system (ore-type and reagents) the top-of-froth bubble size is independent of the initial pulp bubble size. For a defined loading, which is not changed during the pulp bubble size experiments, a maximum bubble size can be stabilised and this does not change. However, what does change is how long the system takes to reach the maximum bubble size criteria, i.e. in a system that drains substantially faster this maximum bubble size will be achieved much earlier, or most importantly, at a lower maximum height. This is the reason that even though significant dynamic stability changes are seen; it does not affect the top-of-froth bubble size and therefore this can be used to define froth stability independent of scale.

5.4.1.2. Top-of-froth Bubble Size as a Function of Ore Type

Section 5.4.1.1 highlighted the fact that top-of-froth bubble size is constant regardless of the starting pulp bubble size for a specific ore type. This is a valuable observation as it points to the fact that scale parameters, such as pulp bubble size, might not affect top-of-froth bubble size which in turn can be used to approximate froth stability. This section will elaborate on this idea and plot the different top-of-froth sizes as a function of ore type with the main question being, are there measurable differences in the top-of-froth distribution when the froth stability is changed? Figure 82 displays the top-of-froth bubble size distribution for all the experimental systems.

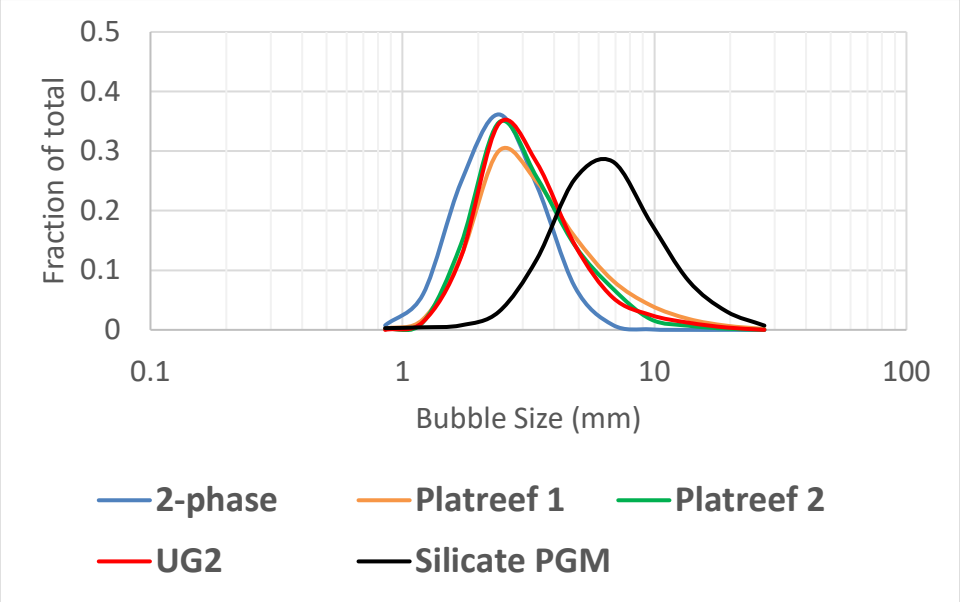

Figure 82: Top-of-froth bubble size distribution as a function of ore type

If the two extremes, 2-phase and silicate PGM ore, are observed the silicate PGM ore has a much larger mean top-of-froth bubble size. This is directly in line with previous observations that the silicate PGM ore generated the most stable froth, i.e. the bubble

has more time to grow, increasing coalescence during this time. Figure 82 also highlights an interesting observation, i.e. the 2-phase, Platreef 1, Platreef 2 and UG2 system all peak at similar bubble sizes. Dynamic froth stability tests have shown the 3-phase systems to be much more stable and therefore it is interesting to observe a similar peak in the aforementioned systems. That being said, all the 3-phase systems (Platreef 1, Platreef 2 and UG2) have a significantly larger portion of bubbles larger than 3 mm and therefore indicates that there is a difference in top-of-froth bubble size. To fully illustrate this the Sauter mean of all the systems is plotted against a stability indicator in Figure 83.

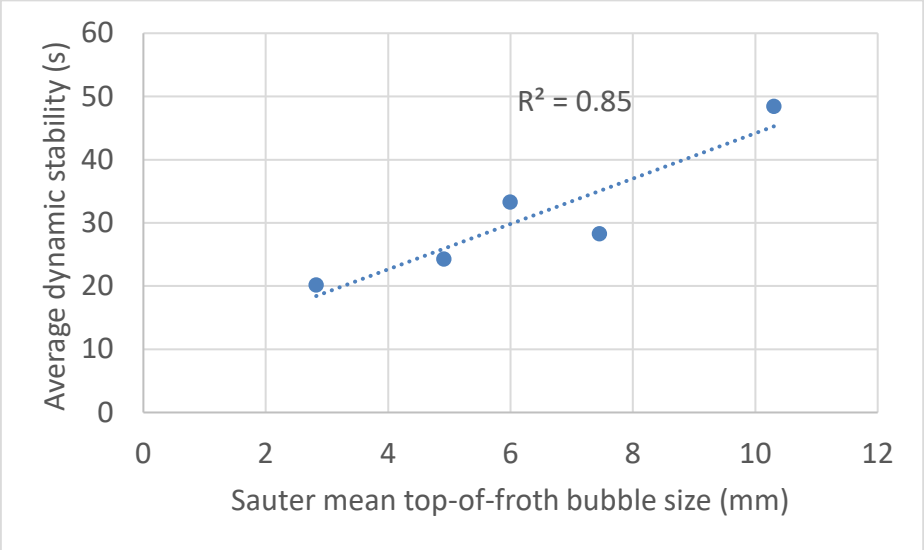

Figure 83: Average dynamic stability for each experimental system as a function of Sauter mean top-of-froth bubble size

Firstly, the parameter plotted on the y-axis of Figure 83 should be defined to avoid any confusion in the meaning thereof. The average dynamic stability is simply the average of the five dynamic stabilities displayed in Figure 76. This parameter has no mechanistic meaning; however, it does provide a quantitative basis from which the different systems can be compared. Figure 83 clearly shows an increase in average dynamic stability with increasing top-of-froth Sauter mean bubble size. It shows that the 3-phase systems are more stable than the 2-phase system which was not explicitly clear in Figure 82. Moreover, the Platreef 1, Platreef 2, and UG2 systems all seem to be close to one another, which was highlighted in Section 5.3. It is encouraging to see both Platreef repeats so close to one another even though there are significant differences in measured dynamic stability.

5.4.2. SIDE-OF-FROTH BUBBLE SIZE

It was mentioned in Section 4.4.2 that viewing bubble size changes for the entire froth height is thought to be more representative than observing a boundary condition such as the top of the froth, which is susceptible to large variance. This section will build

from what has been shown in Section 4.4.2 and therefore a few important observations will be highlighted:

- Variations in both column diameter and pulp bubble size result in vast differences in equilibrium froth height. It is necessary to correct for froth height so that all the experiments can be viewed on a common froth height scale. Equation 18 has been put forth as a correction method and the use thereof will be continued here.
- The column diameter results showed that coalescence rate is a function of corrected froth height and in general an exponential increase in bubble size is seen with increasing froth height. The exponential trend defined for the 100 mm and 200 mm column is similar, showing the usefulness of the scale correction. This will be tested and illustrated with pulp bubble size in this section and seeing as no changes to the material loading onto the bubble are made it is expected to perform similarly. It is predicted that a characteristic exponential trend will emerge for each system and this will be independent of pulp bubble size.

5.4.2.1. Side-of-froth Bubble Size as a Function of Pulp Bubble Size

There were no side-of-froth bubble size measurements done for the 2-phase system due to the difficulty in observing bubble edges. Figure 84 displays the side-of-froth Sauter mean bubble size for the first run with Platreef ore.

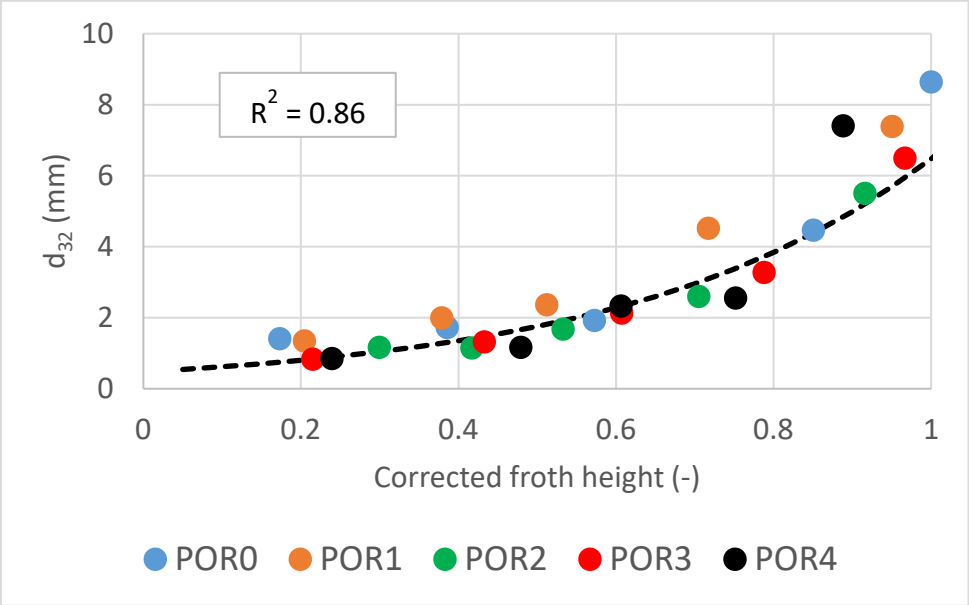

Figure 84: Sauter mean bubble size as a function of corrected froth height for the five different pore size glass frits of the first run with Platreef

As expected all the pulp bubble size experiments fall onto one characteristic line which defines the bubble size increase as a function of corrected froth height. This closely follows the observations made during the top-of-froth discussion as well as the observations made for column diameter, i.e. film stability remains constant throughout,

regardless of the pulp bubble size. Moreover, the detailed side-of-froth data is even more convincing than the single top-of-froth sample that has been shown in the previous section due to the numerous data points. Figure 85 displays the Sauter mean bubble size as a function of corrected froth height for the second Platreef run.

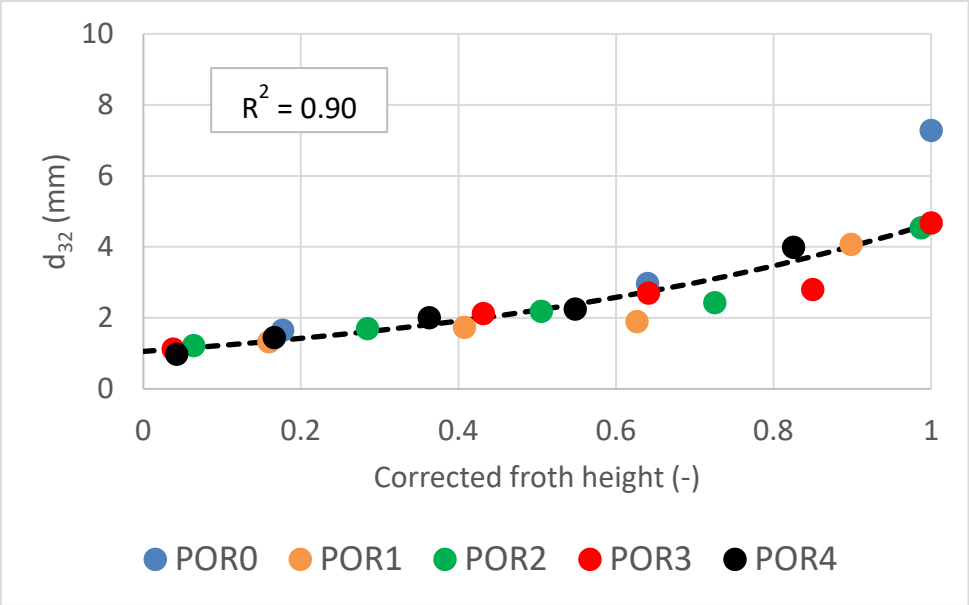

Figure 85: Sauter mean bubble size as a function of corrected froth height for five different pore size glass frits of the second run with Platreef

The shape of the curve in Figure 85 is distinctly flatter than that in Figure 84. That being said, the overall behaviour of the second Platreef run is similar to the first, i.e. all the different pulp bubble size experiments collapse onto one characteristic curve. The reason behind the flatness of the curve is thought to be due to difficulty in gaining a representative top-of-froth sample for bubble size (in Figure 85 the top-of-froth region would be the values close to 1 on the x-axis). Evidence of the variance experienced at the top-of-froth region is evident in Figure 85 as experimental bubble size values range from 4.5 mm to 7 mm at a corrected froth height of 1. This observation has been made throughout the sections discussing bubble size; however, at this point it is thought more background should be given as to the reason behind this. Firstly, one should consider the chaotic behaviour of the bubbles at the top of the froth as bubbles are constantly bursting and/or coalescing. Numerous photographs are taken of this chaotic event and usually only a select few of these photographs are then used for bubble sizing due to time constraints. Secondly, if one photograph is observed, numerous different bubble sizes will be present. Once again, only a select few, usually 100 bubbles per photo, are selected to be sampled for size. The solution to the described sampling errors is taking more photographs for analysis and subsequently more bubbles within those photographs. Unfortunately, due to the fact that bubble size is manually determined this is not feasible as the resulting analysis time would become vastly longer. Figure 86 displays the Sauter mean bubble size as a function of froth height for the UG2 system.

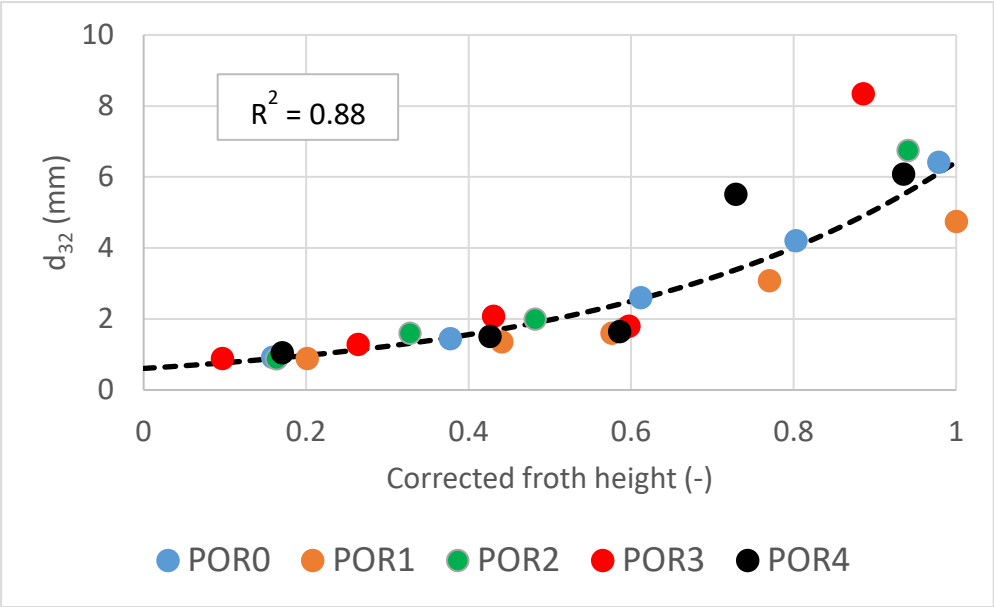

Figure 86: Sauter mean bubble size as a function of corrected froth height for five different pore size glass frits of the UG2 system

It can be seen from Figure 86 that the behaviour of the UG2 system is similar to all the other experimental systems, i.e. bubble growth versus corrected froth height is the same regardless of the starting pulp bubble size. Figure 86 also highlights the significant variation that occurs at the top-of-froth region as was discussed previously. Figure 87 displays the Sauter mean bubble size as a function of froth height for the silicate-rich PGM system.

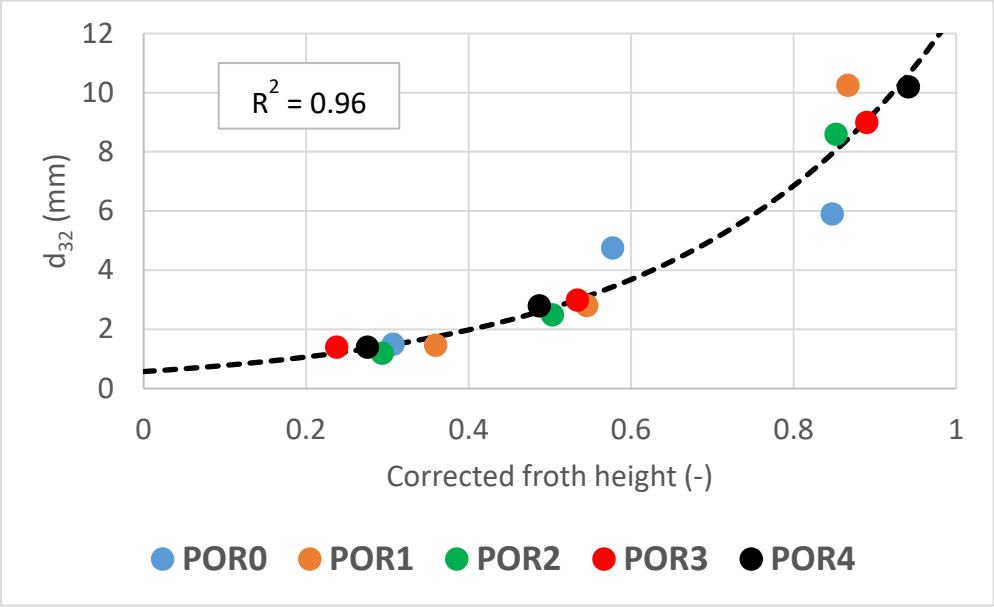

Figure 87: Sauter mean bubble size as a function of corrected froth height for five different pore size glass frits of the Silicate PGM system

The different pulp bubble size runs all collapse onto one curve which has been consistently seen throughout this section. The silicate-rich PGM ore is the most stable

and rheologically complex system tested and therefore it is encouraging to see the consistent behaviour of the side-of-froth bubble size.

In summary of all the side-of-froth bubble growth data displayed in this section – a consistent and repeatable trend is seen throughout, i.e. the rate of bubble growth as a function of corrected froth height is the same regardless of the starting pulp bubble size. This observation is directly in line with what was seen from the top-of-froth data as well as the column diameter data presented in Section 4.4. Changes in pulp bubble size will result in changes in the drainage kinetics and liquid content of the froth and this is known in literature (Farrokhpay, 2011; Koehler, et al., 1999; Saint-Jalmes & Langevin, 2002). However, the material (both quality and quantity) presented to the bubbles are no different and therefore remains constant unless an ore changes or reagent change occurs. Hence, no changes are occurring on the bubble film due to scale parameters and this will manifest as consistent coalescence behaviour at a defined froth height. Therefore, if bubble growth is viewed as a function of froth height, such as is the case for both top-of-froth and side-froth, it will be constant irrespective of the change in drainage caused by scale parameters. This behaviour has been extensively proven throughout this section and the section regarding column diameter and therefore it can be stated with confidence.

5.4.2.2. Side-of-froth Bubble Size as a Function of Ore Type

Displaying all data on one graph shows whether there are measurable differences in the bubble growth kinetics. Figure 88 displays the side-of-froth bubble size as a function of froth height for all the different ore types.

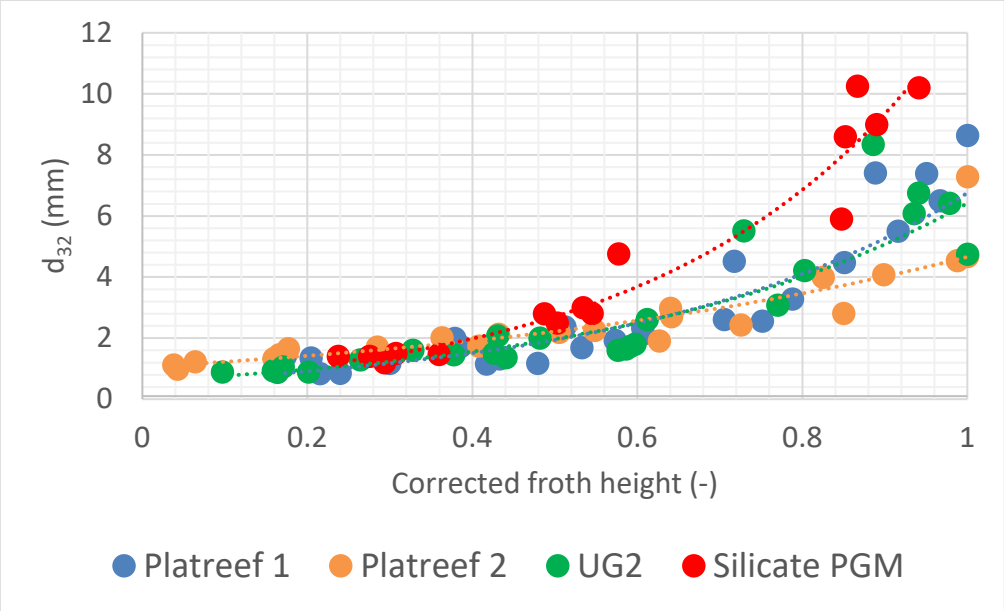

Figure 88: Sauter mean bubble size as function of corrected froth height for all 3-phase experimental systems

Firstly, a defined difference can be seen between the silicate-rich PGM system compared to the other 3-phase systems. The difference is especially prominent as one moves closer to the top-of-froth (approaching 1 on the x-axis in Figure 88). This was seen previously as there is a defined difference in the top-of-froth bubble size distributions; however, where Figure 88 is more insightful is the fact that it gives both the top-of-froth, as well as the gradient (or rate of change) of bubble size to froth height. Moreover, the behaviour of the Platreef and UG2 systems are very similar which points to the fact that film lifetime between these different systems seem to be very similar; a conclusion that was also observed for the top-of-froth bubble size distribution in Figure 82.

CHAPTER SIX:CONCLUSIONS AND RECOMMENDATIONS

6.1. CONCLUSIONS

This section highlights the main conclusions from this experimental work. It will be divided into two distinct sub-sections, namely: column diameter and pulp bubble size effects.

6.1.1. COLUMN DIAMETER EFFECTS

6.1.1.1. MEASURED DYNAMIC STABILITY AS A FUNCTION OF COLUMN DIAMETER

In total three different column diameter experimental data sets were shown. The main conclusion from all these data sets was that measured dynamic stability increases with increasing column diameter up until a maximum dynamic stability is reached. From the limited 2-phase studies on this subject it was seen that in general froth drainage increased with decreasing column diameter (Ambulgekar, et al., 2004; Brannigan & De Alcantara Bonfim, 2001; Papara, et al., 2009). This was attributed to the fact that wall films and Plateau borders drained up to seven times faster compared to interstitial Plateau borders (Papara, et al., 2009). As the column diameter decreases, the relative ratio of column surface area to bulk area increases and therefore this results in an increased drainage rate and subsequently less stable froth.

6.1.1.2. CORRECTING FOR COLUMN DIAMETER

An empirical correction for the significant changes in dynamic stability with column diameter was achieved. As mentioned the literature review highlighted the fact that the stability differences were a direct result of drainage differences between the wall and bulk. At the heart of the empirical correction is a ratio of wall surface area to total bubble surface area to account for the drainage differences which can then be simplified to a bubble size parameter divided by column diameter. There are two extremes for the aforementioned ratio:

1. As the ratio approaches one; the resulting measured dynamic stability will be zero, and;
2. As the ratio approaches an infinitely small value; the measured dynamic stability would reach a theoretical maximum.

This can be summarised in a mathematical form as is shown in Equation 19.

$$\Sigma_{measured} = \Sigma_{\infty}\left(1 - \left(\frac{D_b}{D_c}\right)\right) \qquad \textbf{Equation 19}$$

Equation 19 was then applied to the experimental data sets and in general the relationship described the empirical data quite well. Moreover, an interesting observation from the fitting process was the fact that the bubble size parameter in

Equation 19 was very similar to the experimentally determined top-of-froth Sauter mean. Mechanistically the bubble size parameter is used to calculate the surface area of the available bubbles and therefore it was thought it should represent some global mean of the entire froth. The Sauter mean calculation is inherently biased to large bubble sizes and therefore a global Sauter mean would be very close to a top-of-froth Sauter mean value. Therefore, the correlation seen between the bubble size parameter and top-of-froth Sauter mean is expected and if top-of-froth bubble sizes are available this could be used with relative confidence to reduce the fitting required for Equation 19.

6.1.2. BUBBLE SIZE EFFECTS

6.1.2.1. GLASS FRIT CHARACTERISATION

The froth stability column is quite unique with regards to the fact that glass frits are used to produce the pulp bubble size distribution, as opposed to the conventional rotor-stator assembly. That being said, little attention has been given to the characterisation of these glass frits. The following key observations were made regarding the performance of these glass frits:

1. The Sauter mean bubble size increases linearly with increasing air addition rate at a constant geometric mean pore size.
2. The Sauter mean bubble size increases linearly with increasing geometric mean pore size at a constant air addition rate.
3. Large variation in the Sauter mean between different frits of the same nominal pore size does occur due to manufacturing variance.
4. Frit aging, which refers to the choking of the pores of the glass frit due to solids, influences the Sauter mean and bubble size distribution. This effect is less pronounced at large pore sizes and air addition rates above 6 L/min.

6.1.2.2. DYNAMIC STABILITY AS A FUNCTION OF PULP BUBBLE SIZE

An exponential decrease in measured dynamic stability is seen with increasing pulp bubble size for all experimental systems. This exponential decrease is well-defined and repeatable for all the experimental systems tested and therefore significant confidence can be attached to this behaviour. This conformed to the hypothesis as a decrease in measured dynamic stability with increasing pulp bubble size was expected.

The 3-phase systems are more stable than the 2-phase system for all pulp bubble sizes which is indicative of the stabilising effect solids have on the froth phase. A surprising observation was that the UG2 system generates a similar or slightly larger dynamic stability than both Platreef repeats, even though it is commonly thought that UG2 froths are sparsely mineralised. The response of the silicate-rich PGM ore was of particular interest as this ore contains vastly more altered silicates than any of the

other 3-phase systems. Originally this ore was included for testing due to the rheologically complex froth that would result which would significantly alter the drainage characteristics of the froth. The silicate-rich PGM ore did result in the most stable system due to the reasons discussed above; however, the overall trend of an exponential decrease in measured dynamic stability with increasing pulp bubble size remained.

6.1.3. TOWARDS A SCALE-INDEPENDENT ANALYSIS

Numerous 2-phase studies have illustrated the dependence of bubble size growth as a function of foam height on the amount and type of surfactant present (Chang, et al., 1956; Kostoglou, et al., 2014; Marrucci, 1969; Saint-Jalmes & Langevin, 2002). In 3-phase froth systems where the presence of solids heavily affects the stability it has been found that various physical properties of the particles affect the rate of coalescence (Ata, et al., 2003; Dippenaar, 1982). Therefore, it can be said that the manner in which a bubble responds to growth is heavily influenced by the material loaded onto the bubble film, i.e. for a certain loading, albeit solids and surfactant or just surfactant, a certain maximum bubble size will be stable. This behaviour was confirmed by Morar, et al., (2012), who used machine vision techniques to analyse the top of various flotation froths and found that bubble burst rate, which can be viewed as froth stability, is solely dependent on top-of-froth bubble size and solids loading. If a hypothetical system is now observed where the only change is the column diameter, it can be said that the material quantity and quality presented to the bubble film will remain unchanged. Hence, a constant maximum size should exist for such a system.

The aforementioned assertion has been proven plausible for changes in column diameter and pulp bubble size. This can be further summarised by stating that for a particular experimental system (ore-type and reagents) the top-of-froth bubble size is independent of the starting pulp bubble size and/or the column diameter. For a defined loading, which is not changed during the column diameter or pulp bubble size experiments, a maximum bubble size can be stabilised and this does not change. However, what does change is how long the system takes to reach that maximum bubble criteria, i.e. in a system that drains substantially faster this maximum bubble size will be achieved much earlier, or most importantly, at a lower maximum height. This is the reason that even though significant dynamic stability changes are seen; it does not affect the top-of-froth bubble size and therefore this can be used to define froth stability independent of scale.

Concern has been stated regarding the sampling of bubbles for bubble size. To obtain a statistically accurate estimate of the population it is thought that vastly more bubbles should be sampled especially at the top-of-froth level. This, however, is not practically feasible at the moment as bubble sizing is done manually. Therefore, it was suggested that a side-of-froth bubble growth curve would be more representative. This

methodology, together with the proposed correction to froth height, was used on the data generated from all the experimental systems (column diameter and pulp bubble size). A consistent and repeatable trend is seen throughout, i.e. the rate of bubble growth as a function of corrected froth height is constant regardless of the column diameter and/or the starting pulp bubble size. This observation is directly in-line with what was seen from the top-of-froth data. Changes in scale parameters will result in changes in the drainage kinetics and liquid content of the froth. However, the material (both quality and quantity) presented to the bubbles is no different and therefore remains constant unless an ore change or reagent change occurs. This behaviour has been extensively proven throughout this research and therefore it can be stated with confidence.

6.1.4. GENERAL

An additional observation from the column diameter data sets was the fact that dynamic stability was measured on the same flotation cell, operating with similar superficial gas velocities, with two years separating the measurements. The 2013 data suggested that the dynamic froth stability was much higher than that of the 2015 data set. This highlights a step change in the behaviour of the froth within only 2 years most probably due to an ore change just to mention one possible cause. This is the exact long-term goal this research wants to address as changes in froth stability needs to be incorporated in the control strategy; however, due to lack of measurement this behaviour is quite challenging to predict.

6.2. RECOMMENDATIONS

This section will highlight the main recommendations from this research. Firstly, the design of the froth stability column will be addressed. It is recommended that a column diameter of 200 mm should be used as standard going forward. This is based on the observation that wall effects are negligible in the 200 mm column and upwards. The downside of using a 200 mm column as standard is the fact that much more feed material is used. Therefore, if the amount of feed material is restricted, the operator can continue using smaller column diameters. However, it should be noted that these tests can then only be used in a relative comparison and not in a bid to mimic plant conditions.

The pulp bubble size has been highlighted as a major contributor to the measured dynamic stability. There are two ways forward:

1. Each glass frit must be characterised beforehand to ensure that a constant bubble size is maintained. It has been shown that manufacturing variance does heavily influence the bubble size produced and therefore it is a must that all new glass frits must be characterised. Used frits have shown to drift due to choking of the pores and therefore ideally one would have to characterise

these continuously; however, this could be minimised by using large pore size glass frits and operating above 6 L/min per frit.

2. Online pulp bubble size characterisation should be built into the froth stability column. This is by far the best option; however, it is recognised that this is a large undertaking. It is recommended that an option such as drift flux analysis should be considered.

Lastly, regarding the design of the froth stability column, the current position of the glass frits at the bottom of the column should be redesigned. Not only does the position of the glass frits cause solids to settle onto them which then chokes the pores, but it also makes the process of cleaning the column very tedious. Currently the feed and/or drain pipe is at a level just above the glass frits which leads to some material always remaining within the column, even when it is flushed with water. The normal rotor-stator assemblies within the Leeds batch flotation cell have shown to be very reliable and easy to clean; however, it does not give the operator the freedom to easily manipulate bubble size. It is recommended that a sparging system, such as the ones used in laboratory flotation columns, should be considered as this does provide a certain level of bubble size control.

The plot of side-of-froth Sauter mean bubble size as a function of corrected froth height has been shown to be very useful, especially since it appears to be scale independent. There are two areas that need to be addressed here:

1. The current manual measuring of bubble size is very limiting. Proof of the large variation towards the top of the froth has been highlighted throughout and currently this adds a certain degree of freedom to the results. If the plot of Sauter mean bubble size as a function of corrected froth height is to be used extensively more robust measurements of bubble size are required. It is recommended that an automatic bubble sizing software should be trialled specifically to measure froth bubbles. Currently the Anglo American Platinum Bubble Sizer software which is developed by Stone Three cannot be used due to difficulty in defining bubble edges. An algorithm such as the watershed has been proven to work for froth bubbles and therefore this is an option; however, currently the photographs cannot be segmented correctly due to poor illumination.
2. It has been shown that the Sauter mean bubble size as a function of corrected froth height plot is plausibly scale independent. The question now, however, is what quantitative numbers can be extracted from the plot? The current iteration of the froth model contains within it two froth parameters, namely: time (how long does a certain bubble film remain) and length (a measure of bubble growth) (Harris, 2017). It is possible that the plot of Sauter mean froth bubble size versus corrected froth height can be employed to characterise both these parameters; however, mechanistic relationships are required.

REFERENCES

1. Achaye, I., Wiese, J., Harris, M. & McFadzean, B., 2015. *Effect of particle properties on froth stability,* s.l.: AMIRA P9P.

2. Aktas, Z., Cilliers, J. & Banford, A., 2008. Dynamic froth stability: Particle size, airflow rate and conditioning time effects. *International Journal of Mineral Processing,* Volume 87, pp. 76-71.

3. Ambulgekar, P. V., Dedhia, A. C. & Pandit, A. B., 2004. Liquid drainage in static foam: Analogy with liquid drainage through packed bed. *Indian Journal of Chemical Technology,* Volume 11, pp. 392-400.

4. Ata, S., 2012. Phenomena in the froth phase of flotation - A review. *International Journal of Mineral Processing,* Volume 102-103, pp. 1-12.

5. Ata, S., Ahmed, N. & Jameson, G. J., 2003. A syudy of bubble coalescence in flotation froths. *International Journal of Mineral Processing,* Volume 72, pp. 255-266.

6. Banford, A., Aktas, Z. & Woodburn, E., 1998. Interpretation of the effect of froth structure on the performance of froth flotation using image analysis. *Powder Technology,* Volume 98, pp. 61-73.

7. Barbian, N., Hadler, K. & Cilliers, J. J., 2006. The froth stability column: Measuring froth stability at an industrial scale. *Minerals Engineering,* Volume 19, pp. 713-718.

8. Barbian, N., Hadler, K., Ventura-Median, E. & Cilliers, J., 2005. The froth stability column: linking froth stability and flotation performance. *Minerals Engineering,* Volume 18, pp. 317-324.

9. Barbian, N., Ventura-Medina, E. & Cilliers, J., 2003. Dynamic froth stability in froth flotation. *Minerals Engineering,* Volume 16, pp. 1111-1116.

10. Becker, M., Wiese, J. & Ramonotsi, M., 2014. Investigation into the mineralogy and flotation performance of oxidised PGM ore. *Minerals Engineering,* Volume 65, pp. 24-32.

11. Beneventi, D., Carre, B. & Gandini, A., 2001. Role of surfactant structure on surface and foaming properties. *Colloids and Surfaces A: Physicochemical and Engineering Aspects,* Volume 189, pp. 65-73.

12. Bikerman, J., 1973. *Foams.* s.l.:Springer.

13. Brannigan, G. & De Alcantara Bonfim, O., 2001. Boundary effects on forced drainage through aqueous foam. *Philosophical Magazine Letters,* 81(3), pp. 197-201.

14. Cengel, Y. A. & Cimbala, J. M., 2006. *Fluid Mechanics - Fundamentals and Applications.* 1st ed. New York: McGraw-Hill.

15. Chang, R. C., Schoen, H. M. & Grove, C., 1956. Bubble size and bubble size determination. *Journal of Industrial and Engineering Chemistry,* 48(11), pp. 2035-2039.

16. Crosbie, R. et al., 2009. *The impact of the froth zone on metallurgical performance in a 3 cubic meter RCS flotation cell.* Unpublished, s.n.

17. Deglon, D., Sawyerr, F. & O`Connor, C., 1999. A Model to relate the flotation rate constant and the bubble surface area flux in mechanical flotation cells. *Minerals Engineering,* 12(6), pp. 599-608.

18. Derjaguin, B. & Landau, L., 1941. The theory of stability of highly charged lyophobic sols and coalescence of highly charged particles in electrolyte solutions. *Acta Physiochim. U.R.S.S.,* Volume 14, pp. 633-652.

19. Dippenaar, A., 1982. The destabilization of froths by solids. I: The mechanism of film rupture. *International Journal of Mineral Processing,* Volume 9, pp. 1-14.

20. Durand, M., Martinoty, G. & Langevin, D., 1999. Liquid flow through aqueous foams: From the plateau border dominated regime to the node dominated regime. *Physical Review E,* 60(6).

21. Farrokhpay, S., 2011. The significance of froth stability in mineral flotation - A review. *Advances in Colloid and Interface Science,* Volume 166, pp. 1-7.

22. Gorain, B., Franzidis, J.-P. & Manlapig, E., 1995. Studies of impeller type, impeller speed and air flow rate in an industrial scale flotation cell. Part 1: Effect on bubble size distribution. *Minerals Engineering,* 8(6), pp. 615-635.

23. Gorain, B., Franzidis, J. & Manlapig, E., 1997. Studies on impeller type, impeller speed and air flow rate in an industrial scale flotation cell. Part 4: Effect of bubble surface area flux on flotation performance. *Minerals Engineering,* 10(4), pp. 367-379.

24. Gorain, B., Harris, M., Franzidis, J.-P. & Manlapig, E., 1998. The effect of froth residence time on the kinetics of flotation. *Minerals Engineering,* 11(7), pp. 627-638.

25. Gy, P., 1976. *The sampling of particulate materials - a general theory.* Melbourne, Symposium on Sampling Practices in the Mineral Industries.

26. Harris, M., 2017. *P9Q Discussion document: Simulation of froth flotation in the IES,* s.l.: Centre for Minerals Research.

27. Hilgenfeldt, S., Arif, S. & Tsai, J.-C., 2008. Foam: A Multiphase System with Many Facets. *Philosophical Transactions: Mathematical, Physical and engineering Sciences,* 366(1873), pp. 2145-2159.

28. Horozov, T. S., 2008. Foams and foam films stabilised by solid particles. *Current Opinion in Colloid & Interface Science,* Volume 13, pp. 134-140.

29. Hunter, T. N., Pugh, R. J., Franks, G. V. & Jameson, G. J., 2008. The role of particles in stabilising foams and emulsions. *Advances in Colloid and Interface Science,* Volume 137, pp. 57-81.

30. Hu, Y. & Mokgosi, M., 2014. *The effect of flotation regents on froth stability (4th year project report group 53),* Cape Town: University of Cape Town, Department of Chemical Engineering.

31. Iglesias, E., Anderez, J., Forgiarini, A. & Salager, J.-L., 1995. A new method to estimate the stability of short-life foams. *Colloids and Surfaces A: Physicochemical and Engineering Aspects,* Volume 98, pp. 167-174.

32. Johansson, G. & Pugh, R., 1992. The influence of particle size and hydrophobicity on the stability of minerilised froths. *International Journal of Mineral Processing,* Volume 34, pp. 1-21.

33. Jones, R., 1999. Platinum Smelting in South Africa. *South African Journal of Science,* Volume 95, pp. 525-534.

34. Kantarci, N., Borak, F. & Ulgen, K. O., 2005. Bubble column reactors. *Process Biochemistry,* Volume 40, pp. 2263-2283.

35. Kaptay, G., 2006. On the equation of the maximum capillary pressure induced by solid particles to stabilise emulsions and foams and on the emulsion stability diagrams. *Colloids and Surfaces A: Physicochemical and Engineering Aspects,* Volume 282-283, pp. 387-401.

36. Koczo, K. & Racz, G., 1987. Flow in a Plateau border. *Colloids and Surfaces,* Volume 22, pp. 97-110.

37. Koehler, S. A., Hilgenfeldt, S. & Stone, H. A., 1999. Liquid flow through aqueous foams: The node-dominated foam drainage equation. *Physical Review Letters,* 82(21), pp. 4232-4235.

38. Koehler, S. A., Hilgenfeldt, S. & Stone, H. A., 2000. A Generalised view of foam drainage: Experiment and Theory. *Langmuir,* 16(15), pp. 6327-6341.

39. Kostoglou, M., Lioumbas, J. & Karapantsios, T., 2015. A population balance treatment of bubble size evolution in free draining foams. *Colloids and Surfaces A: Physicochemical and Engineering Aspects,* Volume 473, pp. 75-84.

40. Krishna, E. & S.T., S., 2000. Design and scale-up of the Fischer-Tropsch bubble column slurry reactor. *Fuel Processing Technology,* Volume 64, pp. 73-105.

41. Kruglyakov, P., Karakashev, S., Nguyen, A. & Vilkova, N., 2008. Foam drainage. *Current Opinion in Colloid & Interface Science,* Volume 13, pp. 163-170.

42. Kumagai, H. et al., 1991. Estimation of the stability of foam containing hydrophobic particles by parameters in the capillary model. *Agricultural and Biological Chemistry,* 55(7), pp. 1823-1829.

43. Lemlich, R., 1978. Prediction of changes in bubble size distribution due to interbubble gas diffusion in foam. *Industrial & Engineering Chemistry Fundamentals,* 17(2), pp. 89-93.

44. Magrabi, S., Dlugogorski, B. & Jameson, G., 1999. Bubble size distribution and coarsening of aqueous foams. *Chemical Engineering Science,* Volume 54, pp. 4007-4022.

45. Marrucci, G., 1969. A theory of coalescence. *Chemical Engineering Science,* Volume 24, pp. 975-985.

46. McFadzean, B., 2013. Froth stability characterisation of an industrial flotation cell. *Unpublished.*

47. Morar, S., Bradshaw, D. & Harris, M., 2012. The use of the froth surface lamellae burst rate as a flotation froth stability measurement. *Minerals Engineering,* 36(38), pp. 152-159.

48. Neethling, S. & Cilliers, J., 2002. The entrainment of gangue into a flotation froth. *International Journal of Mineral Processing,* Volume 64, pp. 123-134.

49. Papara, M., Zabulis, X. & Karapantsios, T., 2009. Container effects on the free drainage of wet foams. *Chemical Engineering Science,* Volume 64, pp. 1404-1415.

50. Saint-Jalmes, A. & Langevin, D., 2002. Time evolution of aqeuous foams: drainage and coarsening. *Journal of Physics: Condensed Matter,* Volume 14, pp. 9397-9412.

51. Schouwstra, R., De Vaux, D., Muzondo, T. & Prins, C., 2013. *A Geometallurgical Approach at Anglo American Platinum`s Mogalakwena Operation.* Brisbane, The Second AUSIMM International Geometallurgy Conference.

52. Schouwstra, R. & Kinloch, E., 2000. A Short Geological Review of the Bushveld Complex. *Platinum Metals Review,* 44(1), pp. 33-39.

53. Seaman, D., Franidis, J.-P. & Manlapig, E., 2004. Bubble load measurement in the pulp zone of industrial flotation machines - a new device for determining the froth recovery of attached particles. *International Journal of Mineral Processing,* Volume 74, pp. 1-13.

54. Teixeira, P. & Fortes, M., 2007. Energy and tension of films and plateau borders in a foam. *Colloids and Surfaces A: Physicochemical and Engineering Aspects,* Volume 309, pp. 3-6.

55. Tsatouhas, G., Grano, S. & Vera, M., 2006. Case studies on the performance and characterisation of the froth phase in industrial flotation circuits. *Minerals Engineering,* Volume 19, pp. 774-783.

56. Ventura-Medina, E. & Cilliers, J., 2002. A model to describe flotation performance based on physics of foams and froth image analysis. *International Journal of Mineral Processing,* Volume 67, pp. 79-99.

57. Verwey, E. & Overbeek, J., 1948. *Theory of the stability of lyophobic colloids.* Amsterdam: Elsevier Scientific Publishing Company.

58. Wang, L., 2015. Modeling of bubble coalescence in saline water in the presence of flotation frothers. *International Journal of Mineral Processing,* Volume 134, pp. 41-49.

59. Wang, L., Peng, Y., Runge, K. & Bradshaw, D., 2015. A review of entrainment: Mechanisms, contributing factors and modelling in flotation. *Minerals Engineering,* Volume 70, pp. 77-91.

60. Weaire, D., Cox, S. & Brakke, K., 2005. *Liquid Foams.* [Online] Available at: users.aber.ac.uk/sxc/WORK/cox_weaire_brakke.pdf [Accessed 8 December 2014].

61. Wiese, J. & Harris, P., 2012. The effect of frother type and dosage on flotation performance in the presence of high depressant concentrations. *Minerals Engineering,* Volume 36-38, pp. 2014-210.

62. Wiese, J., Harris, P. & Bradshaw, D., 2010. The effect of increased frother dosage on froth stability at high depressant dosages. *Minerals Engineering,* Volume 23, pp. 1010-1017.

63. Wiese, J., Harris, P. & Bradshaw, D., 2011. The effect of the reagent suite on froth stability in laboratory scale batch flotation tests. *Minerals Engineering,* Volume 24, pp. 995-1003.

64. Wills, B. & Napier-Munn, T., 2006. *Wills` Mineral Processing Technology.* 7 ed. s.l.:Elsevier Science & Technology Books.

65. Zanin, M., Wightman, E., Grano, S. & Franzidis, J.-P., 2009. Quantifying contributions to froth stability in porphyry copper plants. *International Journal of Mineral Processing,* Volume 91, pp. 19-27.

66. Zheng, X., Johnson, N. & Franzidis, J.-P., 2006. Modelling of entrainment in industrial flotation cells: Water recovery and degree of entrainment. *Minerals Engineering,* Volume 19, pp. 1191-1203.

APPENDIX A: DYNAMIC GROWTH CURVES

This section will display the experimentally determined height versus time curves for the various systems tested.

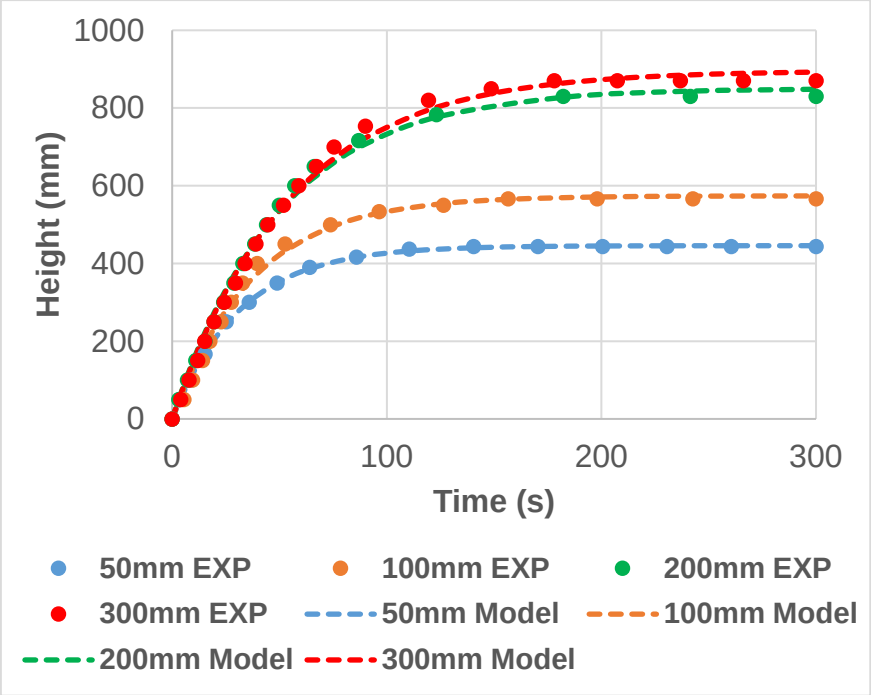

Figure 89: Dynamic froth growth as a function of time for four frothing column diameters performed on the first rougher cell of a PGM operation (dynamic stability data displayed in Figure 53)

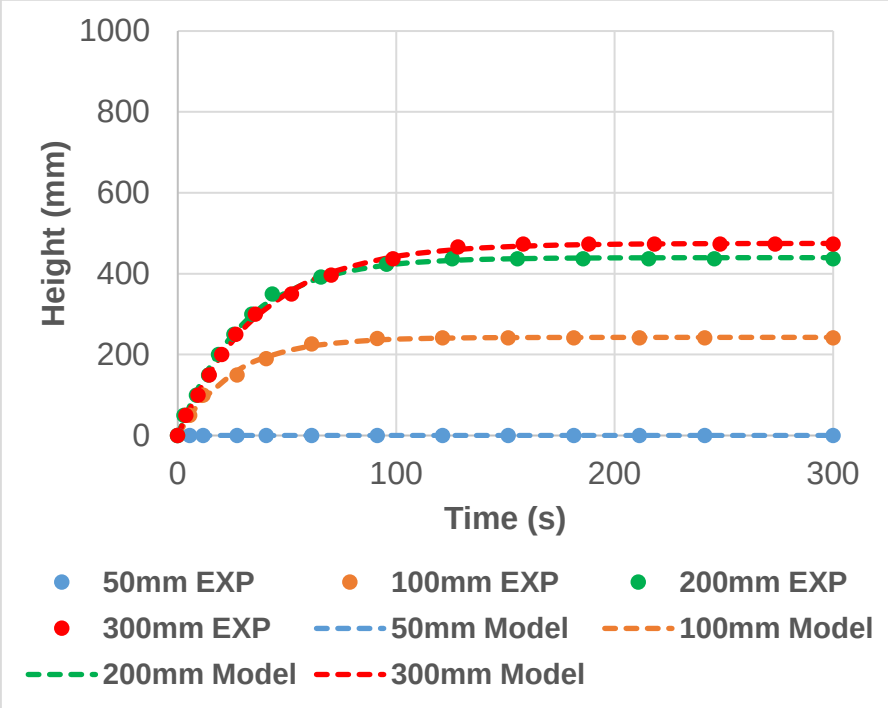

Figure 90: Dynamic froth growth as a function of time for four frothing column diameters performed on the third rougher cell of a PGM operation (dynamic stability data displayed in Figure 54)

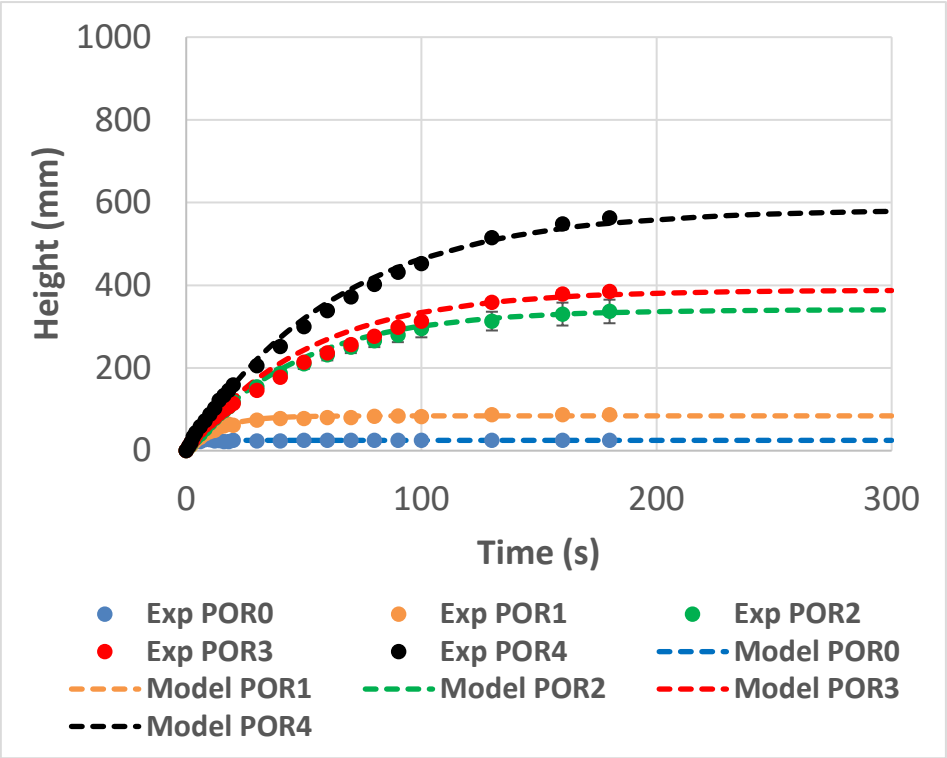

Figure 91: Dynamic foam growth as a function of time for five initial pulp bubble sizes of the 2-phase system operating at 6 L/min (dynamic stability displayed in Figure 76)

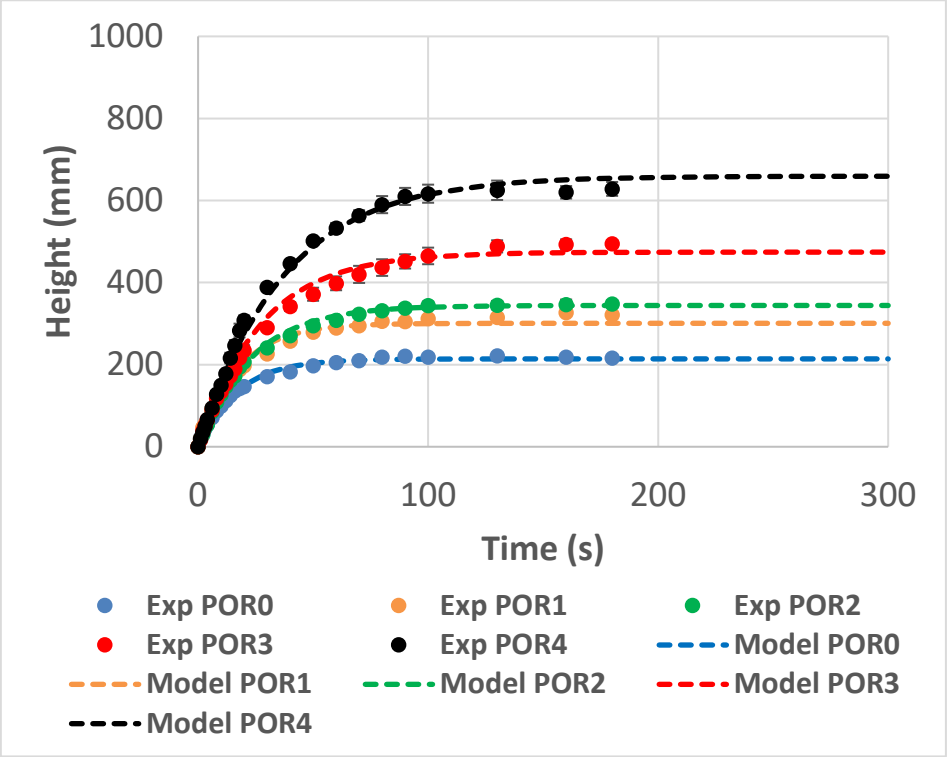

Figure 92: Dynamic froth growth as a function of time for five initial pulp bubble sizes of the Platreef repeat one system operating at 6 L/min (dynamic stability displayed in Figure 76)

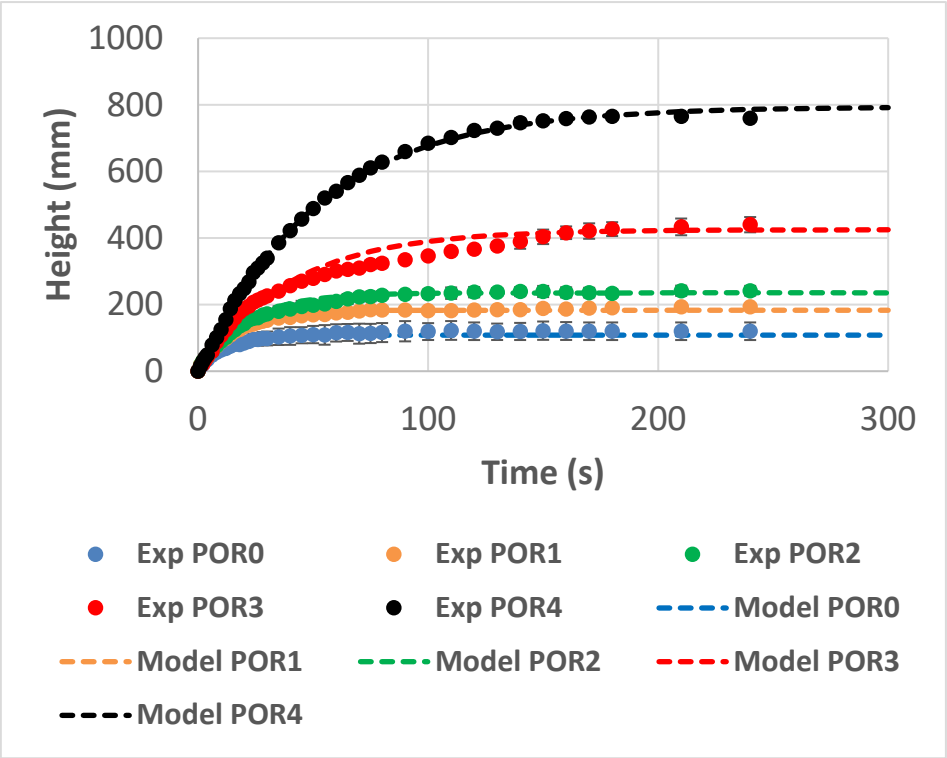

Figure 93: Dynamic froth growth as a function of time for five initial pulp bubble sizes of the Platreef repeat two system operating at 6 L/min (dynamic stability displayed in Figure 76)

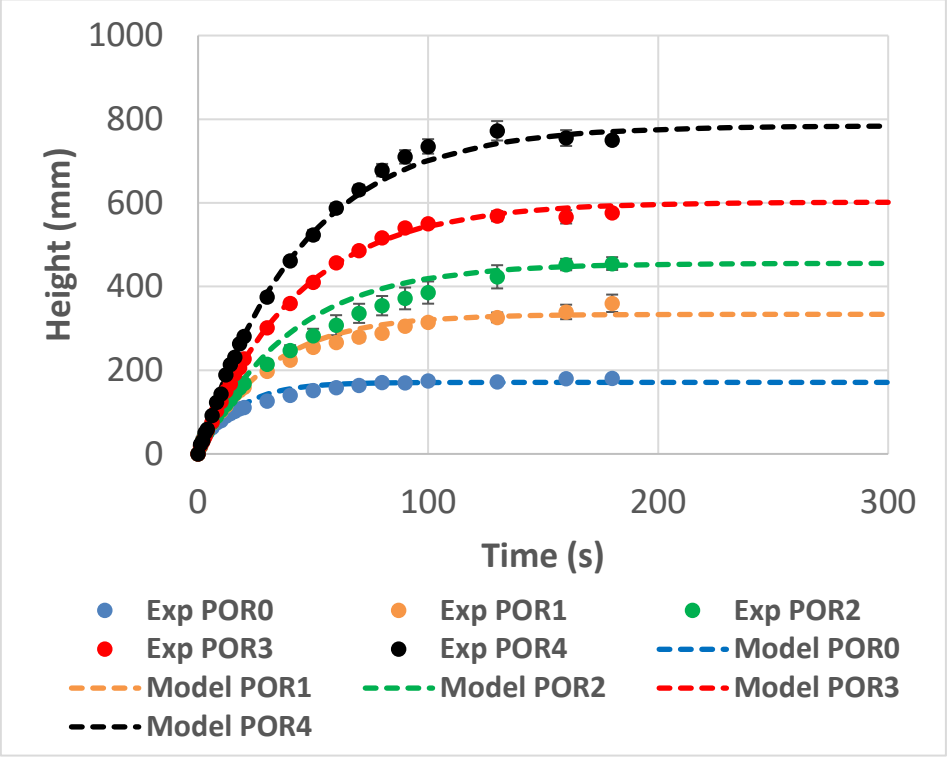

Figure 94: Dynamic froth growth as a function of time for five initial pulp bubble sizes of the UG2 system operating at 6 L/min (dynamic stability displayed in Figure 76)

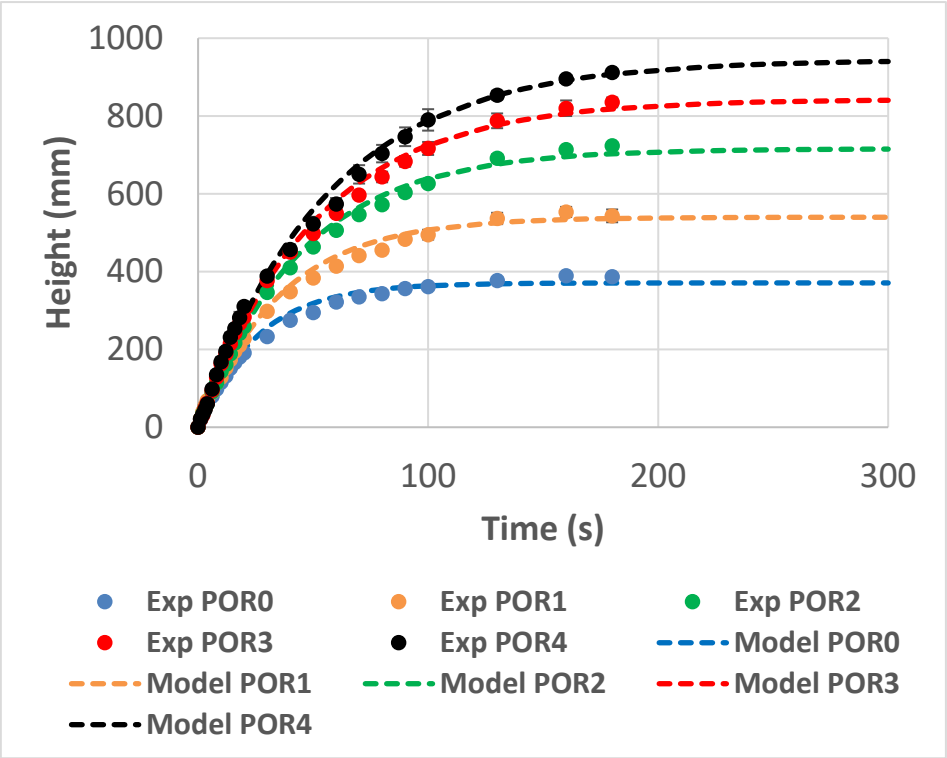

Figure 95: Dynamic froth growth as a function of time for five initial pulp bubble sizes of the silicate-rich PGM system operating at 6 L/min (dynamic stability displayed in Figure 76)